5-2015

Interpretation of Late Cretaceous Volcanic Mounds and Surrounding Gulfian Series Formations Using 3D Seismic Data in Zavala County, Texas

Laura Claire Bennett
University of Arkansas, Fayetteville

Interpretation of Late Cretaceous Volcanic Mounds and Surrounding Gulfian Series Formations Using 3D Seismic Data in Zavala County, Texas

Interpretation of Late Cretaceous Volcanic Mounds and Surrounding Gulfian Series Formations Using 3D Seismic Data in Zavala County, Texas

A thesis submitted in partial fulfillment
of the requirements for the degree of
Master of Science in Geology

by

Laura Claire Bennett
University of Arkansas
Bachelor of Science in Geology, 2013

May 2015
University of Arkansas

This thesis is approved for recommendation to the graduate council.

_____
Dr. Christopher Liner
Thesis Director

_____
Steve Milligan, M.S.
Committee Member

_____
Dr. Doy Zachry
Committee Member

_____
Robert Liner, M.S.
Committee Member

Abstract

The Late Cretaceous Gulfian series is a prominent and important series across the State of Texas that has been extensively studied since the nineteenth century. It is composed of series of southeast-dipping shelf carbonates and clastics deposited on the northwest margin of the Gulf of Mexico Basin. In south Texas, the Gulfian series was deposited in the Rio Grande Embayment and Maverick Basin and is comprised of the Eagle Ford Group, Austin Group, Anacacho Limestone, San Miguel Formation, Olmos Formation, and Escondido Formation that crop out and continue basinward in the subsurface. Late Cretaceous volcanism formed volcanic mounds composed of altered palagonite tuff that are clustered into two fields, including the Uvalde Field centered in Zavala County. Using the Pedernales 3D seismic survey, located in east-central Zavala County, several volcanic mounds were identified and mapped without the use of well log data by identifying structures and characteristics associated with the volcanic mounds. Isolating these mounds through mapping enabled the mapping of the tops surrounding Gulfian formations, Lower Eagle Ford, Upper Eagle Ford, Austin, Anacacho, and San Miguel, for which time-structure, amplitude, similarity/coherency attribute, and isochron maps were generated. By using 3D seismic data, the volcanic mounds and their relation to surrounding rocks can be better interpreted.

Acknowledgements

I would like to thank Stephens Production for their generous donation of the Pedernales survey to the University of Arkansas and allowing me to work on it. It has been a very interesting study, and I am grateful for the opportunity to be able to study a part of my favorite place in the world-Texas.

I would also like to express my sincere and overwhelming gratitude to Kinder Morgan CO2 for hiring me. Seriously. Thank you.

To my advisor, Dr. Chris Liner, the rest of my committee, Dr. Doy Zachry, Steve Milligan, and Robert Liner- thank you for all of your support throughout my graduate (and my undergraduate) career. You have all been so helpful and encouraging throughout this process and I have learned so much. Dr. Liner has taught me so much of his immense geophysical knowledge and general expertise and I am extremely grateful to have had the opportunity to work with him. Without Dr. Zachry's guidance and support as my undergraduate and graduate advisor the past five years, I don't know where I would be. I would also like to thank Dr. Van Brahana, who, although not on my committee, provided me with immense amounts of enthusiasm, encouragement, and edits.

To my fellow graduate students who were always working in Ozark 36, thanks for all the suggestions and advice shared throughout our time together in the basement.

To Daniel Moser, thank you for reminding me every day of how much you believed I could accomplish and for your support through the stressful days.

Lastly, I would like to thank my family, Tony, Denise, and Matthew Bennett, for their unconditional support, without which nothing I've accomplished would be possible. Words cannot express my gratitude.

Dedication

This is dedicated to my grandparents, Johnny and Reva Nell McTyre, who invested in my education and future before I could even walk, and Bill and Dottie Bennett, who loved me unconditionally. This is also to Denise and Tony Bennett, who continued to believe in what I could accomplish, to the rest of my family and friends who have provided me with the support and love that has gotten me where I am today, and especially to Mary Houston.

Table of Contents

List of Figures

I. Introduction

The Gulfian Series in south Texas is composed of the Eagle Ford Group, Austin Group, Anacacho Limstone, San Miguel Formation, Olmos Formation, and Escondido Formation (Fig 1). These rocks constitute a series of carbonates and clastics deposited on the Late Cretaceous northwest Gulf Coast margin through continued eustatic transgression in multiple margin depressions. This work focuses on the Rio Grande Embayment. Structurally, the Rio Grand Embayment inherited the preexisting southeast-dipping structure of the Comanchean platform of the northwest Gulf Coast margin, as well as deep-seated basement faults that were formed during the Paleozoic breakup of Pangea. Extensional fault features resulting from relaxation of the Ouachita thrust belt dominate the northeast area of the Embayment and parallel the thrust belt. In the southwest, compressional fold features dominate, resulting from the Laramide orogeny. A field of submarine volcanoes that formed in the Santonian through Coniacian is centered between the two tectonic provinces.

All of Gulfian rocks have been hydrocarbon producers, including the Eagle Ford, which is currently one of the top oil-producing unconventional plays in North America. These rocks crop out across the state through major Texas cities (Fig 2), and therefore have long been the focus of geologists' attention. Currently, the Eagle Ford Group (commonly referred to as the Eagle Ford Shale) in South Texas is one of the largest oil-producing unconventional plays in North America. Because of its profitability, energy companies have invested to develop this play, enabling geologists to learn more about the Late Cretaceous rocks. While many graduate theses in recent years have been devoted to researching the Eagle Ford, little attention has been paid to the younger Gulfian formations that, in the past, have been hydrocarbon producers.

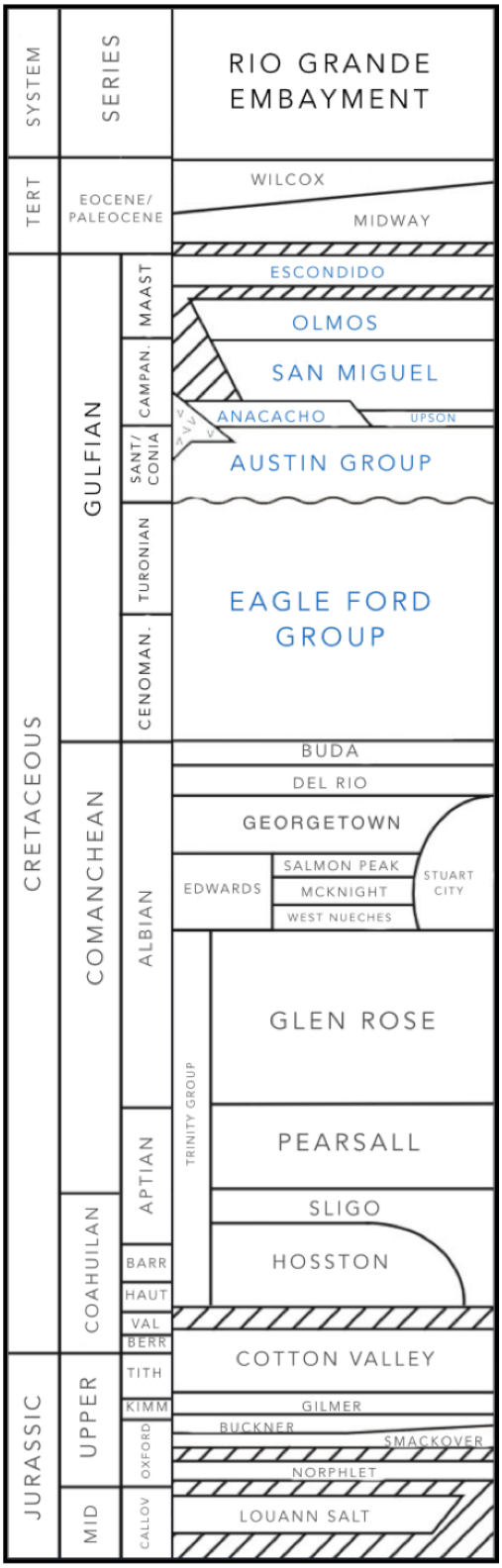

Figure 1: Stratigraphic column of the Rio Grande Embayment. The Gulfian series is highlighted (Condon and Dyman, 2003)

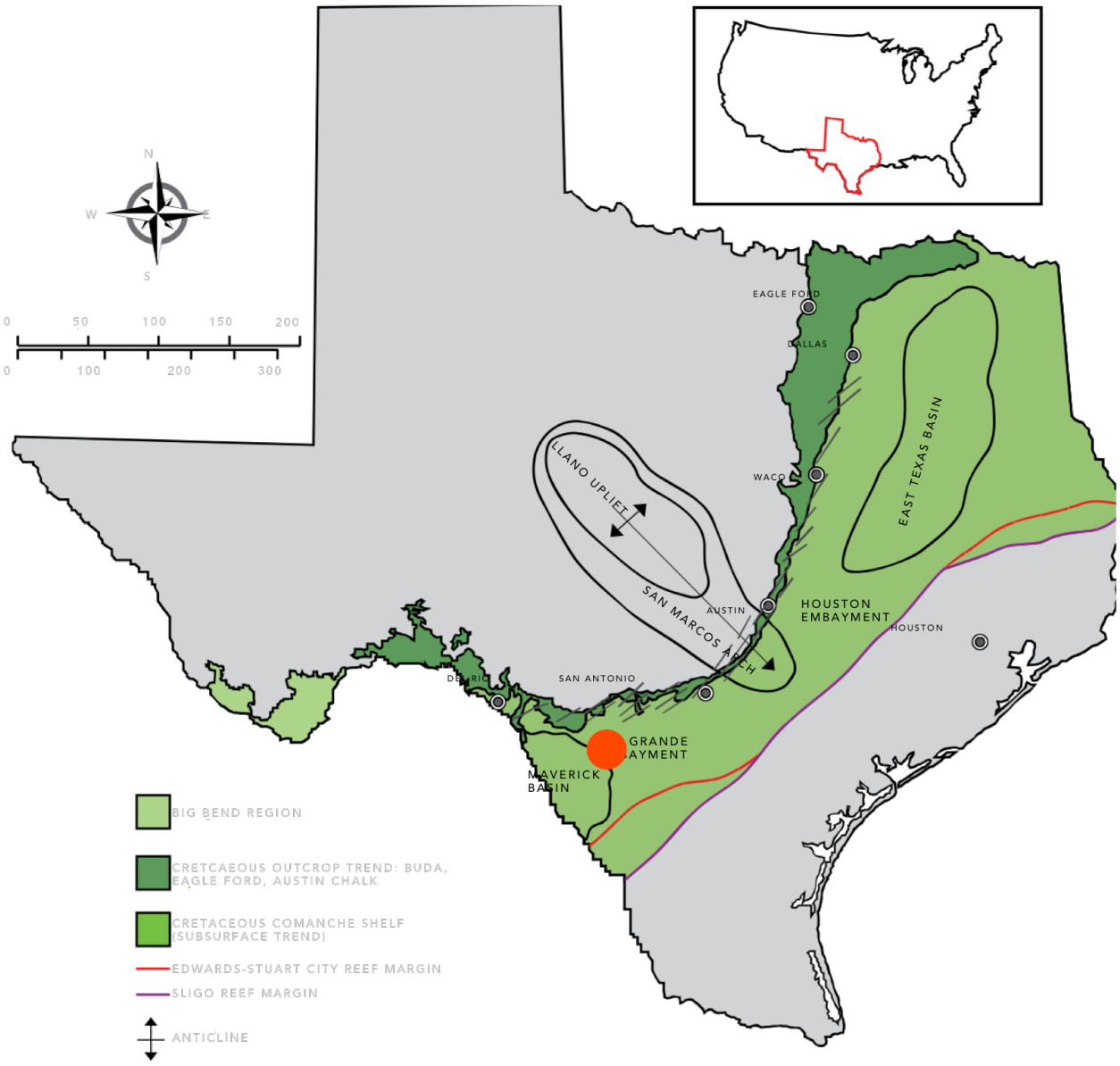

Figure 2: Map of Texas depicting the subsurface trend of the Cretaceous Comanche Shelf. The Maverick Basin is a feature of the larger Rio Grande Embayment, which is separated from the Houston Embayment and East Texas Basin by the San Marcos Arch. Rocks of the Gulfian Series follow this subsurface trend. Approximate location of the work area is denoted by the red dot.

A. Study Location

The 3D seismic survey examined for this thesis is located in east-central Zavala County (Fig 3). Due to the proprietary nature of the survey, exact location cannot be disclosed. The work area is located within the Maverick Basin in the Rio Grande Embayment on the northwest margin of the Gulf of Mexico Basin (GOMB).

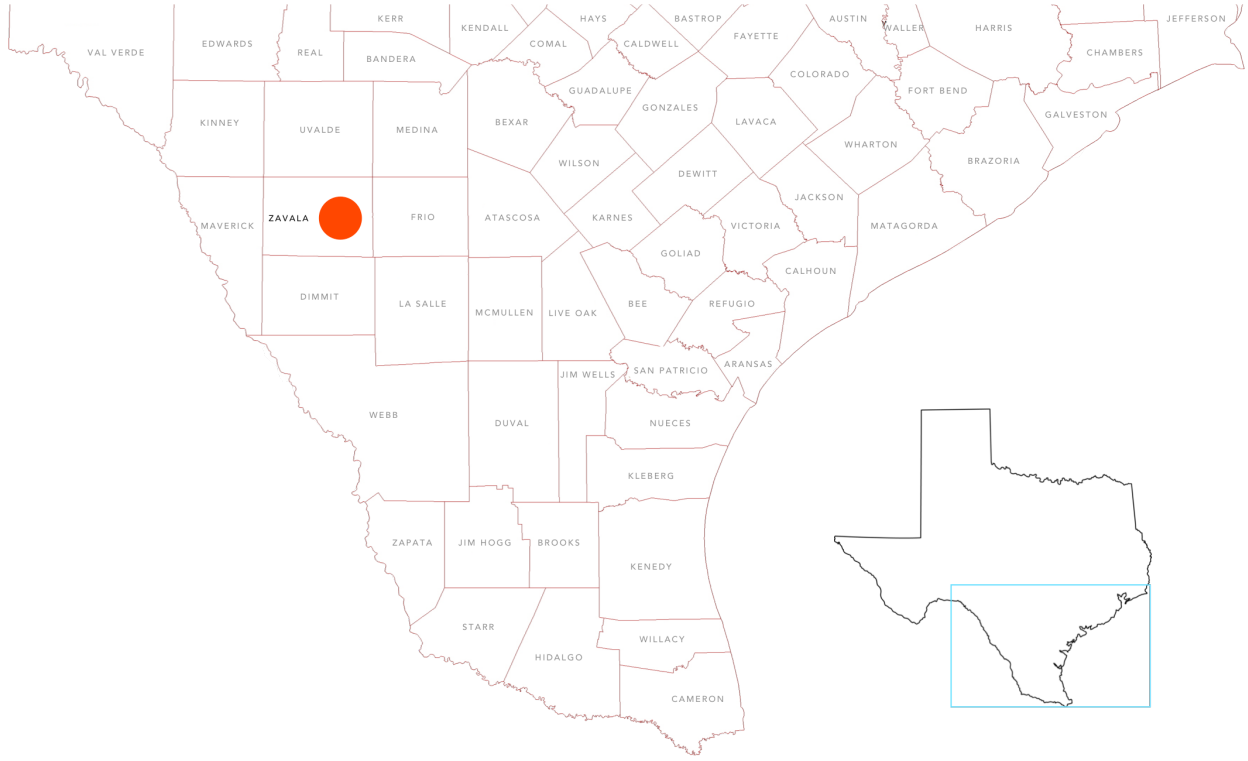

Figure 3 Map of south Texas counties, with approximate survey location indicated by red dot.

B. Previous Works

Early researchers in the late nineteenth and early twentieth century focused intense study on rocks of prominent outcrops that stretched across southwest Texas. Because of their visibility to those researchers, the outcropping rocks (now known to be a part of the Gulfian Series) received a lot of research and academic focus. Not long after the fourth Geological Survey of Texas Bulletin was published in 1889, in which R.T. Hill described several rocks of the Gulfian Series, these rocks were discovered to produce oil in the subsurface. Once they were discovered to be productive, the Gulfian-aged rocks received even more academic focus and research throughout the entirety of the twentieth century. However, due to continuing discovery of more economic hydrocarbon resources, the research on the Gulfian Series slowed.

In 2003, Condon and Dyman published a paper for the United States Geological Survey assessing the undiscovered conventional hydrocarbon resources in the Gulfian series of the Western Gulf Province, specifically in south and southeast Texas. Their assessment compiled cumulative production data for the petroleum system (Fig 4) as well as a century's worth research that detailed lithological descriptions and tectonic and depositional settings of the Gulfian Series in Texas. Because of the assessment's focus on the series as that of a conventional resource (Eagle Ford and Austin source rocks, Anacacho, San Miguel, Olmos, and Escondido reservoir rocks (Fig 5), attention was not paid to the unconventional resource potential of the Eagle Ford Group. In 2008, the mudstones of the Eagle Ford Group (commonly incorrectly referred to as a shale) were discovered to be a highly productive oil-prone unconventional source. Production data for the Eagle Ford from the Texas Railroad Commission through January 2015 can be found in Fig 6. Because of its high productivity, resources were reinvested into exploring and better

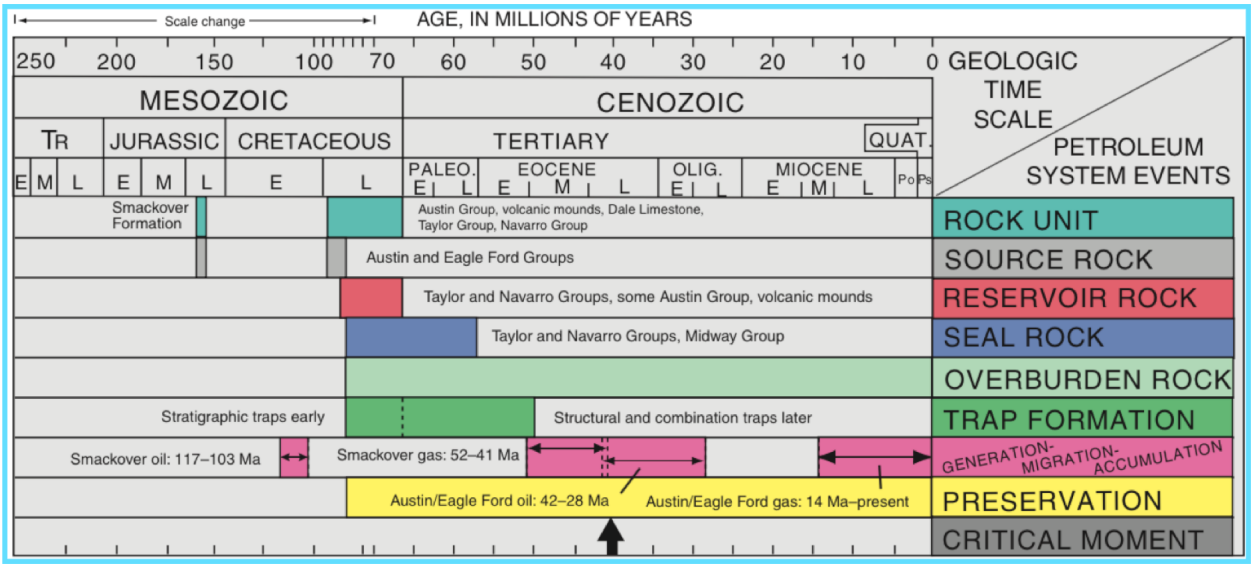

Figure 4 Events chart from Condon and Dyman (2003) showing the timing of key elements in the "Smackover-Austin-Eagle Ford Composite Total Petroleum System"

Producing unit	Produced oil (MMBO)[1]	Produced gas (BCFG)[2]	Approximate no. of leases[3]
Escondido Formation	4	75	450
Olmos Formation	110	1,227	3,700
San Miguel Formation	142	414	1,050
Anacacho and Dale Limestones	11	7	770
Undivided Navarro Group	144	186	4,600
Undivided Taylor Group	29	133	800
Austin Chalk associated with volcanic mounds	2.5	<1	50
Totals	442.5	2,042	11,420

[1]Million barrels of oil.

[2]Billion cubic feet of gas.

[3]Production from a single well may be divided into multiple leases if the well produces from more than one reservoir or has changed operators.

Fig 5 Total oil and gas production of the Smackover-Austin-Eagle Ford Composite Total Petroleum System through February 2003 from Condon and Dyman (2003)

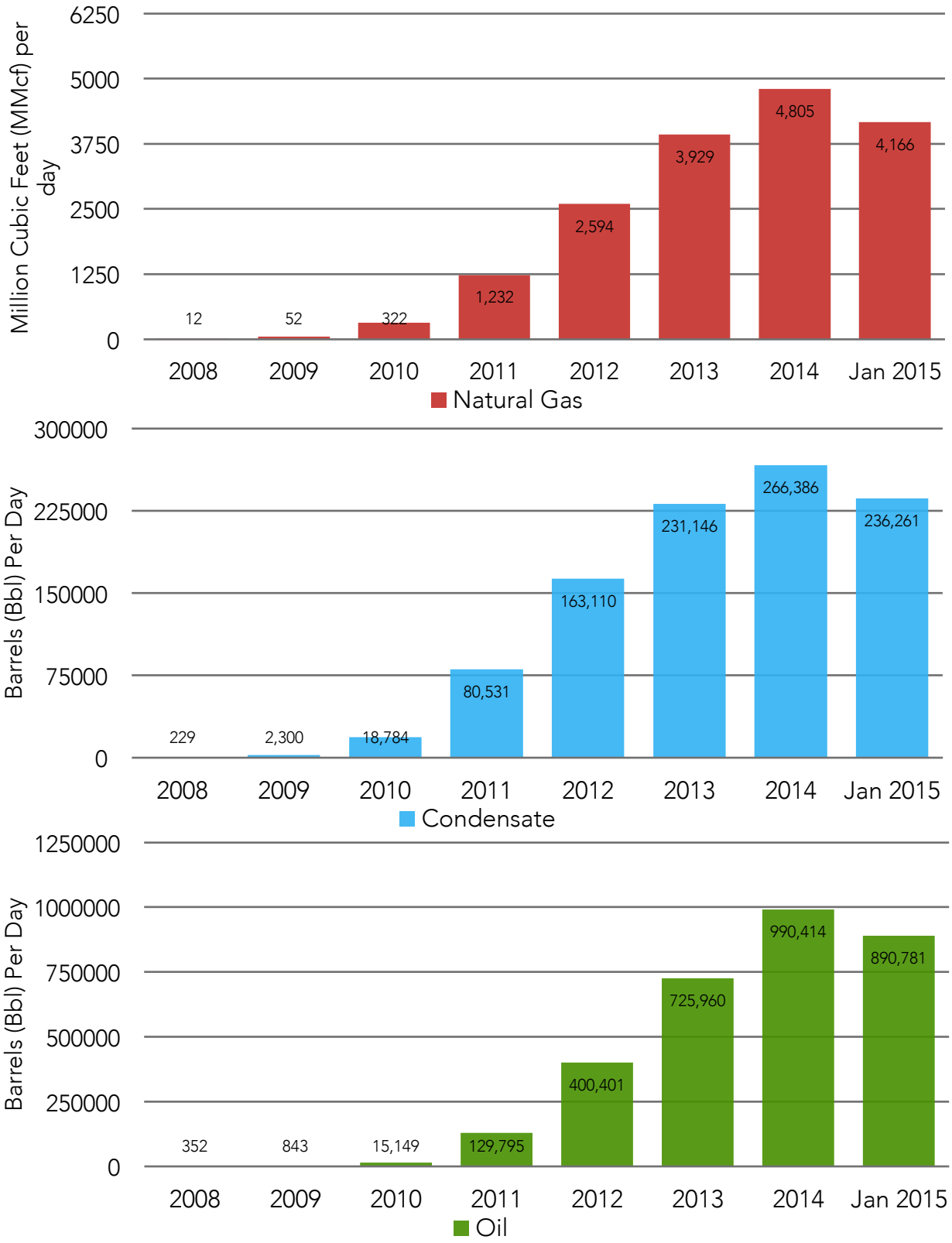

Figure 6: Eagle Ford natural gas, liquid condensate, and oil production from 2008 through January 2015 (Texas Railroad Commission, 2015)

understanding the Eagle Ford Group. With industry and academic focus back on one of the Gulfian Series rocks the Eagle Ford has been explored and understood in new ways thanks to the advancements in data collection and processing such as 3D seismic. Several papers by Treadgold and others in 2010 and 2011 discuss 3D seismic analysis of the Lower and Upper Eagle Ford shale formations.

While much work is being done on the Eagle Ford Group, little recent attention has been paid to the other Gulfian rocks. Because of this, assessments of interesting characteristics in younger Gulfian rocks using newer advanced technologies have not been widely published. Many features in the younger sections were observed using traditional well-log, core, and outcrop analysis, such as Weise (1980) identifying prograding delta formations in the San Miguel, Tyler and Ambrose (1986) identifying prograding delta formations in the Olmos, or Ewing and Caran (1981) that detail the volcanic mounds of the Uvalde and Travis fields using 2D seismic to characterize a seismic pattern for identification. Ewing and Caran describe the volcanic mounds as rising 50-100 m above the paleoseafloor with a thick sheet of tuff or ash spreading out away from the volcano for several kilometers, and observed that the surfaces of larger mounds are flat to irregular, while small mounds rise to a peak, and the sides of the mound typically dip at 5° or less. Further, they observed that the palagonite tuff volcanic centers have low seismic velocity and are encased by high velocity carbonates. The characteristic seismic pattern yielded from the higher P-wave velocities of the Anacacho (11,000 to 12,500 ft/s), Austin (13,000 to 14,000 ft/s), and Eagle Ford (11,000 to 15,000 ft/s) surrounding the low P-wave velocity palagonite tuff (around 9,500 ft/s in Wilson County) allowed tuff thicker than 95 feet to be mapped between the peaks of negative pulses on top and positive pulses below (Fig 7). The edges of the volcanic center would show tuning, followed by outward decrease in

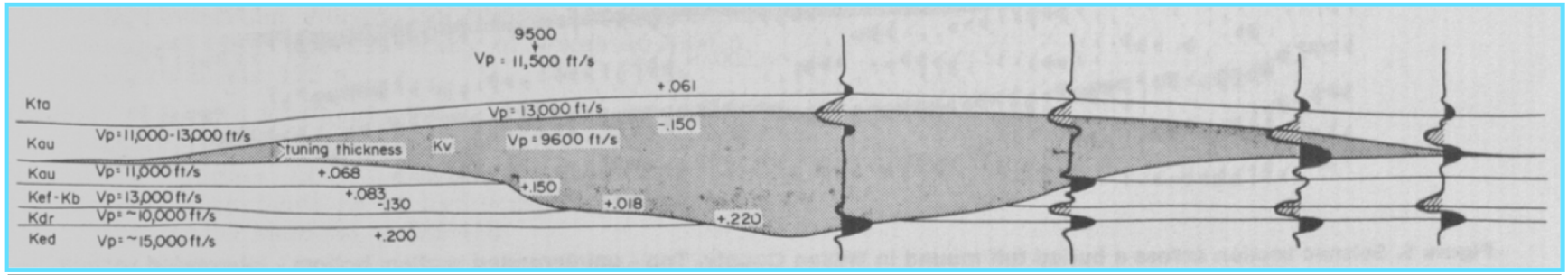

Figure 7 Velocity and seismic model of a buried tuff mound in Wilson County from Ewing and Caran (1981). On the left are sonic velocity values from a well. Decimal fractions are estimated reflection coefficients for various contacts. On the right is the predicted response at different locations on the tuff mound; note the tuning or additive response in the outer part of the mound.

amplitude to normal background levels. Crestal normal faults and velocity pull-downs could also be observed in relation to the mounds. They also observed mafic igneous rocks, which were found in the Uvalde field, that had substantially higher P-wave velocities ranging from 18,000 to 24,000 ft/s, which, when observed in seismic data, should produce a strong positive reflection, a shadow zone (the result of most of the seismic energy being reflected), and a substantial pull-up of underlying reflectors resulting from the low velocity tuff wedge.

Ogiesoba and Eastwood (2013) discuss mapping the volcanic mounds, as well as the Eagle Ford and the Austin, using 3D seismic data and attribute analysis (Fig 8). They describe the volcanic ash mounds as having high clay content corresponding to low acoustic impedance (AI) and lower frequency due to absorption by high clay content. High impedance sediments directly below the volcanic mound were also observed to exhibit chaotic features, which would likely be the result of eruptions shattering surrounding carbonate rocks and depositing them along with volcanic ash. In their study, well data provided an interval velocity for the palagonite tuff of about 11,400 ft/s, which is higher than velocity reported by Ewing and Caran (1981) but still lower than that of the encasing carbonate rocks that range from 14,500 to 16,500 ft/s. They explained that the lower interval velocity found associated with these mounds is the result of the diagenetic alteration of the magma to palagonite, which has a lower interval velocity than that of the original magma, which was described by Ewing and Caran (1981) to be of considerably higher velocity.

In addition to their analysis of the features within the volcanic mounds, Ogiesoba and Eastwood (2013) analyzed the possible magma pathways that led to the formation of the volcanic mounds. No pathways could be observed directly below the mounds that

could have led to their emplacement which would mean that the mounds probably formed from magma that came through any of the nearby faults by explosive eruption. They mapped the pathway as a zone of underlying faults and fractures through which magma travelled that can be seen some distance away from the center of the volcanic mound (Fig 8).

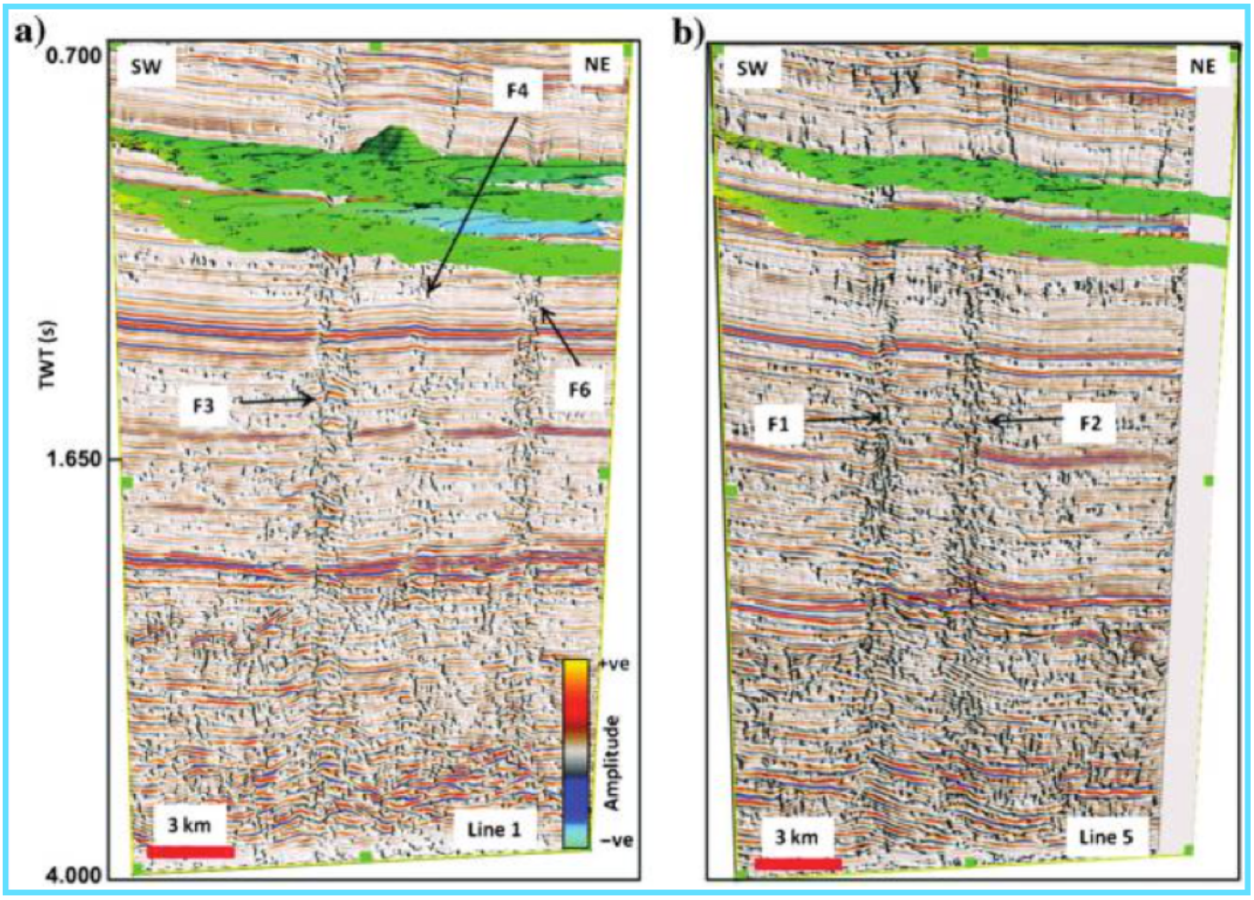

Figure 8 Seismic line from Ogiesoba and Eastwood (2013) that transects faults associated with volcanic mounds. Top horizon located near the Austin Chalk Horizon and the lower horizon is at the base of the Eagle Ford.

II. Geologic Setting

A. Tectonic Setting

The Late Cretaceous (mid-Cenomanian-Maastrichtian) Gulfian Series (Fig 1) was deposited along the Cretaceous northwest margin of the GOMB on top of a shelf that formed on the drowned Early Cretaceous Comanche Platform (Comanchean Series) (Fig 2). Because of the preexisting Comanche architecture, the Gulfian formations exist in the subsurface along a belt that trends from the southwest to northeast and dip basinward in the southeast direction, which gradually lessens upsection (Fig 2). The Cretaceous northwest margin of the GOMB is divided into three main areas: the Rio Grande Embayment, Houston Embayment, and East Texas Basin (Fig 2).

The Rio Grande Embayment is separated from the Houston Embayment and the East Texas Basin by the northwest-to-southeast trending San Marcos Arch (Fig 2), a structural high that is an extension of the Paleozoic Llano Uplift. The Rio Grande Embayment (Fig 9) is a negative feature aligned along a northwest-trending Precambrian Texas Lineament along the Rio Grande River to the southwest. The buried Ouachita Orogenic Thrust Belt, which curves along the south and east sides of the Llano Uplift and consists of faulted and folded Paleozoic rocks, defines the northwest limit of the Rio Grande Embayment. The San Marcos Arch marks the northeast limit, and the upper Cretaceous Sligo Reef Margin marks the southeast limit of the Rio Grande Embayment.

Faulting and folding from the latest Cretaceous through the Tertiary dominate the structural architecture of South Texas. Fault zones, which are thought to have developed in the latest Cretaceous related to extension and subsiding in the GOMB, trend southwest-to-northeast and roughly parallel the Ouachita Orogenic belt (Condon and Dyman, 2003). Of the major Rio Grande Embayment fault zones, only two (Balcones and Luling) may have

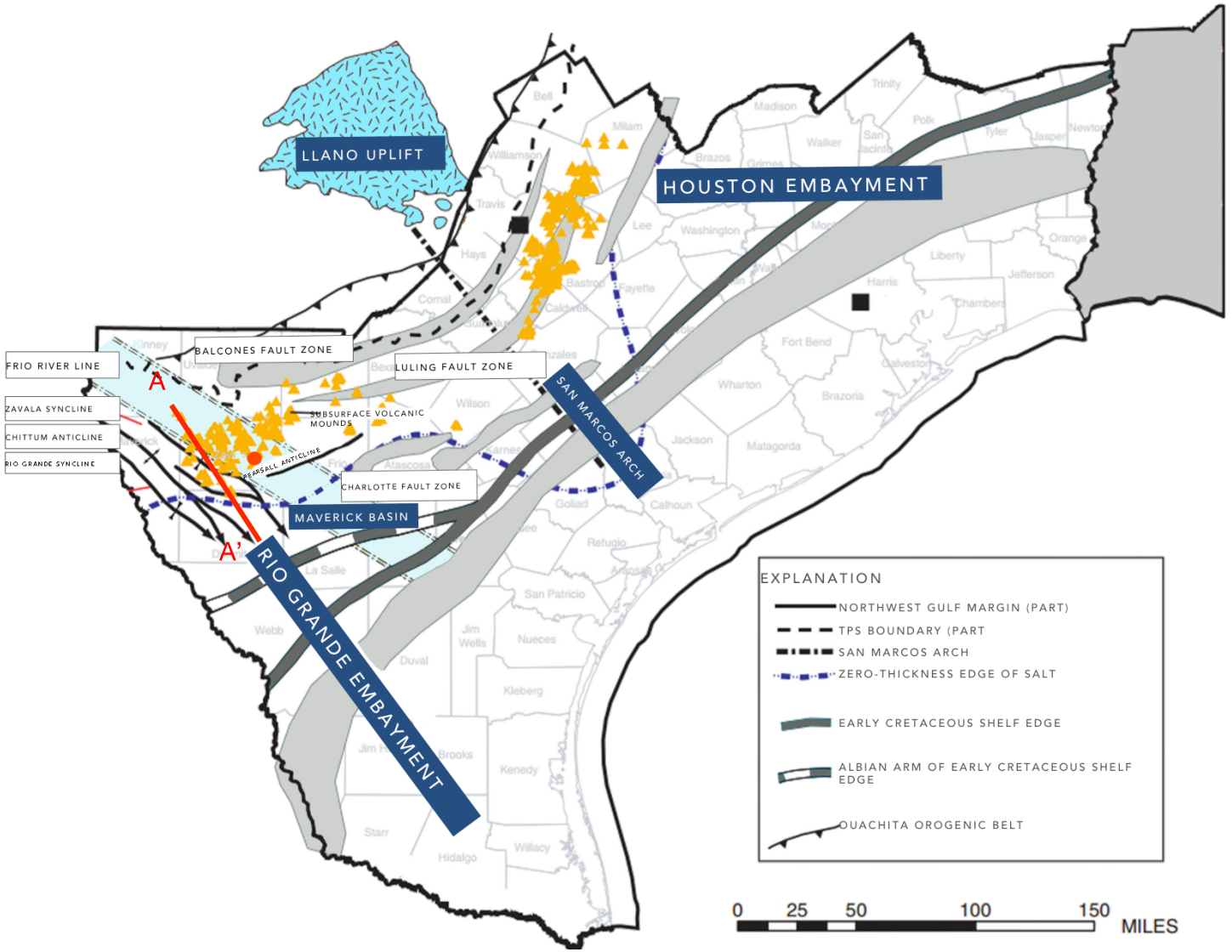

Figure 9: South Texas Region map showing prominent structural features. Red dot indicates approximate location of work area. Line A-A' is shown for Fig 10

direct impact on the Maverick Basin and this research area. The Balcones fault zone marks the craton margin of the central North American continent, parallels the Ouachita thrust belt, and consists of normal faults with down-to-the-southeast displacements that can exceed 1600 feet and extend into Paleozoic rocks. The Balcones fault zone (Fig 9) extends from Williamson County, TX southwest into Uvalde County, TX (Condon and Dyman, 2003). The Luling fault zone (Fig 9), which extends from Williamson County in the north to Medina County in the south, is parallel to and southeast of the Balcones fault zone. Normal faults of the Luling have down-to-the-northwest displacements, opposite to those of the Balcones, and range from 1,000 to 2,000 feet, and extend at least to Paleozoic basement rocks. Together, the Luling and the Balcones bound a broad, down-dropped graben (Condon and Dyman, 2003).

Within the bounds of these two faults systems, there is a belt of igneous rocks referred to as the Balcones Igneous Belt (Fig 9). This Late Cretaceous (Santonian-Campanian) belt, made up of buried and exposed volcanic mounds, extends approximately 250 miles, with the highest concentrations of volcanics clustered in the Uvalde volcanic field and the Travis volcanic field near Austin, TX. The Uvalde field is a cluster of more than 200 volcanoes centered in Zavala County (Fig 9) (Condon and Dyman, 2003). These volcanic mounds are composed of pyroclastic material that erupted from and accumulated on top of volcanic vents. Other structural features are associated with these volcanic mounds, including radial faults over the mounds that were the result of collapse of overlying deposits due to overburden. Also, differential compaction of sediments around the mounds produced local domes and tensional graben systems, as well as overlying thin depositional sequences. Distribution of these mounds suggests that they are the result of magma intrusions that travelled through faults that cut pre-Cambrian

and Paleozoic rocks, moved up along fracture zones related to the Balcones fault zone, then finally penetrated Santonian-Campanian deposits (Simmons, 1967).

While the Travis volcanic field is clearly associated with the Balcones and Luling Fault Zones, the Uvalde field, which contains the most volcanic mounds, does not appear directly related to the fault zones (Fig 9) (Condon and Dyman, 2003). The Uvalde volcanic field occurs where the Balcones and Luling fault zones intersect a transition zone called the Frio River Line (Fig 9), which separates faulting in the northeast from folding in the southwest. The northwest-southeast oriented Frio River Line is a linear zone that divides the Rio Grande Embayment and is thought to divide two areas with different structural histories (Condon and Dyman, 2003; Matthews, 1986). The Ouachita thrust-related fault systems in the northeast (i.e., Balcones and Luling fault zones) terminate at the Frio River Line, and transition to a compression fold belt related to the Laramide Orogeny to the southwest (i.e., Rio Grande and Zavala synclines, and Chittum Anticline) (Fig 9) (Matthews, 1986). The Frio River Line transition zone is thought to be of Mesozoic age, which would suggest it resulted from structural adjustments during the coalescence of plates to form Pangea and subsequent disruption (Condon and Dyman, 2003). However, its alignment atop the Precambrian Texas Lineament, which was one of a series of transform faults related to the opening of the Proto-Atlantic Ocean (Salvador, 1991), could have implications on its origin and character.

Folding features in the Rio Grande Embayment are mostly northwest-to-southeast-trending (Fig 9). The Rio Grande foldbelt includes the Rio Grande and Zavala Synclines, and the Chittum Anticline. The Rio Grande Syncline extends from Maverick County southwest into Dimmit County and the Zavala Syncline extends southwest from Maverick County through Zavala and Dimmit Country. The southeast-plunging Chittum Anticline

separates the two. The only fold with orientation subparallel to faults is the southwest-northeast trending Pearsall Anticline that passes through Frio County and southeast Zavala County (Condon and Dyman, 2003). The Maverick Basin is a subset of the Rio Grande Basin (Fig 9 and Fig 2) and is a local depression in the northern part that formed as a part of a northwest-southeast trending rift zone composed of a series of half-grabens representing a failed rift that developed during the opening of the Gulf Coast Basin (Scott, 2004). In the Albian, reactivation of the rift system caused increased subsidence in the Maverick Basin, resulting in locally thicker Late Cretaceous units (Scott, 2004).

B. Stratigraphic Setting

The thickest upper Cretaceous deposits in the Gulf Coast Basin occur as the Gulfian Series in the Rio Grande Embayment of South Texas. Throughout the Cretaceous, carbonate sedimentation dominated until the middle Late Cretaceous when terrigenous clastic sedimentation took over for the remainder of the Cretaceous. The oldest three formations in the Gulfian series (Eagle Ford, Austin, Anacacho) are dominantly carbonate formations deposited on a marine shelf and the youngest three formations (San Miguel, Olmos, Escondido) are mainly clastics derived from late Cretaceous tectonic uplifts to the west and northwest of the Maverick Basin (Fig 10) (Weise, 1980).

Eagle Ford Group

The oldest of the Gulfian series in South Texas is the Eagle Ford Group (Cenomanian-Turonian). An extreme marine highstand resulted in the deposition of deep-water, organic and carbonate-rich mudstones of the Eagle Ford conformably atop the shallow-platform lime mudstone of the Buda Formation (Hentz and Ruppel, 2010;

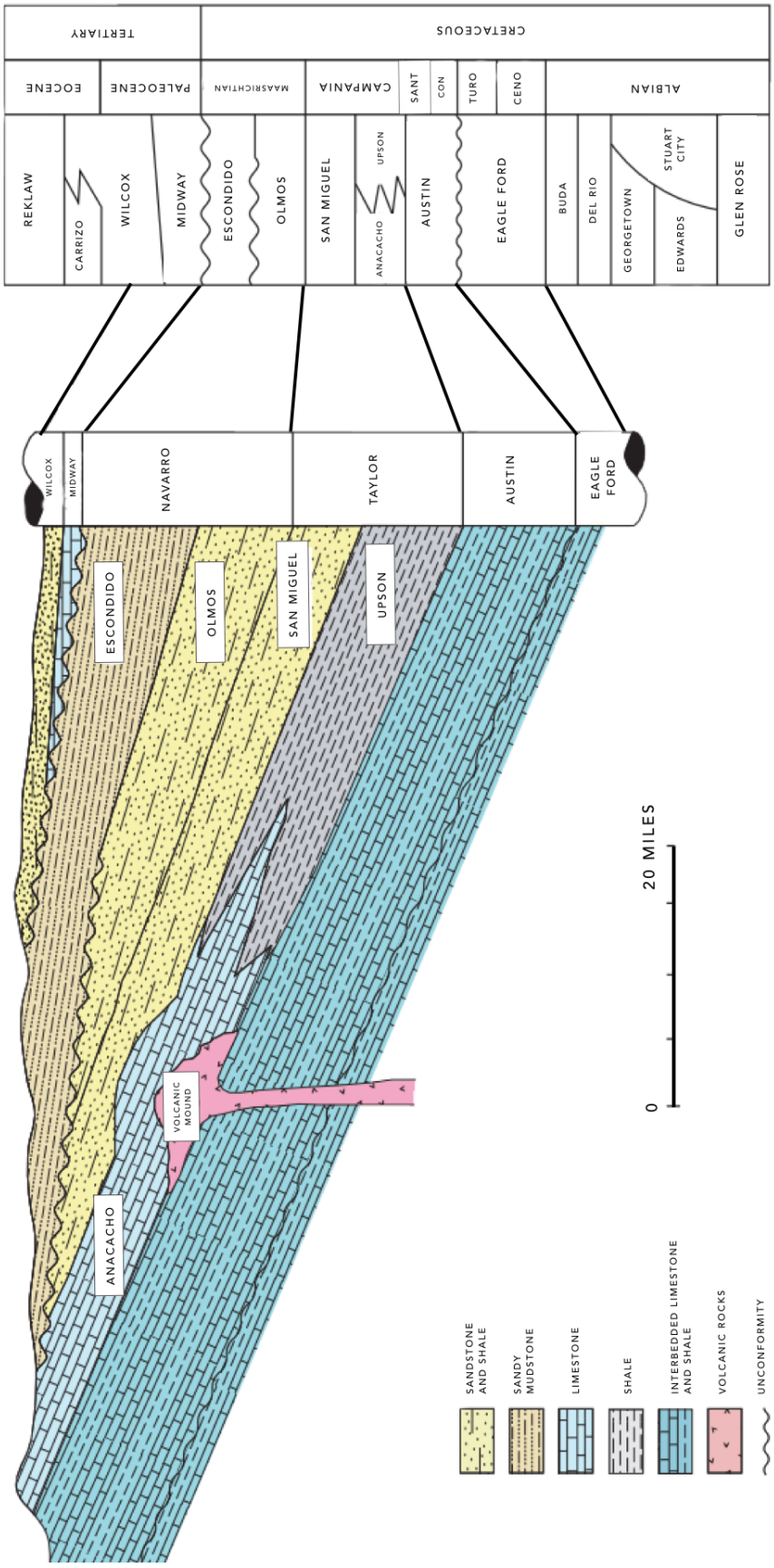

Figure 10 Northwest-southeast cross section through the Maverick Basin (modified by Condon and Dyman, 2003 from Tyler and Ambrose, 1986). Location of cross section shown on Fig 9.

Treadgold et al., 2011). The Eagle Ford south of the San Marcos Arch in the Rio Grande Embayment and the Maverick Basin varies from the unit found to the north of the arch (Fig 11). In the Maverick Basin, the Eagle Ford is subdivided into an organic-rich lower unit that is found throughout the basin and a carbonate-rich upper unit, which is only found in the Maverick Basin. The Lower Eagle Ford (LEF) was deposited during a transgressive episode and is composed of dark-gray mudrock with some locally developed light-gray calcareous mudrock, marl, and possibly limestone (Hentz and Ruppel, 2010). The LEF is characterized by 7-15% porosity and total organic content (TOC) ranging from 4-7% (Treadgold et al., 2011). The Upper Eagle Ford (UEF) consists of interbedded light- and dark-gray calcareous mudrock deposited during a regressive highstand (Hentz and Ruppel, 2010; Dawson, 2000). The UEF has lower porosity and organic content than the LEF, with 7-12% porosity and 2-5% TOC (Treadgold et al., 2011). The combined LEF and UEF is thickest in the Maverick Basin in Maverick, Zavala, and Dimmit counties, reaching around 500-600 feet and thinning downdip to the southeast (Condon and Dyman, 2003). LEF thickness reach a maximum of approximately 250 feet in west-central Maverick County (Hentz and Ruppel, 2010). The UEF is much thicker than the lower unit, due to prolonged subsidence and deposition, and reaches a maximum thickness of 480 feet (Hentz and Ruppel, 2010).

Austin Group

The Austin Group, named for its characteristic Austin Chalk Member, is dominated by chalks and marls and was deposited between the Coniacian and the Santonian. A disconformity separates the underlying Eagle Ford from the Austin (Fig 10), which is commonly regarded as a paraconformity (Ogiesoba and Eastwood, 2013). Furthermore, the contact between the Eagle Ford and the Austin is not easily discernable due to the high

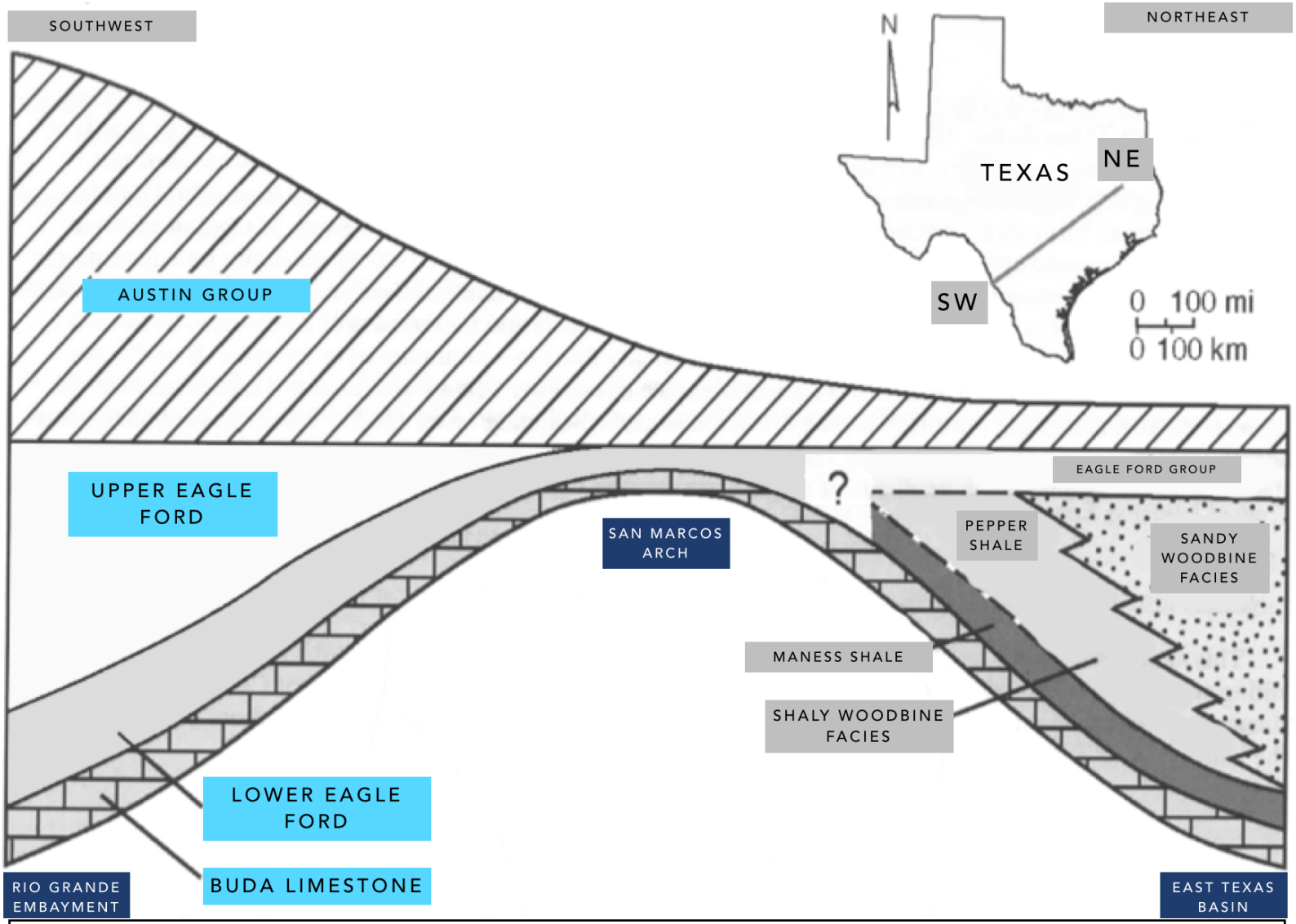

Figure 11 Southwest-northeast schematic strike cross section illustrating the differences in the Eagle Ford in the Rio Grande Embayment, over the San Marcos Arch, and in the East Texas Basin

carbonate content of the UEF. The Austin Formation can be divided into three lithologically distinct formations (upper, middle, and lower) (Ogiesoba and Eastwood, 2013; Condon and Dyman, 2003). The upper and lower formations are composed of alternately bedded chalk and marl and are separated by a mostly marl middle formation (Ogiesoba and Eastwood, 2013). Updip, the rocks of the upper and lower formations were deposited in shallow-marine shelf and normal-marine environments that were well-oxygenated, resulting in lower organic matter preservation (Grabowski, 1984; Dawson et al., 1995). The Austin Group is thickest updip, reaching a maximum of 800 feet (Ogiesoba and Eastwood, 2013). The Austin is darker, less fossiliferous, and less bioturbated in downdip areas; these rocks were deposited below wave base in outer-shelf and upper-slope environments in nearly anoxic conditions, making them higher in organic content (Grabowski, 1984; Dawson et al., 1995). In these downdip areas, at present depths exceeding 5000 feet, Austin rocks can have TOC as high as 3.5% (Ogiesoba and Eastwood, 2013). The type I and type II kerogen preserved to generate hydrocarbons in the Austin Group is thought to originate from marine plankton and algae (Grabowski, 1984; Dawson et al., 1995).

The Austin Group has low average porosity (around 4%) and permeability (0.02-1.27 mD). Original porosity was reduced by carbonate recrystallization resulting from compaction and pressure solution (Ogiesoba and Eastwood, 2013; Dravis, 1981). Austin Group permeability, however, is enhanced by extensive fracturing, consisting of tectonic fractures and microfractures. Net permeability of the Austin Group can reach values as high as 2000 mD (Ogiesoba and Eastwood, 2013; Snyder and Craft, 1977; Berg and Gangi, 1999).

Igneous Rocks

Igneous rocks in the Rio Grande Embayment are the result of volcanic activity that

began at the end of the Austin Group deposition and continued throughout the Campanian Taylor episode (Fig 10). These rocks are restricted to a northeast trending belt from Zavala County to Milam County where volcanic activity occurred (Fig 9). Within this area, three different types of igneous rocks can be found: 1) massive igneous rocks ("basalts") which form laccoliths, plugs, sills, and dikes; 2) thin beds of fine-grained, bentonitic ash, transported away from the volcanic center by air before settling in quiet water; 3) thick accumulations of palagonitic volcanic tuff, forming mounds which mark the centers of volcanic eruption (Ewing and Caran, 1982). Argon-Argon dating in the Uvalde Volcanic field provided an age range on these volcanic mounds from 78-71 Ma correlating to Campanian and early Maastrichtian stages of the Cretaceous period (Miggins et al., 2002). These igneous bodies were originally termed "serpentine plugs" by Collingwood and Rettger (1926) because they were thought to be intrusive in origin (thus the plug designation) and subsequently altered to serpentine (Matthews, 1986). They are now understood to be the result of submarine volcanic vents that produced ash and lapilli that accumulated around a crater to form tuff mounds, which were subjected to wave action and mass wasting, and later filled with lava flows (Roy et al., 1981; Ewing and Caran, 1982; Matthews, 1986). The volcanic material was altered to palagonite by immediate exposure to seawater and is now recognized as a complex assemblage of hydrated magnesium aluminum silicates derived from the alteration of extrusive basaltic rocks consisting of olivine nephelinite, basanite, alkali basalt and phonolite (Ewing and Caran, 1982; Matthews, 1986; Spencer, 1969). High magnesium and nickel content, along with mantle xenoliths that characterize these volcanic rocks, suggest a deep magma source. Although this chemistry is similar to ocean-island basalts, the volcanoes are considered to be a part of a passive continental margin as opposed to rifting or plume activity (Wittke and Mack, 1993;

Ewing and Caran, 1982).

Anacacho Limestone

The Anacacho Limestone is a fringing reef carbonate that formed on topographic highs built by the marine volcanoes in the early Campanian and is considered the basal formation of the Taylor Group (Fig 10)(Condon and Dyman, 2003). More specifically, the Anacacho is an accumulation of carbonate grainstones reworked from atoll reefs that grew on and around seamounts (Tyler et al., 1986). The Anacacho consists of biohermal reef rock and reworked skeletal debris, mollusk shells, forams, and other microorganism remains in chalky or coarsely crystalline limestone matrix, deposited in water depths of less the 150 feet (Harville, 1959). The predominantly organic fragmental limestones of the Anacacho are interbedded with bentonitic clay beds, from altered pyroclastic material, which are the result of continued volcanic activity that interrupted reef building (Harville, 1959). Whereas the porosity would have been high originally, burial and compaction of the Anacacho reduced the primary porosity and formed fractures and stylolites. All observed porosity, which on average is around 15%, is secondary porosity created by groundwater circulation (Wilson and Wilson, 1984, Harville, 1959).

Because of the Anacacho's direct relation to the late Cretaceous seamounts, it is not laterally extensive and is restricted locally to the Balcones volcanic belt in the updip part of the Rio Grande Embayment and grades into the Upson Clay downdip (Fig 10). With continued accumulation, these carbonates coalesced and spread across the shallow-marine shelf areas away from the mounds (Condon and Dyman, 2003). The maximum thickness of the Anacacho Formation is approximately 800 feet in north-central Frio County and southern Zavala County; the average thickness around 275 feet (Wilson and Wilson, 1984; Condon and Dyman, 2003).

San Miguel Formation

The San Miguel was deposited conformably atop the Anacacho in the middle-to-late Campanian and forms the upper unit of the Taylor Group in the Maverick basin (Fig 10). While deposited during a time of relative sea level rise and transgression, wave-dominated deltaic deposits of minor regressive phases best characterize the deltaic-sandstone dominated San Miguel (Weise, 1980). These deltaic sandstones are interbedded with marine shales representing the overall marine transgression. Porosity and grain size increase upward in individual sandstone beds (Weise, 1980). These sandstone beds were deposited from updip fluvial systems, as indicated by dip-aligned sandstone trends observed by Weise (1980) and can be generally observed in the Fig 10 cross section. Updip in southwestern Zavala county, San Miguel porosity and permeability average 27% and 100 mD, respectively, and reaches a maximum thickness of about 1500 feet (Lewis, 1977; Condon and Dyman, 2003). Formation thickness decreases downdip through southern and southeastern Zavala County to a mean of approximately 575 feet, and porosity and permeability decrease to 19-21% and 6-7 mD, respectively (Layden, 1976; Tyler et al., 1986). The observed porosity is secondary, since much of the original porosity was occluded by kaolinite or calcite cement; later dissolution of the calcite cement created secondary porosity (Jacka, 1982; Merritt, 1980).

Olmos Formation

The Olmos Formation constitutes the lower unit of the Maastrichtian age Navarro Group (latest Cretaceous ~70 Ma) that conformably overlies the San Miguel Formation (Fig 10). The Olmos is a low-relief sand shoal that accumulated in the middle to outer shelf under low-energy conditions and slow rates of deposition (Conrad et al., 1990). Like the San Miguel, the Olmos was deposited during an overall transgression, with pulses of

sedimentary accumulation in the western and eastern depocenters during minor regressive phases, and therefore has lithology similar to San Miguel characterized by sandstones bodies separated by interlayered shales (Tyler and Ambrose, 1986). However, lithofacies within the Olmos are a much more complex assemblage than the San Miguel, representing a wider range of delta environments. These lithologies include minor coal, shale, siltstone, and locally fossiliferous sandstone beds (Snedden and Kersey, 1982; Snedden and Jumper, 1990; Tyler and Ambrose, 1986; Conrad et al., 1990).

Eight individual Olmos sandstone bodies have been identified that are composed of a lithofacies of either a clean, biodestratified reservoir-quality sandstone, a shaly, biodestratified nonreservoir sandstone and siltstone, or a stacked sequence of both (Tyler and Ambrose, 1986; Conrad et al., 1990). Net sandstone thicknesses of individual sandstone bodies range 60-150 feet. Total thickness of the Olmos is greatest along the United States-Mexico border (maximum 1600 feet) and thins to the north and east, with mean thickness of 695 feet (Condon and Dyman, 2003).

In addition to similarity of deposition and lithology, the Olmos appears to have undergone the same diagenesis as the San Miguel (Merritt, 1980). Primary porosity was largely destroyed by compaction and calcite precipitation, and secondary porosity was created during two periods of dissolution, which subsequently partially filled by late-stage cements (Condon and Dyman, 2003). Observed porosity in the Olmos ranges from 9-28% (average 24%) and permeability ranges from 0.01-422 mD (average 83 mD) (Tyler and Ambrose, 1986; Dennis, 1987).

Escondido

The youngest formation of the Gulfian Series is the Escondido, deposited in the late Maastrichtian. This uppermost Navarro unit in the Maverick Basin is separated from the

underlying Olmos by a transgression-caused erosional surface (Fig 10) (Condon and Dyman, 2003). Lithologically, the Escondido is composed of alternating mudstone and sandstone beds, divided into lower, middle, and upper units. The mudstones were probably the result of coastal bay and lagoon deposits, and the sandstone beds formed from shoreface deposits and shallow marine shelf bars (Cooper, 1971, 1973). Fossiliferous mudstones, medium- to thick-bedded, fine-grained sandstone beds, and argillaceous, fossiliferous limestones comprise the lower part of the Escondido. Thick shell breccias and lenticular, coarser-grained sandstone beds of higher porosity make up the middle part. The upper part is composed of glauconitic, calcareous, sandy mudstone and siltstone, argillaceous limestone, and fine-grained sandstone (Pessagano, 1969; Cooper, 1971). Together, these lower, middle, and upper parts form a series of progradational, shallowing-upward parasequences deposited in a transgressive systems tract (Snedden, 1971). The Escondido formation is thickest in the southern part of the Maverick Basin in northeast Webb and southwest LaSalle Counties, reaching a maximum of ~2550 feet, and thinning northward, which can be generally seen in the Fig 10 cross Section (Condon and Dyman, 2003). Mean thickness calculated by Condon and Dyman (2003) is 923 feet.

Sandstone porosity and permeability in the eastern part of the Maverick Basin from one well in the Leming field ranged from 15.9 to 30.7%, with an average of 22.9%, and 0 to 1295 mD, with an average 143 mD (McDonald, 1986).

C. Depositional and Tectonic Evolution

Deposition of the Gulfian Series in the Late Cretaceous was largely controlled by earlier events that took place along the North American continental boundary. Breakup of a Precambrian supercontinent and coalescence and subsequent breakup of the Pangea supercontinent in the Paleozoic produced the underlying structure and setup for platform development and then shelf development. Most structural features were also inherited from basement features produced during these events.

Precambrian through Paleozoic

In the Precambrian, northeast-trending rifts offset by northwest-striking transform faults developed during the breakup of a supercontinent and the opening of the Proto-Atlantic Ocean (Fig 12). One of these transform faults, called the Texas transform or lineament, roughly parallels the lower course of the Rio Grande River and is believed to have shaped the southern rifted margin of the North American Plate in the Paleozoic (Salvador, 1991).

In the late Paleozoic (Pennsylvanian/Permian), the African, South American, and North American Plates collided to form the supercontinent Pangea (Condon and Dyman, 2003). During collision, thrusting directed toward the North American Craton resulted in the formation of the Ouachita orogenic belt (Condon and Dyman, 2003; Salvador, 1991). Along the sutured margin between the North American and South American plates, the Ouachita orogeny created folding, northward and northwestward thrust faulting, and uplift of Paleozoic rock (Fig 13) (Ewing, 1991). One such uplift is the Llano uplift of central Texas (Fig 9), around which curves the zone of compressed Paleozoic rocks of the Ouachita orogenic belt (Ewing, 1991). After initial compression in the Late Permian, the Ouachita thrust belt began a period of relaxation that lasted until the Early Tertiary and

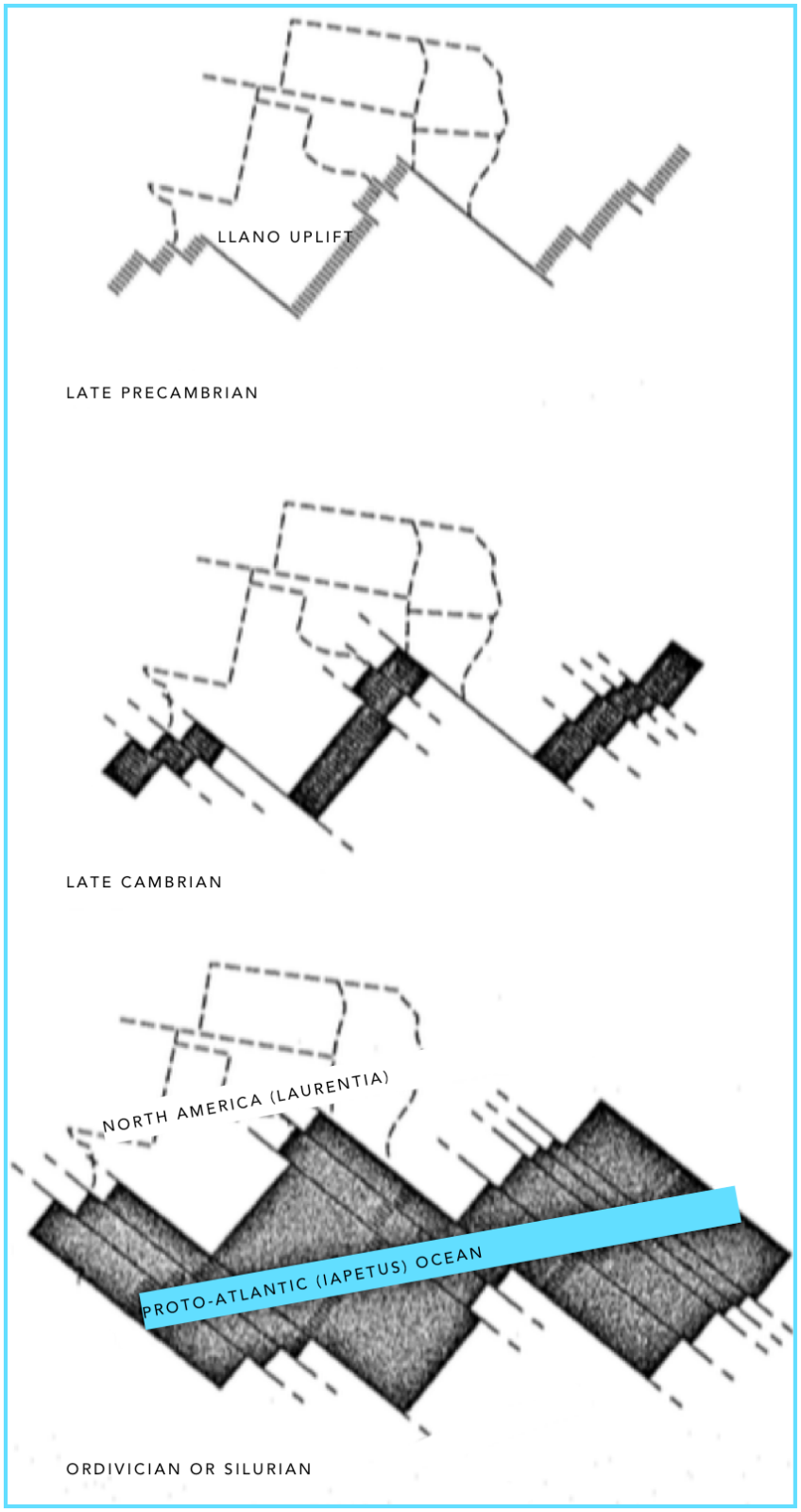

Figure 12 Opening of the Proto-Atlantic Ocean from Late Precambrian through early Paleozoic along the Texas transform, which is shown as a broader zone of transform faults (illustrated by Thomas, 1977, 1988; from Salvador, 1991)

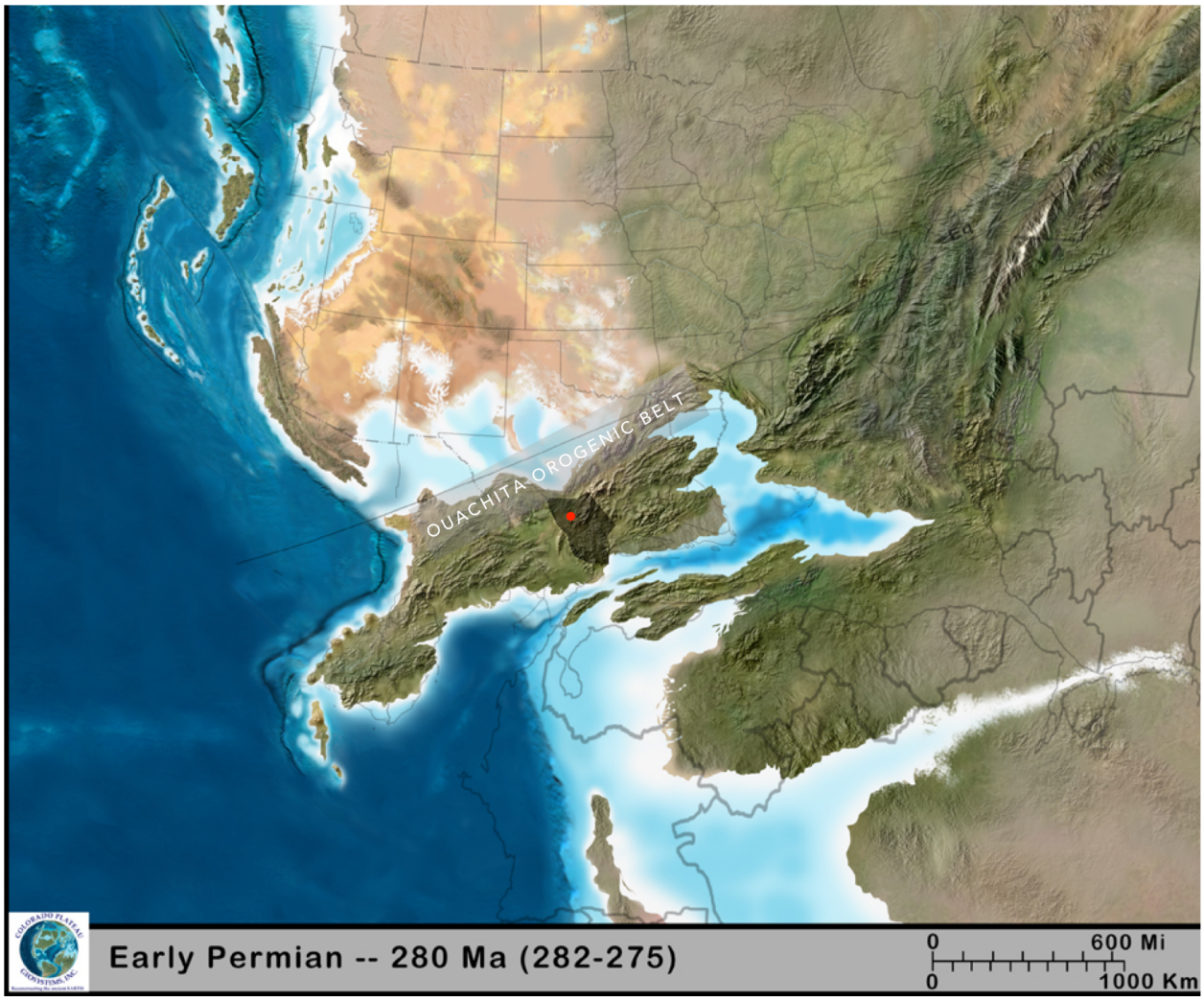

Figure 13 Early Permian (280 Ma) paleogeographic map of North American continent as a part of the Pangea supercontinent. Uplifted rocks and mountains of the Ouachita orogenic thrust belt can be seen throughout Texas and Arkansas. (Blakey, 2011)

formed a rift zone that paralleled the continental edge (Clark, 1982). It is within this rift zone that the major fault zones of the Rio Grande Embayment (i.e. Balcones and Luling) eventually formed through continued extension initiated in the Triassic that led to the breakup of Pangea (Matthews, 1986; Salvador, 1991; Galloway, 2008).

Along the margins of the spreading boundary between the North American and South American plates during the breakup of Pangea, aulacogens began to form that would become the sub-basins that define the northern margin of the GOMB (Salvador, 1991; Tyler and Ambrose, 1986). An aulacogen may have preferentially formed in south Texas and later become the Rio Grande Embayment, because of the preexisting structure of the Texas lineament and the Llano Uplift, Rifting continued throughout the Early and Middle Jurassic, and seawater periodically flooded the continental rift basin between the North American and South American plates (Fig 14), depositing thick sequences of Louann Salt across the basin and within the margin aulacogens (Salvador, 1991).

The continental rift basin continued to expand and, in the Late Jurassic, the GOMB opened with deposition of thick, course, terrigenous clastic ramp sediments (Galloway, 2008; Salvador, 1991). By late Jurassic time, the Rio Grande Embayment had grown to become a distinct, structurally negative area that received sediments from the basin margins (Weise, 1980). This era dominated by tensional deformation ended in the Late Jurassic, when a second, quieter tectonic phase of intermittent subsidence took over, resulting from the cooling of oceanic crust that had extruded along the spreading center of the basin and thermal subsidence (Salvador, 1991). This was accompanied by onset of marine transgression that continued into the earliest Cretaceous with only minor period of regression or sea level drop (Fig 15) (Salvador, 1991).

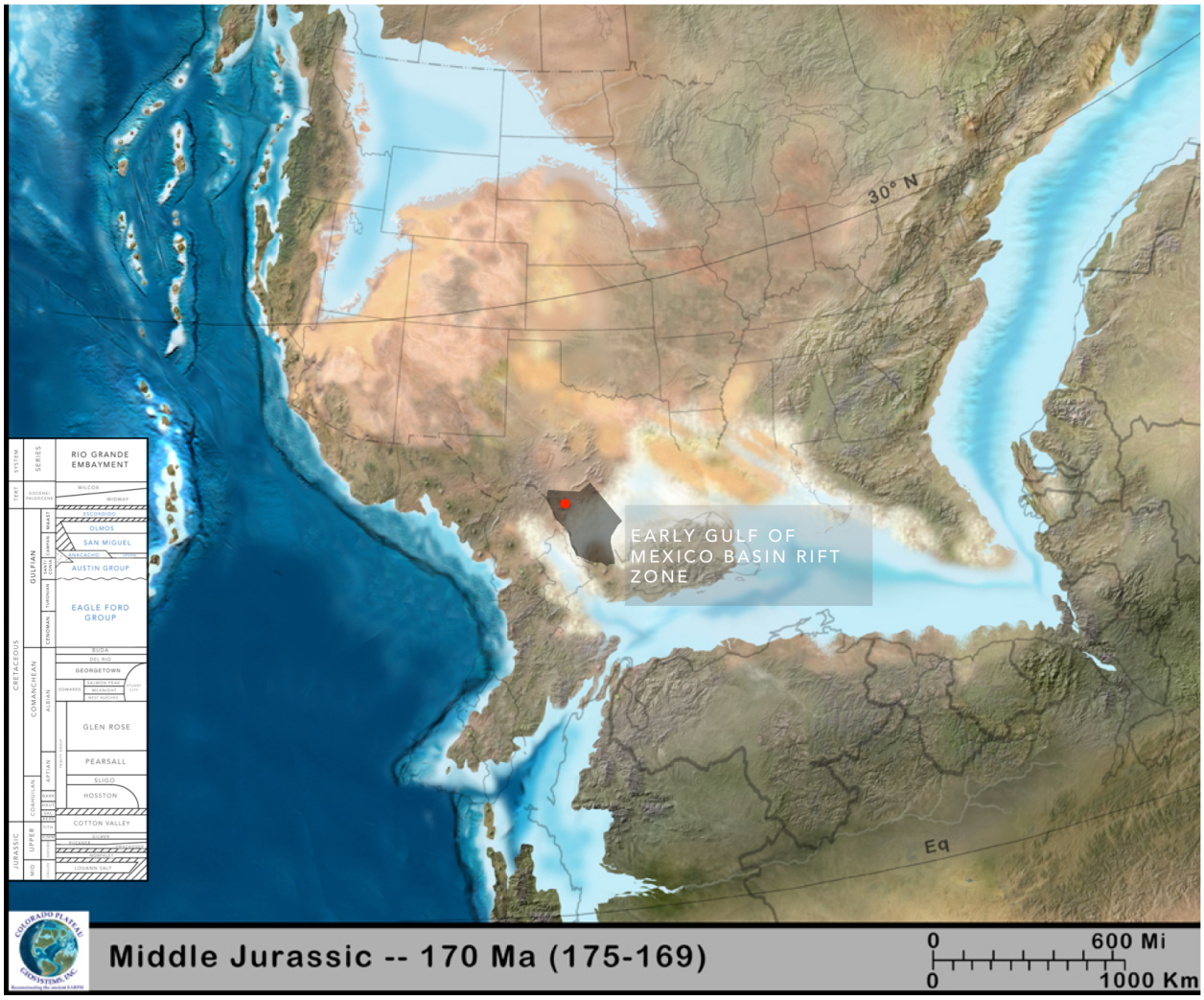

Figure 14 Middle Jurassic (170 Ma) paleogeographic map of the North American continent during the breakup of Pangea Seawater sourced from the Pacific Ocean can be seen invading the areas being rifted apart and connecting to the proto-Atlantic Ocean. (Blakey, 2011) Western Interior Seaway is established in the northwest. Future Rio Grande Embayment highlighted with approximate seismic location indicated by red dot.

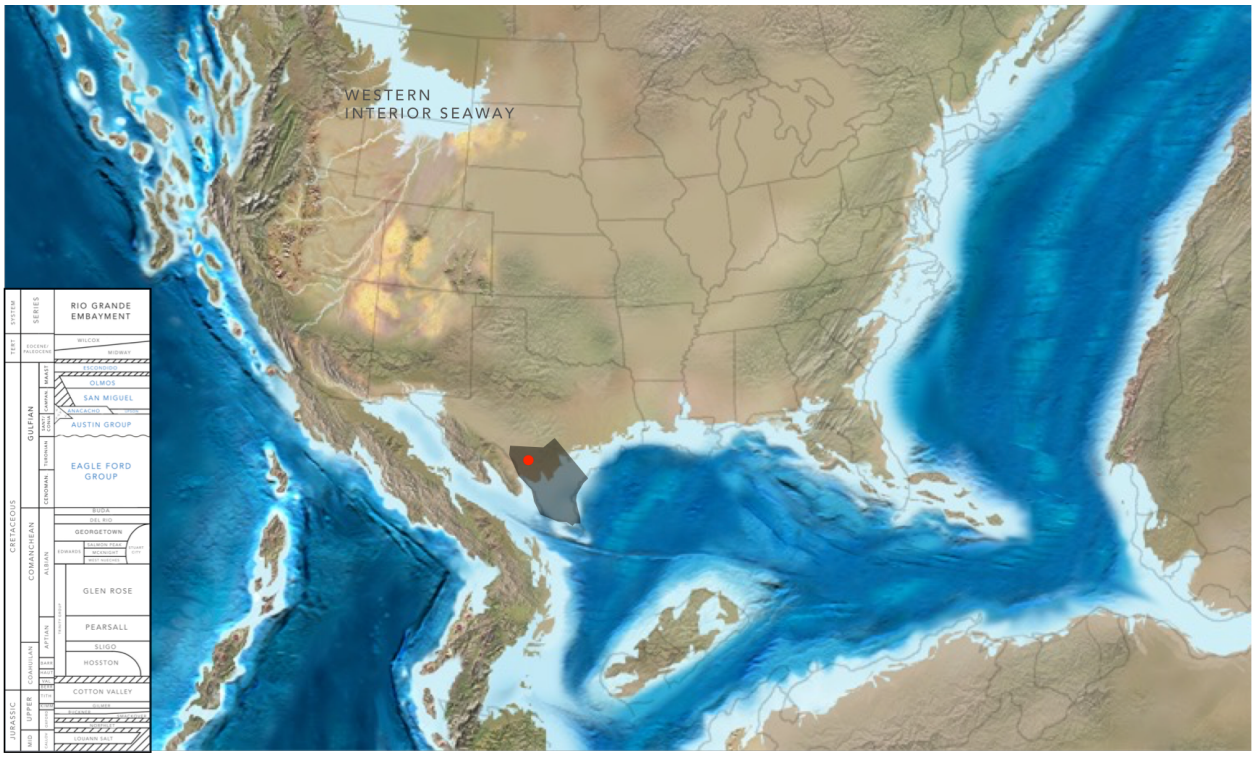

Figure 15 Late Jurassic (150 Ma) paleogeographic map of the North American Continent. Rift margin between North and South American has been flooded and marine transgression has begun pushing the North American coast northward. Western Interior Seaway extends southward. (Blakey, 2011)

Cretaceous

In the northern GOMB, the Cretaceous was a time of relative tectonic stability, and activity was restricted to deformation of Jurassic Louann Salt and to listric normal growth faulting around the rims of depositional centers and along progradational shelf margins (Condon and Dyman, 2003; Salvador, 1991). Thermal subsidence that had dominated the Gulf Basin since the Late Jurassic was replaced by sedimentary loading subsidence in the Middle Cretaceous (Salvador, 1991).

Comanchean Series

Stable shelves, ramps, and platforms began developing along the gulf margins (Fig 16) due to the persistent influx of terrigenous coarse clastic sediment in the early Cretaceous (Salvador, 1991). These became the sites of widespread carbonate deposition, which marks a major change in sedimentation of the basin from clastic to carbonate and allowed for the formation of the Early Cretaceous Comanche shelf and accumulation the Comanchean Series (Salvador, 1991; Tyler and Ambrose, 1986). The Comanche Shelf developed as a reef-rimmed platform atop northwest margin depocenters through transgressive-regressive cycles that were characterized by deposition of prograding reef-rimmed carbonate depositional episodes, which were intermittently interrupted by transgression-induced platform drowning that would result in deposition of organic-rich deep-marine shale (Harbor, 2001; Galloway, 2008; Phelps et al., 2014). Continued marine transgression had connected the Western Interior Seaway to the GOMB by the Albian. These phases of regional progradation of the reef-rimmed carbonate margin of the Comanche platform produced a well-defined shelf edge by Albian time, which defines the basinward extent of the overlying late cretaceous deposits (Galloway, 2008).

Figure 16 Early Cretaceous (130 Ma) paleogeographic map of the North American Continent. GOMB has developed, along with the Comanche Platform in Texas. Western Interior Seaway had receded since the late Jurassic. (Blakey, 2011)

In the Cenomanian, just prior to Eagle Ford deposition, eustatic regression and uplift cut off the Western Interior Seaway from the GOMB, causing a break in deposition referred to as the Mid-Cretaceous Unconformity (MCU) (Salvador, 1991). Although the MCU is recognized across a large area and used as a marker to separate the Early from the Late Cretaceous, it is not found in intrashelf basins like the Rio Grande Embayment and the Maverick Basin because they remained underwater while the rest of the shallow shelves and platforms were exposed (Salvador, 1991). This is why the deposition observed in the Rio Grande Embayment is continuous from the Cenomanian into Turonian. Uplift also intensified the surficial expression of the San Marcos Arch, an extension of the Paleozoic Llano Uplift, making it a dominant structural feature of the Late Cretaceous shelf and creating a greater divide between the Rio Grande Embayment, the Maverick Basin, and the rest of the Comanche platform.

After the drop in sea level in the Cenomanian, an ocean anoxic event was accompanied by another widespread marine transgression, which permanently drowned the platform and reestablished connection with the Western Interior Seaway (Harbor, 2011). The drowning of the platform changed the depositional architecture from the rimmed Comanche shelf platform to an open shelf ramp (Harbor, 2011; Galloway, 2008). In addition to a depositional architecture shift, movement along basement structures from the failed Rio Grande rift coupled with salt withdrawal led to the further development of the Maverick Basin as a significant negative feature within the Rio Grande Embayment (Harbor, 2011).

Gulfian Series

The Late Cretaceous depositional history of the northwest Gulf margin consisted of an early phase of carbonate sedimentation initiated by a widespread marine transgression

followed by deposition of terrigenous clastic deltaic sediments during short regressive pulses of overall transgressive events (Tyler and Ambrose, 1986). Late Cretaceous sedimentation took place on the shelf that had built atop the broad Comanche platform, from which it inherited its shelf edge, the Stuart City Reef margin (Fig 9). In the Rio Grande Embayment, the Late Cretaceous Gulfian Series accumulated as mixed carbonate and clastic aggradation of continental margins from the Turonian through Maastrichtian and can be divided into the Eagle Ford, Austin, Taylor, and Navarro depositional episodes (Fig 10) (Salvador, 1991; Galloway, 2008).

The first carbonate depositional episode in the Gulfian Series was the Eagle Ford, deposited as the result of the ocean anoxic event that drowned the platform after the MCU in the late Cenomanian through Turonian. The separation of the Rio Grande Embayment (and the Maverick Basin) from the rest of the shelf by the San Marcos Arch influenced lithology of the Eagle Ford on each side of the arch (Fig 17). Northeast of the arch, detrital siliciclastic sediment was supplied to the East Texas basin from eastern highlands. Southwest of the arch, the San Marcos Arch blocked the siliciclastic sediment supply and the Western Interior Seaway supplied carbonate sediments to the Rio Grande Embayment and Maverick Basin (Jennings and Antia, 2013; Harbor, 2011). In the Maverick Basin, previously mentioned syndepositional faulting and prolonged salt withdrawal that deepened the basin allowed for the deposition of a thicker Eagle Ford unit than in the Maverick Basin (Fig 11) (Harbor, 2011). A second order transgressive systems tract deposited the LEF and the UEF was deposited during the marine regression that followed (Harbor, 2011), terminating with regional flooding and the development of a late Turonian condensed maximum flooding horizon across the shelf (Galloway, 2011).

The Austin depositional episode began in the Coniacian and continued through the

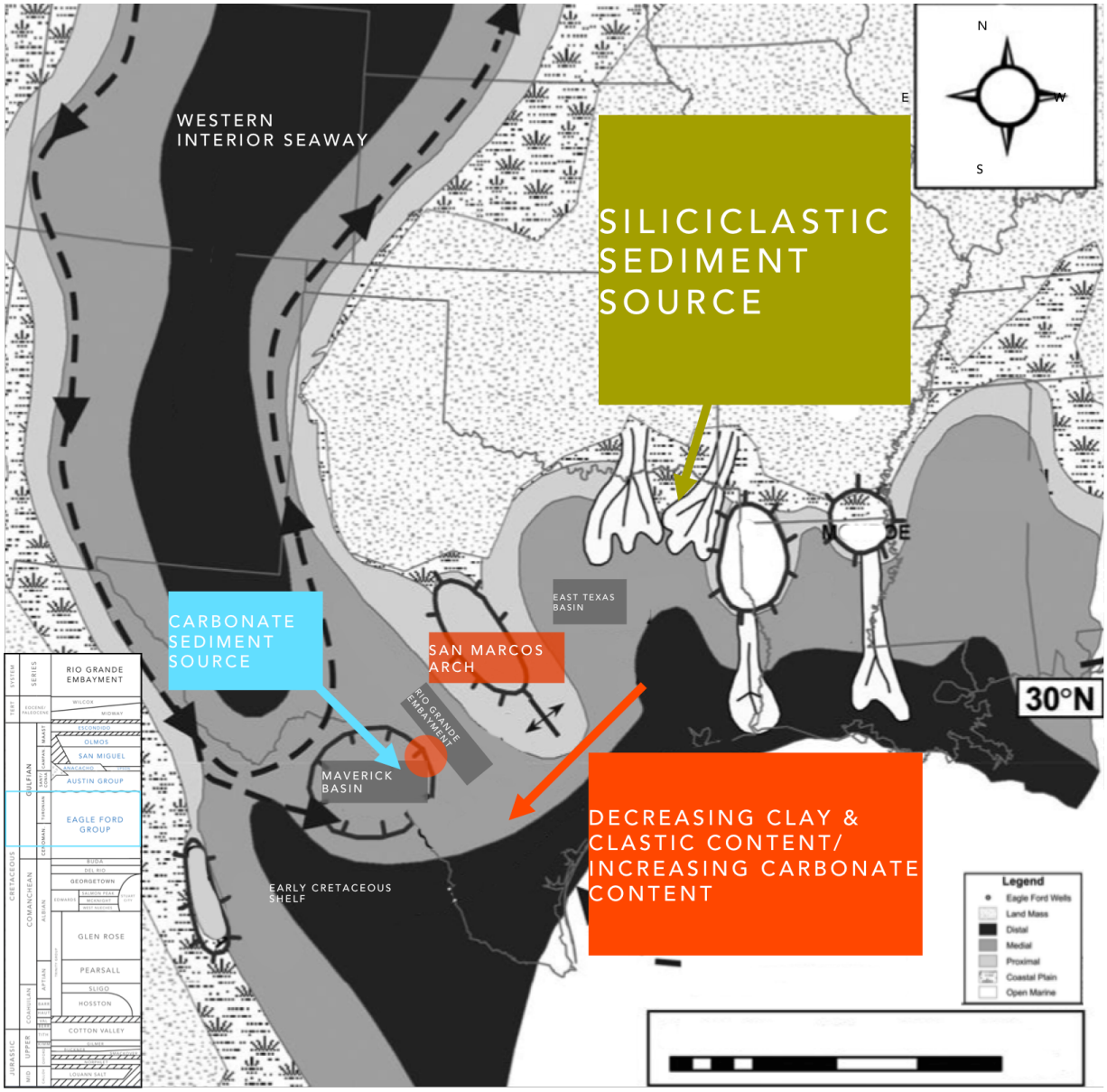

Figure 17 Late Cenomanian paleogeography and structure modified from Jennings and Antia (2013) and Hentz and Ruppel (2011). Eagle Ford sediment supplies are shown for the Maverick Basin and the East Texas Basin.

end of the Santonian (Fig 18). The laterally extensive open marine micrites of the Austin Group were deposited during a time of global eustatic sea level high stand (Tyler and Ambrose, 1986; Galloway, 2008). The northwest gulf margin was dominated by extensive deep carbonate shelves during the Austin depositional episode, evidenced by the presence of coccolith oozes and globigerinids that characterize the chalks, and remained connected to the Western Interior Seaway that supplied carbonate sediment to the shelf and created distinctive intraformational scours and hard grounds. Overall, the Austin Formation records a shoaling cycle bounded by periods of relatively deep water (Galloway, 2008).

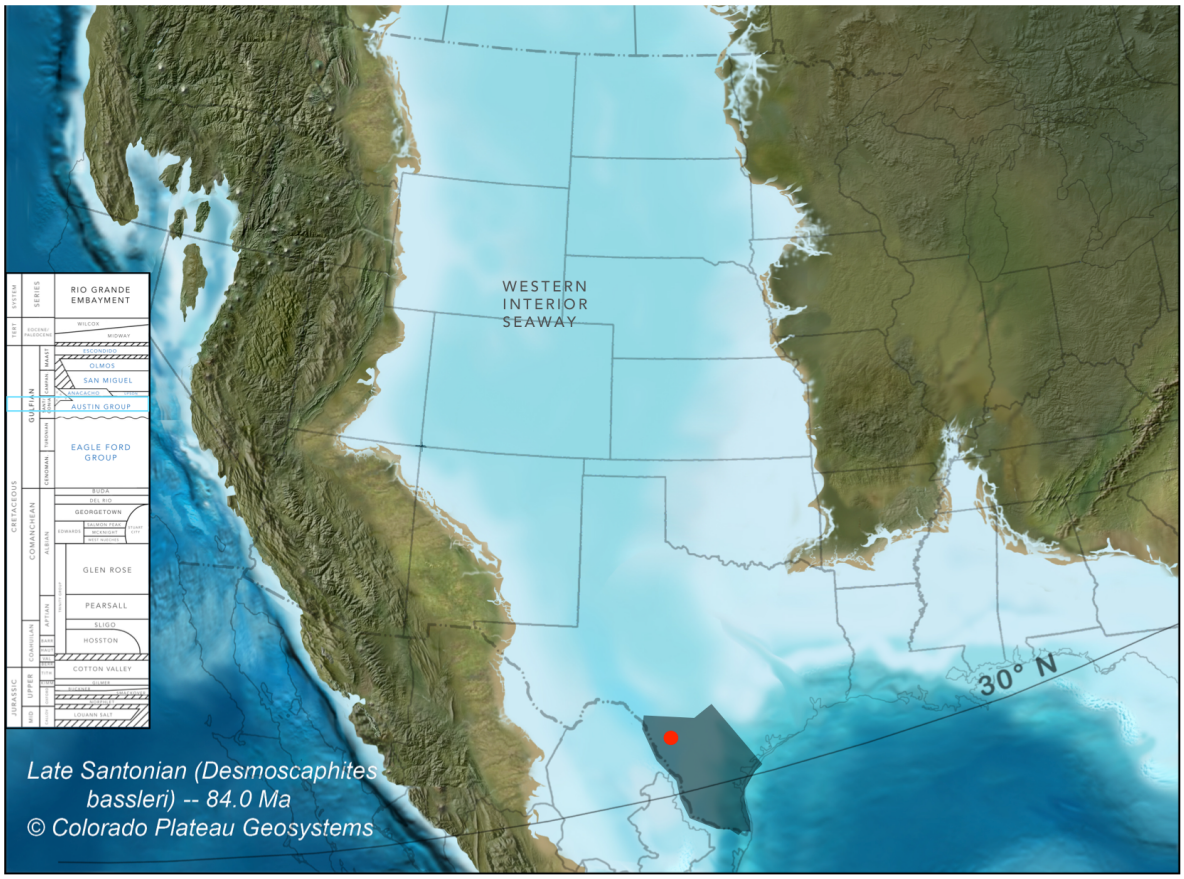

Figure 18 Santonian (84 Ma) paleogeographic map of the North American continent showing drop in sea level from Coniacian. Rio Grande Embayment highlighted with approximate seismic location indicated by red dot. (Blakey, 2011)

At the end of the Austin depositional episode, volcanic activity began to occur on the shelf floor that lasted through the Taylor episode (Fig 19). As the result of a magmatic event during the Santonian, Campanian, and likely the Maastrichtian, volcanic mounds formed on the sea floor, in some cases growing large enough to extrude above the surface. These volcanic mounds occur along a northeast-trending belt that reflects the buried Ouachita thrust belt and are the result of continued extension of the rift zone that parallels the thrust belt in the Balcones fault zone (Fig 9); therefore, this volcanic belt is referred to as the Balcones volcanic province (Matthews, 1986; Salvador, 2991). This distribution of volcanic mounds suggests magma intruded into the marine section by traveling upward from the mantle along basement faults through Precambrian and Paleozoic rocks of the Ouachita complex then further up along fracture zones related to the Balcones fault zone (and possibly the Pearsall Anticline) where it spread out among multiple fractures in Austin and Taylor deposits, eventually reaching the surface (Weise, 1980; Simmons, 1967). The primary magmas of this igneous province were silica-deficient alkalic basalts and rarer basanite and olivene nephelinite magmas that were derived from partial melting of the mantle from 80-150 km deep, indicating that major faulting penetrated the crust to allow magma to ascend (Fischer and Schmincke, 1984). The evidence for deep faulting explains their alignment along major fault systems and the Ouachita thrust belt and supports the postulation that they are directly related to this system (Matthews, 1986).

Once the magma breached the seafloor, interaction with water resulted in immediate conversion to steam, likely causing explosive phreatic eruptions. These may have occurred at or below sea level, since water depth was between 100 and 300 feet during the Austin and Taylor episodes (Matthews, 1986; Martinez, 1982; Caran and Ewing,

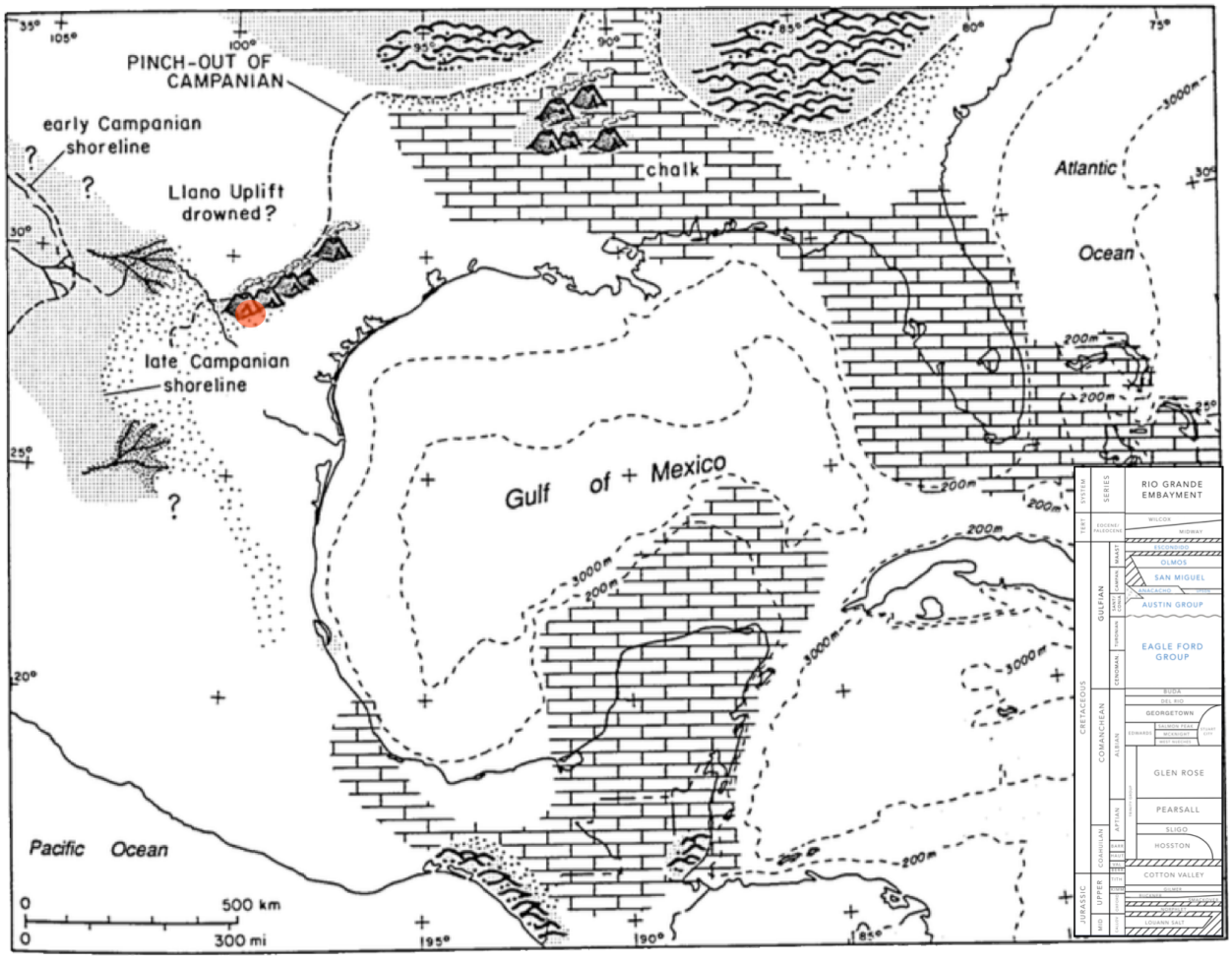

Figure 19 Campanian paleogeography of the GOMB region (Salvador, 1991)

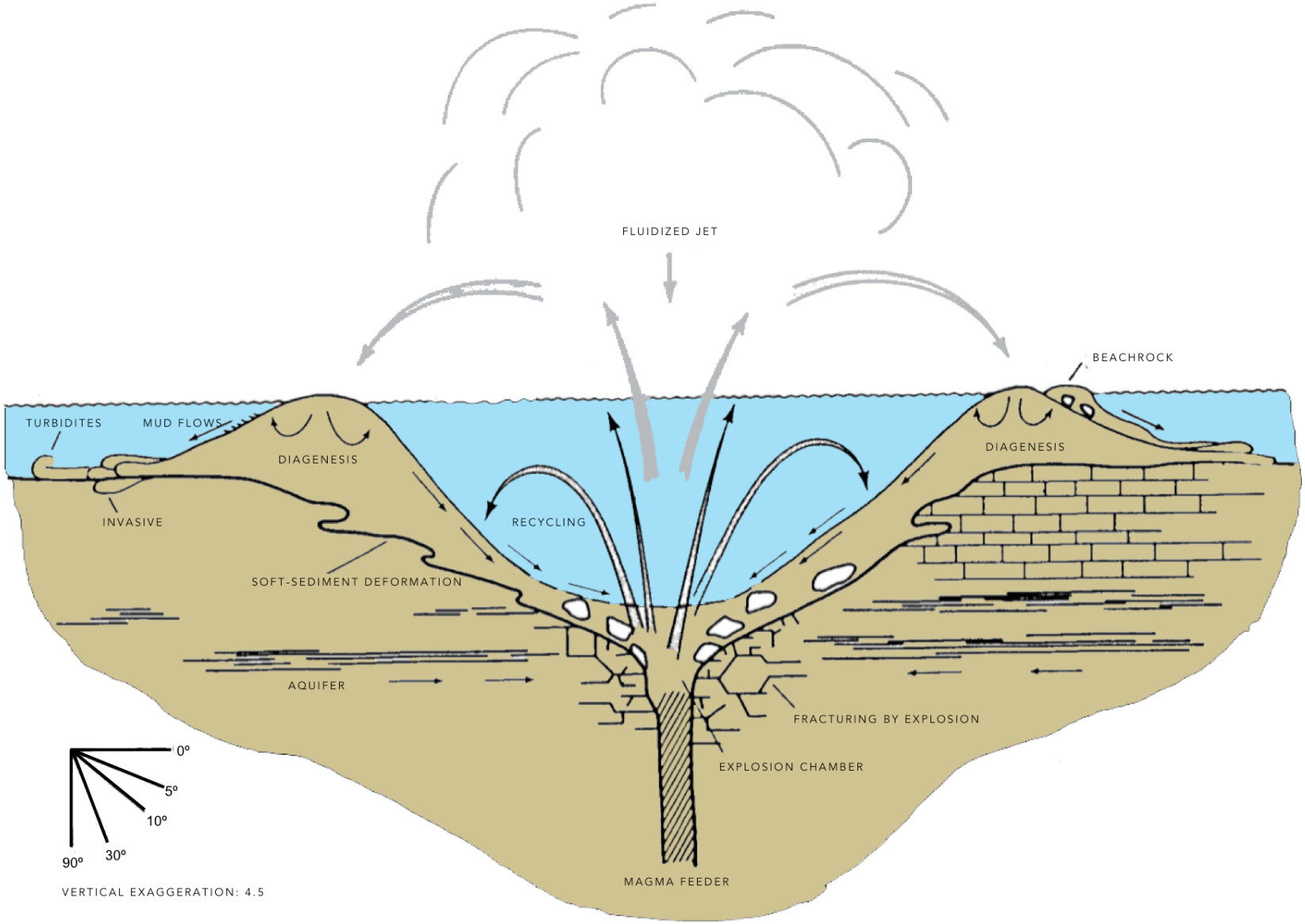

Figure 20 A schematic model of an erupting submarine volcano (Ewing and Caran, 1982)

1982). The explosive eruptions created craters in the underlying sedimentary strata, with a central vent through which ash and lapilli were ejected upwards in a fluidized jet stream and may have also caused intense fracturing of surrounding country rock (Fig 20) (Ewing and Caran, 1982; Young et al., 1982; Matthews, 1986).

The fluidized jet carrying steam and rock particles probably broke the relatively shallow water surface; finer ash carried by wind drifted and settled into thin, finely laminated beds away from the vent (sometimes meters away). Coarser material fell back into the crater and formed an accretionary tuff ring around the vent. Once the volcanic material was deposited, it was immediately subjected to intense seawater diagenesis, altering the volcanic glass to palagonite. Additionally, wave action and gravitational instability caused repeated reworking of volcanic material, significantly altering the igneous rocks from their original state (Ewing and Caran, 1982). Eventually, accumulation of tuff over multiple eruptions and possible regional doming grew the mounds above sea level and lava flows and ash falls replaced the phreatic eruptions and filled the crater to form a gently sloping tuff mound (Ewing and Caran, 1982; Matthews, 1986). The formation of these mounds is similar to the present day South Pacific, where magma is actively being ejected into the sky from under the sea and resultant mounds are located away from the vent (Ogiesoba and Eastwood, 2013) These mounds created topographic highs where shallow-water carbonates built up during the early Taylor episode of the Campanian.

In the Balcones volcanic province, accumulation of the shallow-water carbonates prolonged the period of carbonate-dominated deposition through the early Campanian. The Anacacho Limestone in the Uvalde field and its equivalent Dale Limestone (also referred to as the McKown Formation) in the Travis field are shoal water carbonates that were deposited on top of the volcanic mound margins and the Austin Formation (Tyler and

Ambrose, 1986). Initially, the shoals and reefs preferentially developed on the southwestern sides of the mounds as a result of prevailing winds or ocean currents from the northeast distributing volcanic material (Luttrell, 1977; Roy et al., 1981). They grew as patchy biostromes, deposited in less than 150 feet of water in a high-energy environment that reworked material and transported skeletal debris and carbonate material from northeast to southwest (Hartville, 1959; Tyler and Ambrose, 1986; Wilson, 1986). Eventually, the carbonates coalesced and spread across the shallow marine shelf away from the mounds. Periodic eruptions from the volcanoes on which the reefs grew interrupted carbonate accumulation and buried the carbonate rock with ash, which was altered to bentonitic clay (Condon and Dyman, 2003).

Elsewhere on the shelf, clastic sedimentation had already begun to dominate as a result of renewed tectonism, depositing the Anacacho time-equivalent Upson Clay of the Taylor Group in the Rio Grande Embayment. On the Pacific margin of the North American plate, nearly horizontal subduction of an oceanic plate resulted in the Laramide orogeny, which developed a series of lengthy fold and thrust belts across the western United States and Mexico (Salvador, 1991). Early Laramide folding to the west and northwest created a clastic sedimentary source for the embayment while there was a progressive reduction in marine connection that began in the Campanian, leading to the influx of terrigenous sedimentation and basinward progradation of deltaic and associated coastal plain fluvial systems of the Taylor and Navarro groups of Campanian and Maastrichtian age (Tyler and Ambrose, 1986). The San Miguel of the Taylor episode and the Olmos and Escondido Formations of the Navarro episode are a series of clastic wedges that were deposited on a broad, stable, low-energy shallow shelf (Tyler and Ambrose, 1986; Weise, 1980).

The San Miguel Formation was deposited conformably atop the Anacacho

Limestone as a series of several progradational sequences during a time of relative sea-level rise and transgression. A total of ten minor regressive pulses (recorded as individual sandstone bodies) interrupted the major transgressive event that lasted the entirety of San Miguel deposition, during which progradational sequences would develop from dip-oriented distributary systems that carried north- and northwest-sourced sediments from early Laramide folding into the Rio Grande Embayment in high-destructive, wave-dominated deltas (Tyler et al., 1986; Weise, 1980). Some of those sediments were transported along strike to the southwest by longshore drift (Tyler et al., 1986). After deposition, resumed transgression and intensified wave action reworked the sediments into beach-ridge plains (Weise, 1980; Tyler et al., 1986). Overall sea level would rise after each episode, leading successively younger deltas to form progressively landward and resulting in coastal onlap (Weise, 1980).

During the deposition of the San Miguel, two main depocenters formed, primarily as a result of depositional features rather than structural features, in which two distinct series of sand were deposited from two different source areas. The western depocenter received sediments sourced from the northwest in New Mexico or northern Mexico and developed the bulk of the sandstone units. The smaller eastern depocenter source was to the north. Both depocenters may have received debris from local eroded volcanic mounds, or by continued volcanic activity of the mounds (Weise, 1980).

The San Miguel was the first in a series of overlapping near-shore and fluvial-deltaic facies and is predominantly composed of a spectrum of wave-modified and wave-dominated sandstones, sandy limestones, and siltstones derived from uplifted areas to the west and northwest that grade basinward to increasingly shaly sequences (Matthews, 1986; Tyler and Ambrose, 1986; Salvador, 1991). Deposition was continuous from the

Campanian into the Maastrichtian (Fig 21a) (Salvador, 1991). The Olmos Formation was deposited conformably on top of the San Miguel Formation and reflects the depocenters and the depositional sequences of the San Miguel, with morphology and sandstone facies varying to a greater degree. Tyler and Ambrose (1986) divided the Olmos of the western depocenter into five individual sandstone bodies that display alternating periods of wave dominated deltaic sedimentation along strike followed by high constructive deltaic deposition that prograded seaward to the shelf edge. Each individual sandstone unit was deposited by a wide range of deltaic depositional environments including wave-dominated to high-constructive delta, barrier/strandplain, and coastal plain and fluvial deposits (Tyler and Ambrose, 1986).

Continued deposition increased overburden pressure atop the fine-grained volcanic mounds, causing them to collapse and form radial faults in overlying strata that extend out from the volcanic center and up through the Anacacho Limestone, San Miguel and Olmos Formations. If the volcanoes were younger, these faults can extend up into the Escondido Formation.

Maximum deltaic and shore-zone progradation occurred by the onset of Escondido deposition in the mid-Maastrichtian (Galloway, 2008). Transgression following the termination of Olmos deposition created an erosional surface, atop which the Escondido Formation was deposited in open marine, ebb-tidal delta, shoreface, and marginal marine environments (Condon and Dyman, 2003; Snedden, 1991). Coastal bay and lagoonal mudstones and shoreface and shelf bar sandstones of the Escondido were deposited as a series of progradational, shallowing-upward parasequences in a transgressive systems tract (Cooper, 1971; Snedden, 1991). The termination the Navarro depositional episode is marked by a marine regression (Fig 21b) that caused sea level to drop and deposition of

the Escondido Formation to end. The sea level drop also caused the disconnection of the Western Interior Seaway from the northwest gulf margin, effectively ending the Gulfian depositional series (Salvador, 1991). Intensification of the Laramide Orogeny in the early Eocene deformed the Gulfian rocks in south Texas. Compressional folding deformed the Maverick Basin south of the Frio River line, creating a system of synclines and anticlines.

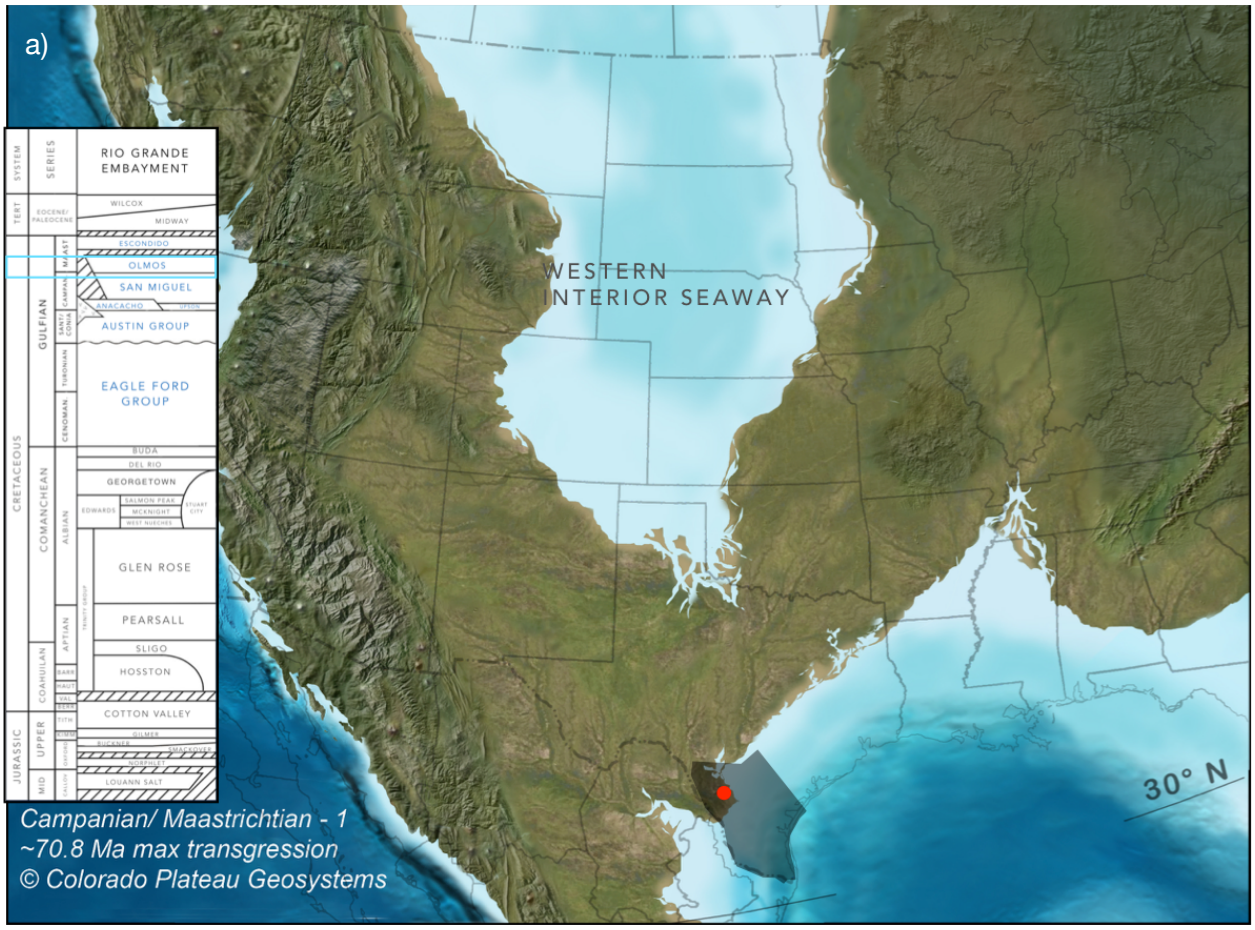

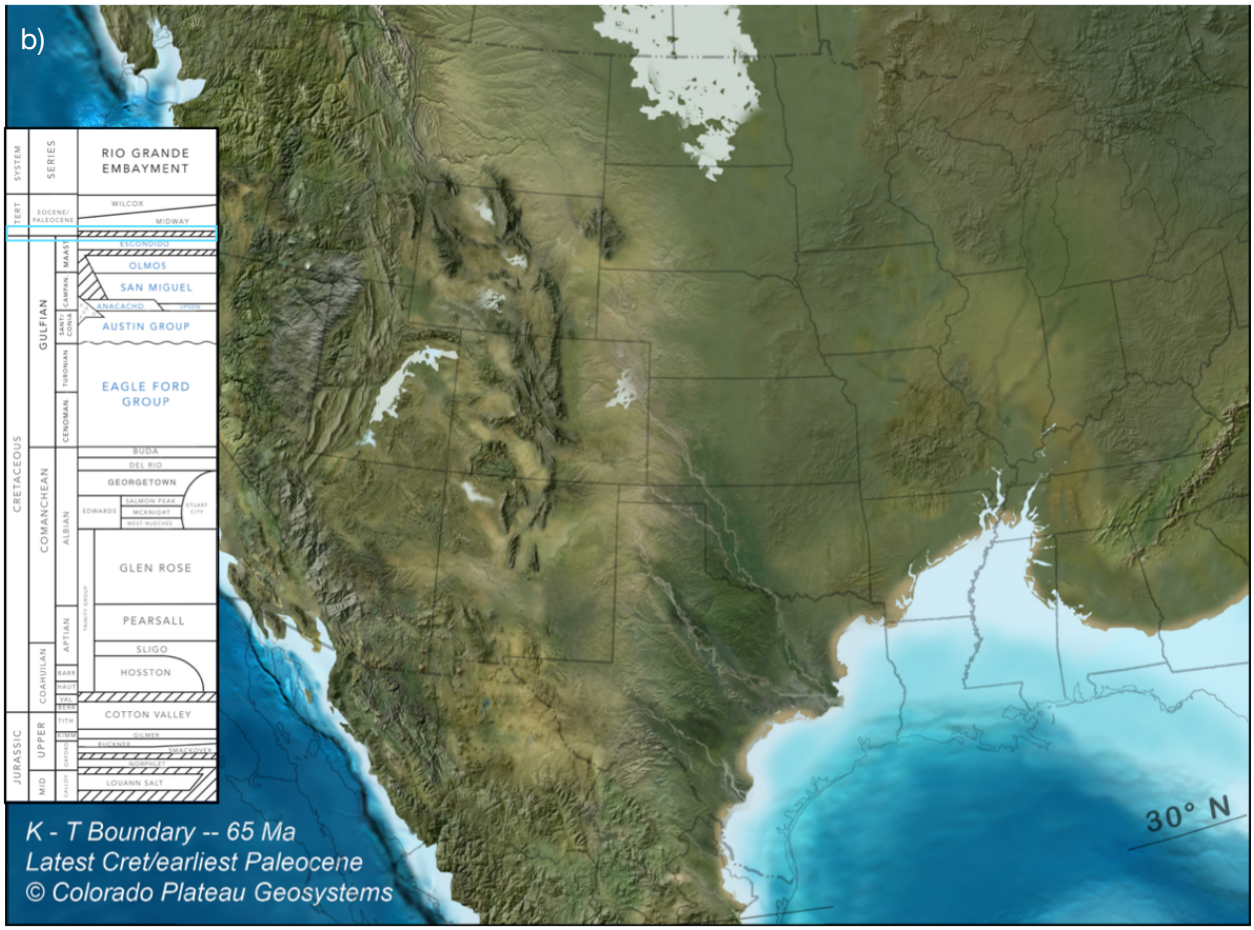

Figure 21 a) Campanian/Maastrichtian paleogeography of the GOMB region b) Cretaceous-Tertiary boundary paleogeography of the GOMB (Blakey, 2011)

IV. Methods and Analysis

A. Survey Overview and Scope

Stephens Production of Fort Smith Arkansas donated the Pedernales survey to the University of Arkansas for scholarly use. The Pedernales was shot in east-central Zavala County, Texas in 2008 and is about 42 square miles, or 27,000 acres (Fig 22). Specific processing info and survey data can be found in Appendix A. For this 3D seismic analysis, OpendTect version 4.6 software was mainly used for seismic interpretation, and IHS Kingdom was used only for synthetic seismogram generation.

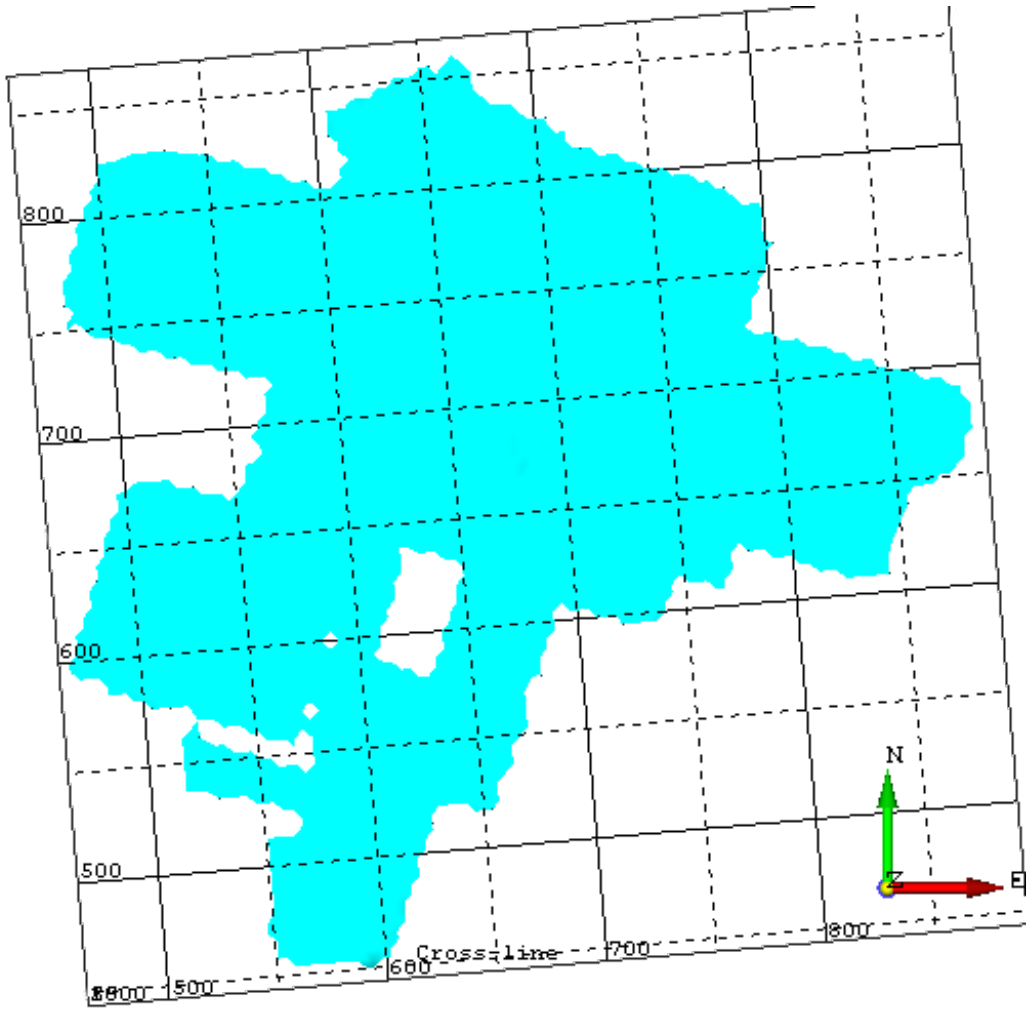

Figure 22 Base map of the Pedernales 3D seismic survey. Crossline values are shown on the x-axis and inline values are shown on the y-axis.

This study analyzes the Eagle Ford Group, Austin Group, volcanic mounds, Anacacho Limestone, and San Miguel Formation of the Gulfian Series in south Texas (Fig 23). These formations were deposited while the Western Interior Seaway was still mostly intact with the GOMB, which provided a carbonate source for these early-Late Cretaceous rocks. Only during the late Campanian did the very early stage of the Laramide orogeny provide a clastic sediment source for the northwest gulf margin, resulting in the deposition of mixed series of sandstones, sandy limestones, and siltstones that graded into marine shales. Therefore, this series of carbonate rocks that is capped by a mixed carbonate and sandstone formation was a logical interval for which to do a 3D seismic analysis.

The workflow for analysis reported in this thesis is shown in Fig 24. The first step is data loading of the SEGY prestack migration data volume into OpendTect (OD). Faults were then identified and picked in OD. To correlate seismic events and well formation tops, a synthetic seismogram was generated on the Holdsworth Nelson well using IHS Kingdom software. Reflection event identification was jump-correlated from Kingdom to OD to identify key seismic events. Once the key seismic events were fully tracked, the method of which is described later in this chapter, the time-depth, amplitude, and similarity attribute maps were created. Using these maps, subresolution structural features were mapped and more details of the volcanic mounds were gathered. The volcanic mounds were tracked last, so the greatest attention could be paid to detail and so that surrounding formation tops that had been previously tracked could be adjusted. Time-depth and similarity attribute maps were subsequently generated.

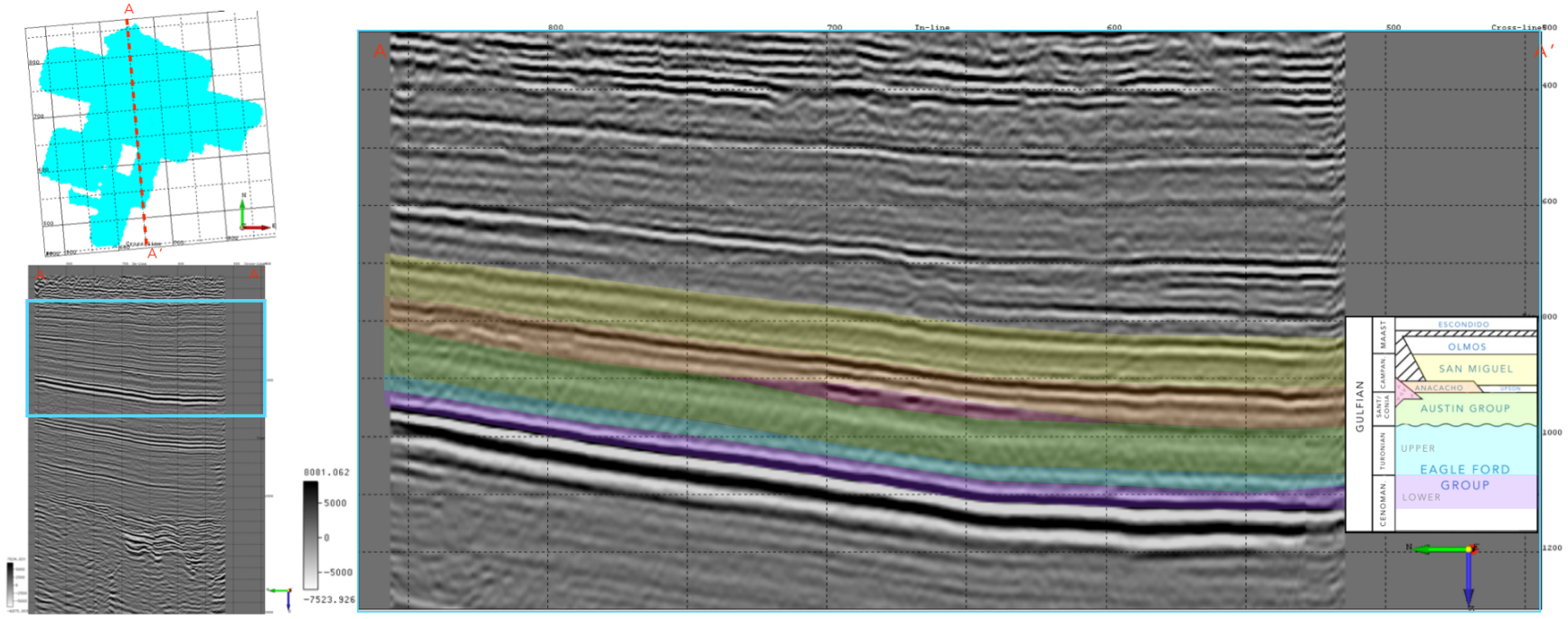

Figure 23 Crossline 650 with the stratigraphic units analyzed highlighted. Both seismic lines are vertically exaggerated 2.75:1

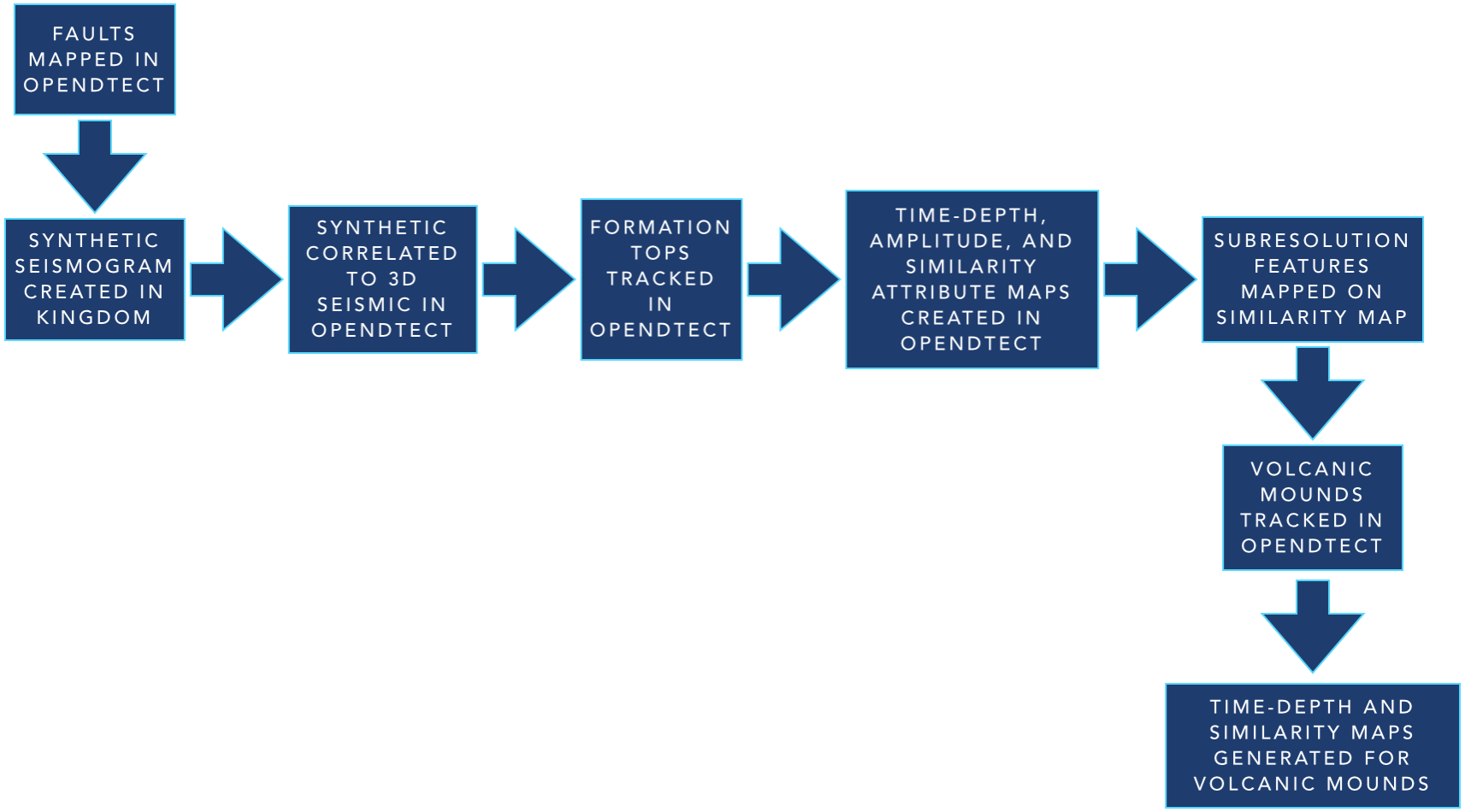

Figure 24 Workflow for Pedernales 3D seismic interpretation

B. Fault Tracking

Faults were tracked in Opendtect before the horizons were mapped, following the traditional order of structural interpretation before stratigraphic interpretation. Many faults exist in the Pedernales survey that have significant displacement but only appear in 10 or 20 lines. Therefore, instead of tracking individual faults one at a time, the faults were tracked using fault-stick set tracking. This tracking method allows the user to track multiple faults on the same inline under one set. The individual sticks can then be reassigned to individual faults. Two fault-stick sets were established, one for those tracked on crosslines and one for those tracked on inlines. Fault-sticks were tracked every fifth line for both sets on seismic lines, showing amplitude with a similarity attribute overlay at 50% transparency. Once the survey was covered, these fault sticks could be viewed in time-slice to observe the extent and trend of the faults picked. Once a general idea was gathered for the nature of the faults in the area, the inlines and crosslines were retraced to reassign sticks to individual faults. The faults mapped, totaling 41 individual faults, are shown in Fig 25a. They are normal faults; most trend north-south and many are part of small horsts or grabens, like Faults 1 and 2 (Fig 25 a and b). These faults also tend to curve, which could be attributed to the extensional tectonics that formed the faults near volcanic mounds. Fault 3 (Fig 25 a and c) is one of the only faults that trends east-west, and it eventually curves northward before intersecting another fault. The groups of faults that directly overlie volcanic mounds (Fig 25 a) are radial faults that extend out from the center of the mound and will be discussed later.

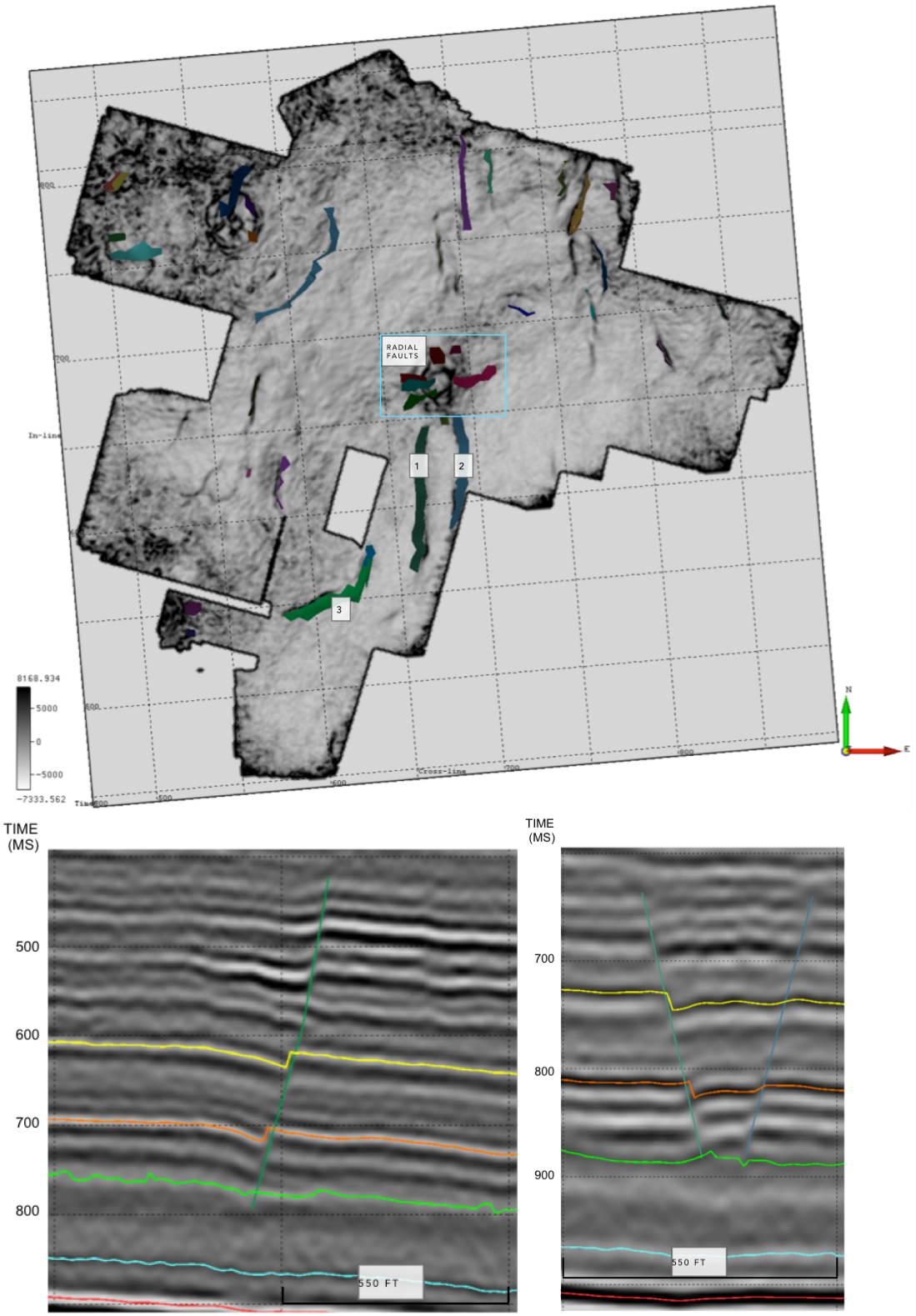

Figure 25 a) Z-slice 860 with similarity attribute showing the faults tracked in the survey b) close up of seismic crossline transecting fault 3 c) close up of seismic inline transecting faults 1 and 2. Seismic lines vertically exaggerated 2.75:1

C. Synthetic Seismogram

The synthetic seismogram used to map the formation tops in the Pedernales survey was generated using IHS Kingdom. Stephens provided two wells with sonic logs and formation tops, the Whitecotton and Holdsworth Nelson, although density logs were not present. Of those two, the Holdsworth Nelson had the best synthetic to seismic fit so it was used to pick formation top horizons in the Pedernales survey (Fig 26). While working with S. Milligan, the synthetic seismogram generated matched the frequency data of the Pedernales survey with an Ormsby wavelet of 65 Hz and was rotated 22° based on observed matches with tops. Analyzed with the tops provided by Stephens, the trace and the synthetic were a good fit. For formation abbreviations used in this chapter, please reference the key given in the caption of Fig 26.

The sonic log was also used to generate average velocities for the formations, using the equation:

$$v_{avg} = \frac{1000000}{avg\ sonic}$$

The average velocities of individual formations were used to calculate the vertical resolution and lateral resolution of the formations.

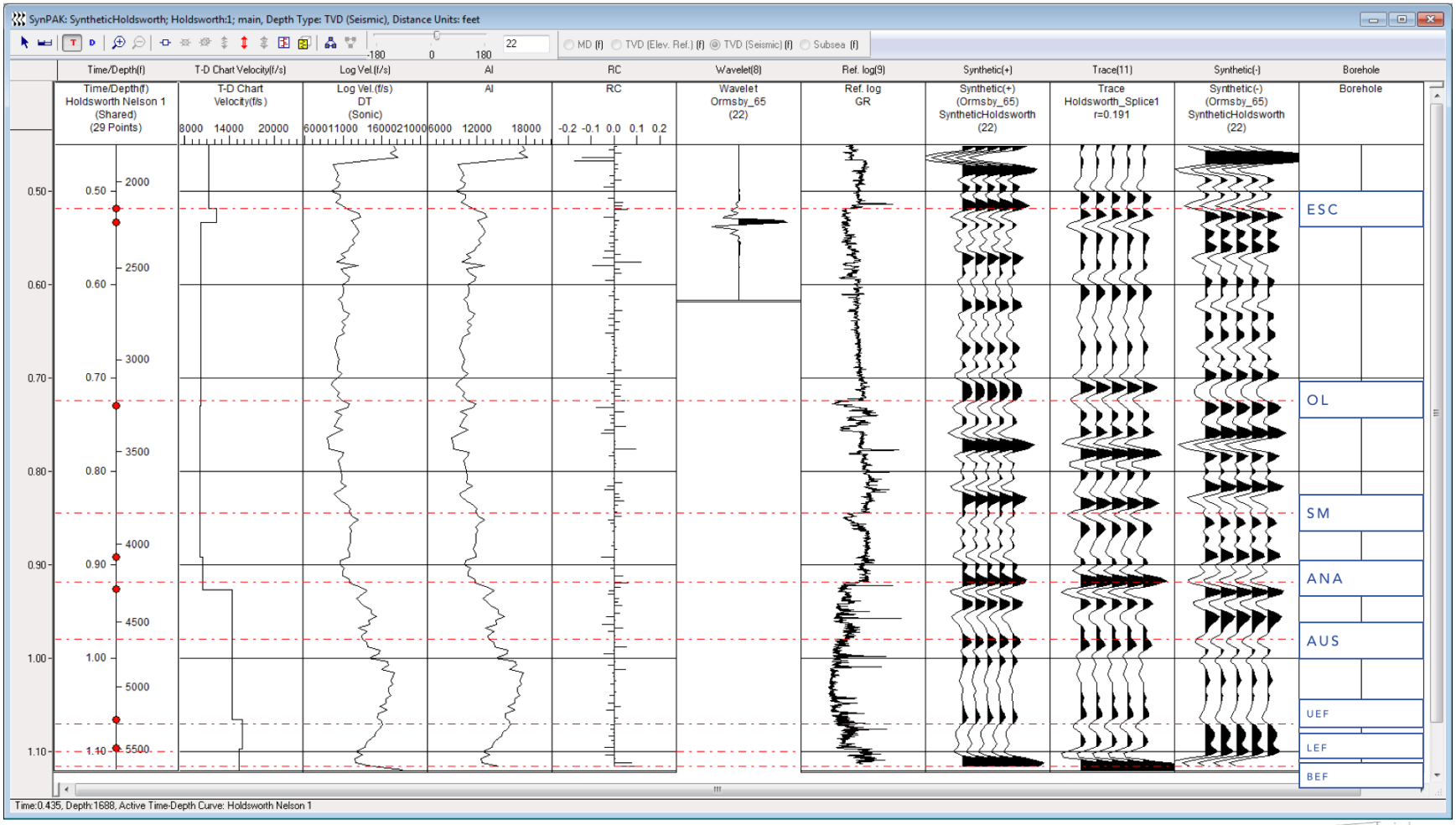

Figure 26 Synthetic seismogram generated on IHS Kingdom for the Holdsworth Nelson well. BEF=Base of Eagle Ford, LEF= Top Lower Eagle Ford, UEF= Top Upper Eagle Ford, AUS= Top Austin, ANA=Top Anacacho, SM=Top San Miguel, OL=Top Olmos, ESC=Top Escondido. Base map shows well location in the seismic survey area. This well intersected a normal fault with significant bed displacement so resulting sonic log values are only slightly deviated due to influence of younger offset beds directly adjacent to the well.

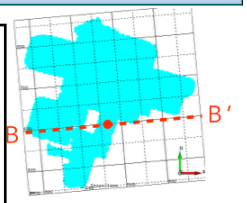

D. Horizons

Volcanic Mounds

Scanning through the seismic data before in-depth analysis, the most obvious structural features in the Pedernales survey are approximately circular volcanic mounds, with steepening dip toward the center (Fig 27A). These mounds are part of the large Uvalde volcanic field previously described in Chapter 2. Areas near these mounds appear to be more faulted than others, especially in rocks directly overlying the mounds. When observed in a time slice, the faults appear to be radiating out from the central, highest point of the mound (Fig 27B). These are the result of collapse due to overburden and can be difficult, if possible at all, to track due to the chaotic displacement and their laterally short and discontinuous nature. The original mound shape is obscured by the radial faults, but an overall flatness of some mounds and sharpness of others can be seen. Below the larger mounds, there appears to be a significant dip in underlying sediments which are not an actual structural feature, but the result of a pull-down effect due to the lower velocity of the palagonite tuff in the mound transitioning laterally and vertically to much higher velocity carbonates (Fig 27A).

Aside from the structure of these mounds that makes them so distinct, the amplitudes associated with the mounds is striking as well. Amplitude anomalies outline the structures in overlying and underlying horizons (which will be discussed in the later section). Chaotic arrangements of amplitudes and horizons inside the mounds are not continuous or trackable (Fig 27A), again likely related to velocity contrast between the mounds and encasing carbonate rock. Observed in the Pedernales were three complete large volcanic mounds, two possible smaller volcanic mounds, and several partial volcanic mounds that were cut off along the edges of the survey. Only the completely imaged

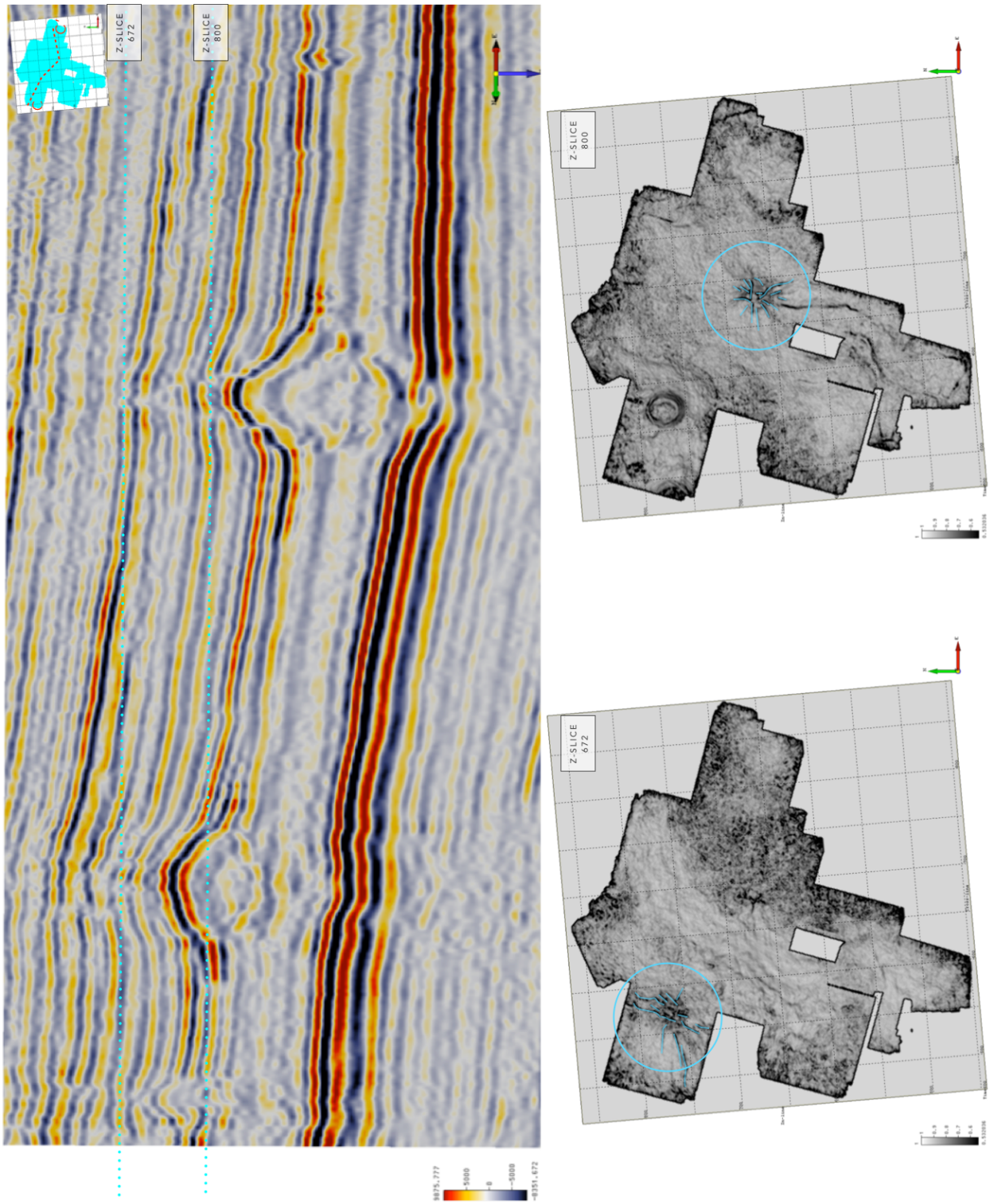

Figure 27 a) Uninterpreted 3D seismic line of the volcanic mounds across a Arbitrary line C-C. Seismic line vertically exaggerated 2.75:1 b) Z-slices 800 and 672 with similarity attribute above volcanic mounds that show radial faults overlying the tops of the volcanic mounds

mounds were analyzed for this study, although the structure and resulting stratigraphy of the partial volcanoes affected the picking of faults and horizons.

To better track the mounds, the seismic was vertically exaggerated to a 2.75:1 scale. This better displayed the nuances of the mound structures and the relationships of the observed horizons. The tops and bottoms of the volcanic mounds were tracked as negative and positive horizons, respectively, using the line tracker on every inline between the perceived extent of the horizons for better control and outcome. The tracking parameters are shown in Fig 28. Along the edges of the mound, the bed thickness is below the vertical resolution limit, which for the Austin group is ~100 ft, and top-base events merge into a single event (Liner, 2004). Where the mounds reach subresolution thickness, the tracking was stopped, although they could possibly extend further. Where the mounds reach subresolution thickness, the tracking was stopped, although they could possibly extend further. Using these tracking methods, the top and base events of two large volcanoes, VM1 and VM2 were mapped that can be seen in (Fig VM).

In order to interpret the volcanic mounds, the formation of these mounds should be considered. These mounds initially formed as craters, around which a tuff ring built up and ash was deposited some distance laterally (Fig 20). With continued eruption, the tuff rings built up, eventually rising above sea level. Once the vent was no longer underwater, the craters were filled in with lava flows, taking on a mound shape instead of a crater shape. Eruptive events slowed while reefs would build on the sides of the mounds and in between the mounds. Sporadic eruptions would interrupt the carbonate factory and bury the reefs with lava flows and ash. When observing these mounds in a vertical seismic line all the stages can be identified, despite faulting that obscures much of the original structure of the mounds. Ignoring the effect of velocity pull down that makes the mounds appear to have a

a)

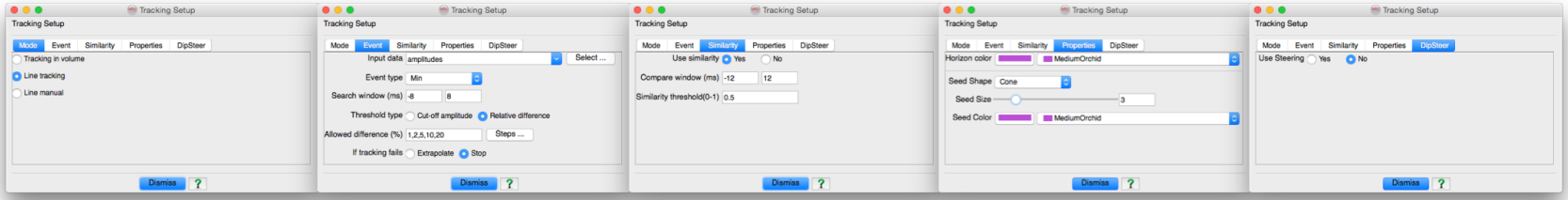

b)

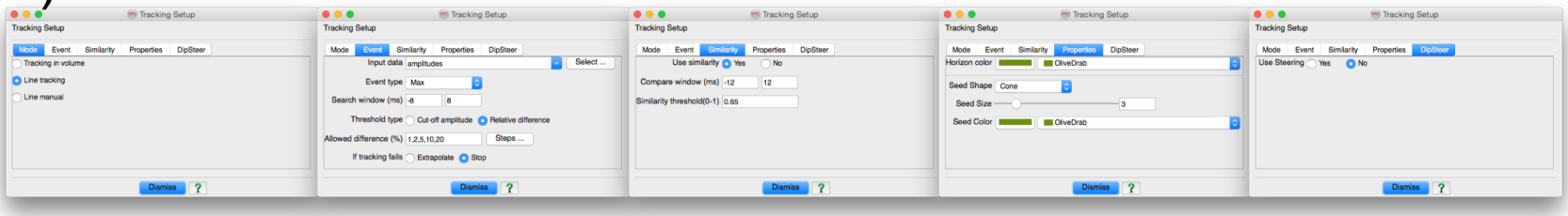

Figure 28 Tracking parameters for the top (a) and base (b) of VM1. The same parameters were applied to VM2.

a)

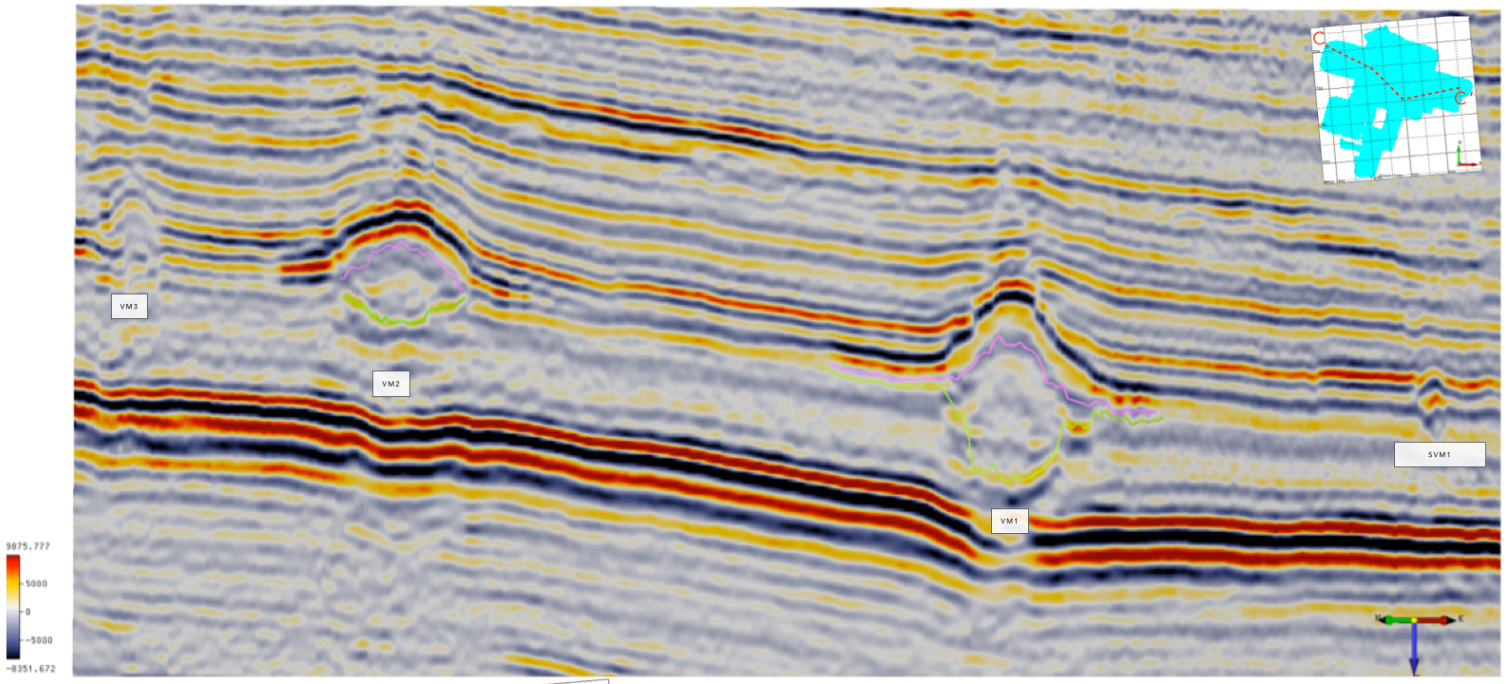

b)

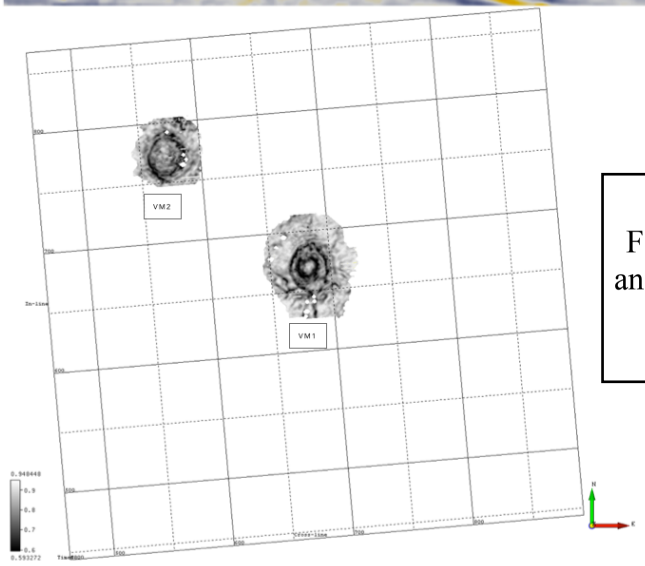

Figure 29 a) Arbitrary Line C-C' with tops and bases of VM1 and VM2 tracked. Seismic line vertically exaggerated 2.75:1 b) similarity attribute map for the tops of VM1 and VM2.

severe dip below them, an original shape of the periphery of the crater can be distinguished in VM1 and VM2 in Fig 29a. The pull-down below VM2 is not as significant as that of VM1, likely due to its smaller size, so the structure can best be observed on VM2. The base of the palagonite tuff rock is the positive/peak horizon shown in Fig 29a, the result of the transition from the low-density palagonite tuff into the denser underlying carbonates (relative velocities can only be assumed, since there was no well log penetrating the mound). The dome-shaped negative horizon that overlies the crater form is the lava flow that filled in the center of the crater, forming the top of the palagonite tuff. However, the amplitudes are not bright or smooth, which is not what is expected from the transition to a material with such a large change in velocity.

There are structural differences between mounds VM1 and VM2. Mound VM2 does not appear to be as deeply rooted as VM1, and its top appears flatter than VM1 (Fig 29 a and b). VM1 has steeper dipping sides, with a maximum dip angle of ~14°, than VM2, whose sides dip a maximum of ~11°. Both mounds are approximately elliptical in map view with long axis roughly north-south (Fig 29b). Mound VM1 appears to have to concentric bands of collapse faults, one of which extends to the south.

Reflection events above the volcanic mounds show amplitude brightening, likely due to lateral impedance changes and dip effects. This may represent bioherm deposits that are part of the Anacacho Limestone Formation, but no firm conclusions are possible at this seismic resolution. Mound VM2 shows evidence of attic faulting progressing upward for a considerable distance, approximately 1000 ft, likely due to compaction of volcanic material by overlying strata.

Formation Tops and Packages

Before formation tops could be mapped in OpendTect, the synthetic seismogram

from Kingdom was matched to inline 600 (Fig 30) and formation tops were identified on the seismic line. Horizons were picked every fifth crossline, (picking parameters shown in Fig 31). Crosslines were chosen to pick initial tracking seeds to align with regional southeast dip. Inlines run southwest to northeast, parallel to strike, and the crosslines run northwest to southeast, parallel to dip. After crossline tracking was completed, the every fifth inline was tracked. After inlines and crosslines were thoroughly examined and tracked, volume autotracking was used to infill between the tracked lines. The volume tracking function in OpendTect allows the user to track horizons across surveys using only a few seeds, but when attempted on horizons in the Pedernales survey, the result was noisy and often jumped to incorrect events, so horizons were tracked on the grid described.

For each horizon, three maps were generated: Time structure, amplitude, and a similarity attribute. The time structure map for each horizon has color bar shown in time (seconds) and depth (ft, measured depth) approximated by the time depth curve calculated from the Holdsworth Nelson sonic log (Fig 32). Amplitude maps were extracted from prestack time migrated (PSTM) amplitude data processed (Appendix B). The similarity attribute, also known as coherence (Bahorich and Farmer, 1995), was created from PSTM amplitude data using a -12 to 12 ms time gate to create a detailed structural map. This time gate was selected based on parameter testing done prior to mapping. Selected isochron maps were generated between horizons as a proxy for thickness of the associated rock interval. Approximate thicknesses were calculated using the equation:

$$\Delta x = \frac{v * \Delta t}{2}$$

where v is the average velocity of the formation calculated from the Holdsworth Nelson sonic log.

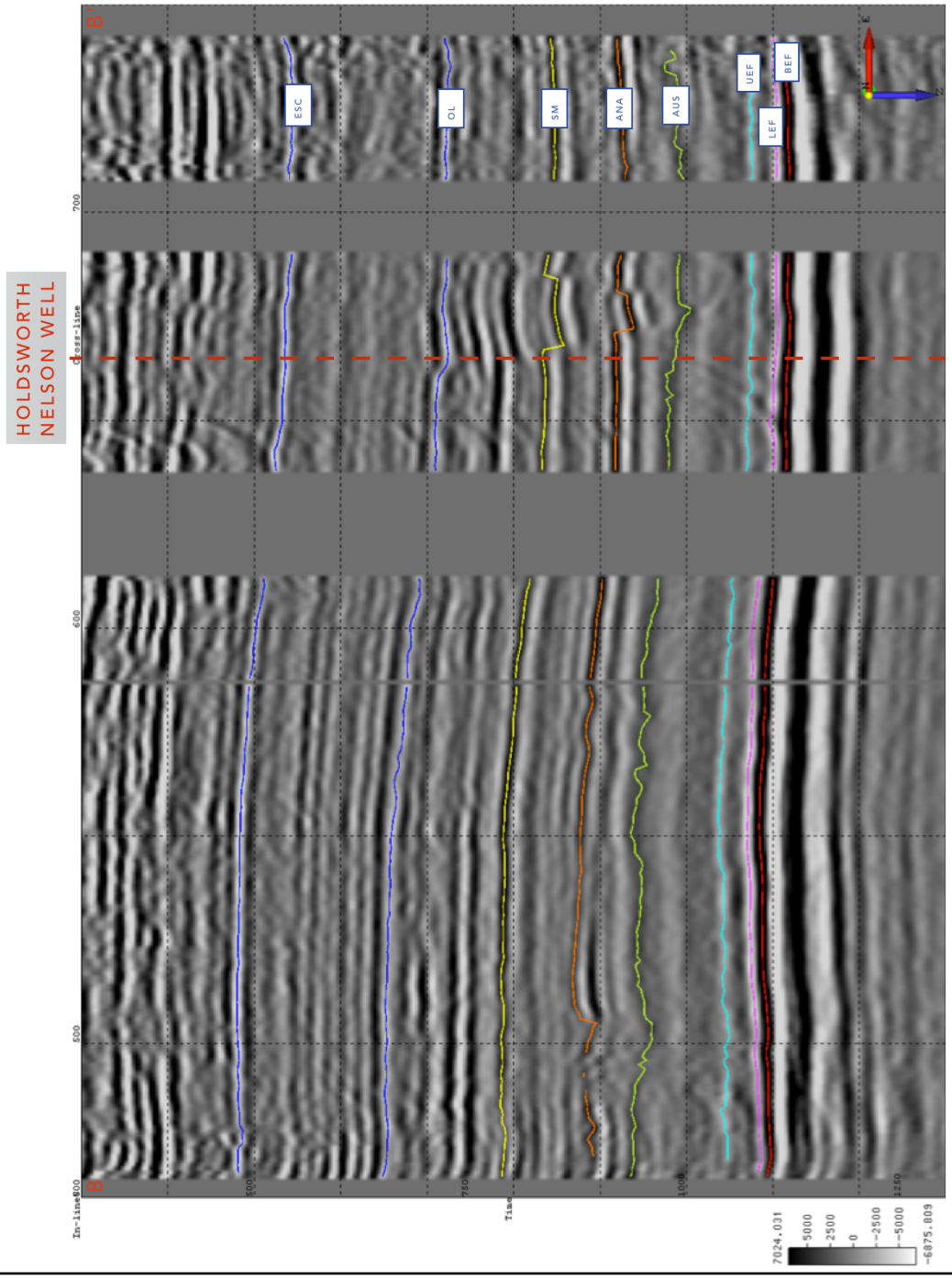

Figure 30 Seismic Inline 600 with major Gulfian Horizons tracked based on synthetic seismogram from the Holdsworth Nelson well. Seismic line vertically exaggerated 2.75:1

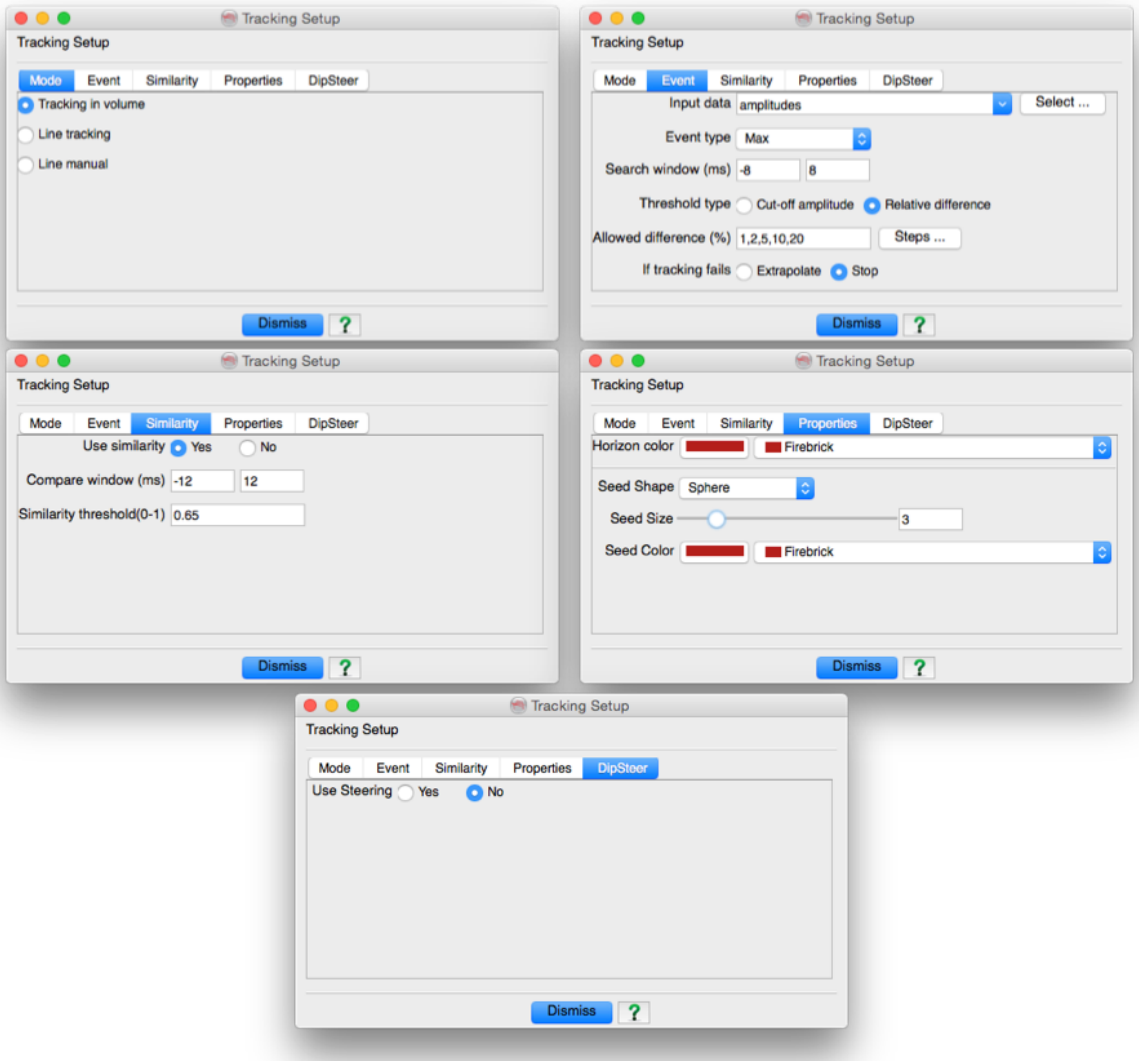

Figure 31 Tracking parameters for horizon tracking of the BEF. The input data is the poststack time-migrated amplitude values provided by Stephens and event type varied based on the top being picked. Similarity was also used for better accuracy and for the complicated arrangements of horizons surrounding the volcanic mounds. Dip steering was not used. For explanation, see OpendTect User Documentation version 4.6 Chapter 3.3 Fig 32

Base of Eagle Ford

The base of the Eagle Ford Group was tracked as a waveform peak (Fig 26) at depths ranging from approximately 5,250 ft to 6,635 ft (Fig 32a). The positive amplitude of this horizon represents the transition from organic-rich, porous mudstones of the LEF to the underlying tight carbonates of the Buda Formation. High porosity and total organic content (TOC) make the LEF less dense compared to the low-porosity massive micritic wackestone that underlies it (Treadgold et al, 2011), causing the strong positive reflection as P-wave velocity increases from an average of 13,294 ft/s in the LEF to the Buda ranging between 17,646 ft/s and 19,964 ft/s. This strong reflection is evident in the high amplitude values seen in the BEF horizon (+6000 to +23000 amplitude units) (Fig 32b). The relatively widespread nature of the high amplitude BEF shown in Fig 32b supports the conclusion that the values are the result of a lithology change, as opposed to the presence of hydrocarbons. Low amplitude is observed directly below volcanic mounds and along fault trends (likely due to weakened, low-impedance rock in the fault vicinity). Perhaps due to seismic wave scattering by the conical mounds, amplitudes show a dimout directly below the structure at BEF level and below. Additionally, the northwest corner of the survey appears to be generally low amplitude on the BEF, perhaps indicating a lithological variation in either the LEF or the Buda in this particular area.

The amplitude map of the BEF also sheds light on the structure of the horizon that is emphasized by a similarity attribute map (Fig 32c). The time structure map (Fig 32a) shows a relatively smooth structure dipping to the southeast (with local pulldown from the overlying volcanic mounds) and no faults were detected in vertical seismic lines. Low amplitude areas on the amplitude map are revealed as faults on the similarity attribute map, including some that visibly offset overlying formations but not the BEF, LEF, or UEF.

Using these maps, subresolution faults were picked that penetrate not only the AUS, but to the top of the Buda, if not further.

a)

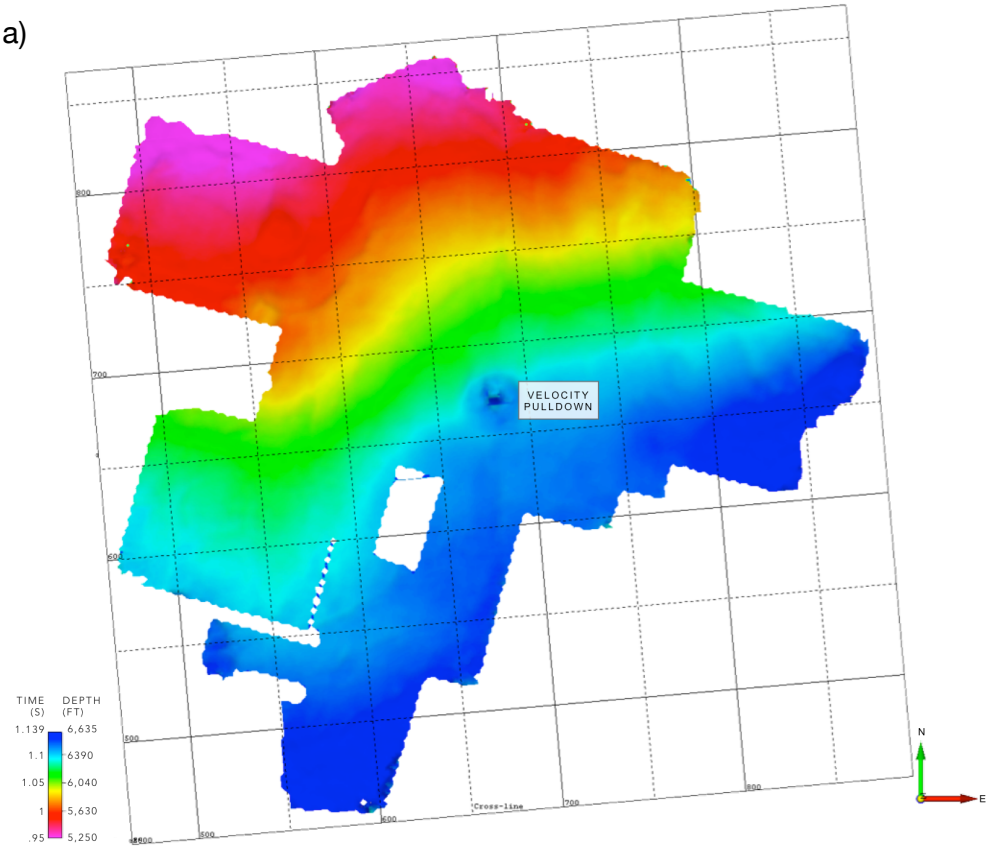

b)

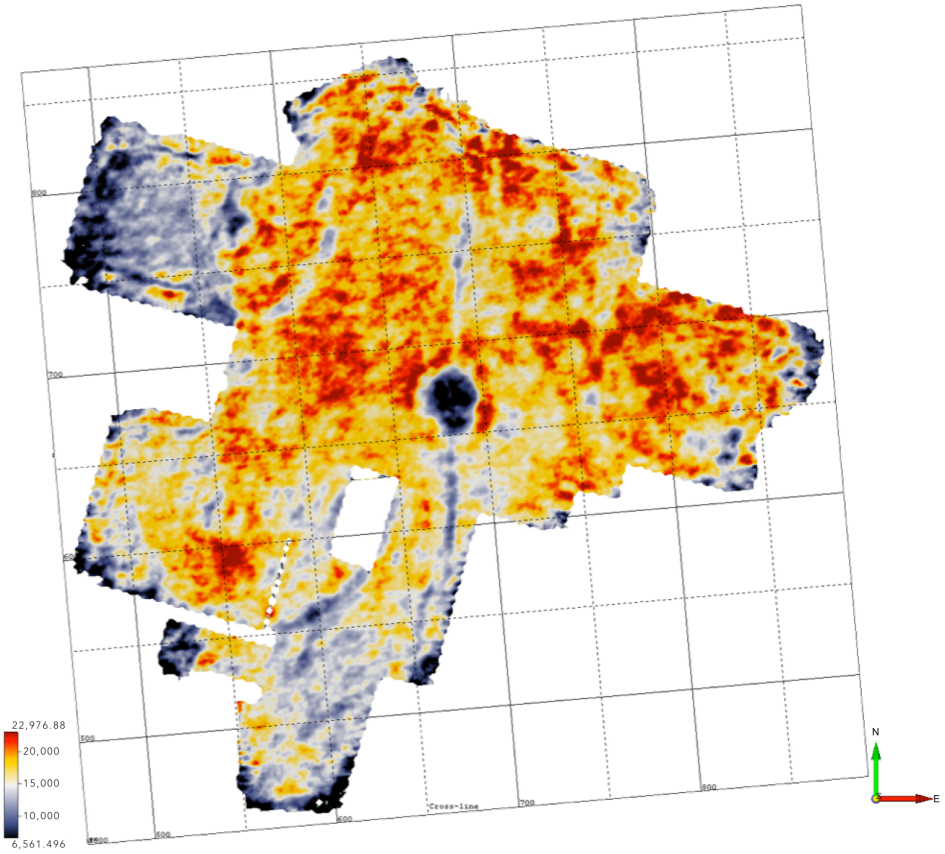
22,976.88
20,000
15,000
10,000
6,561.496
Cross-line
N
E

c)

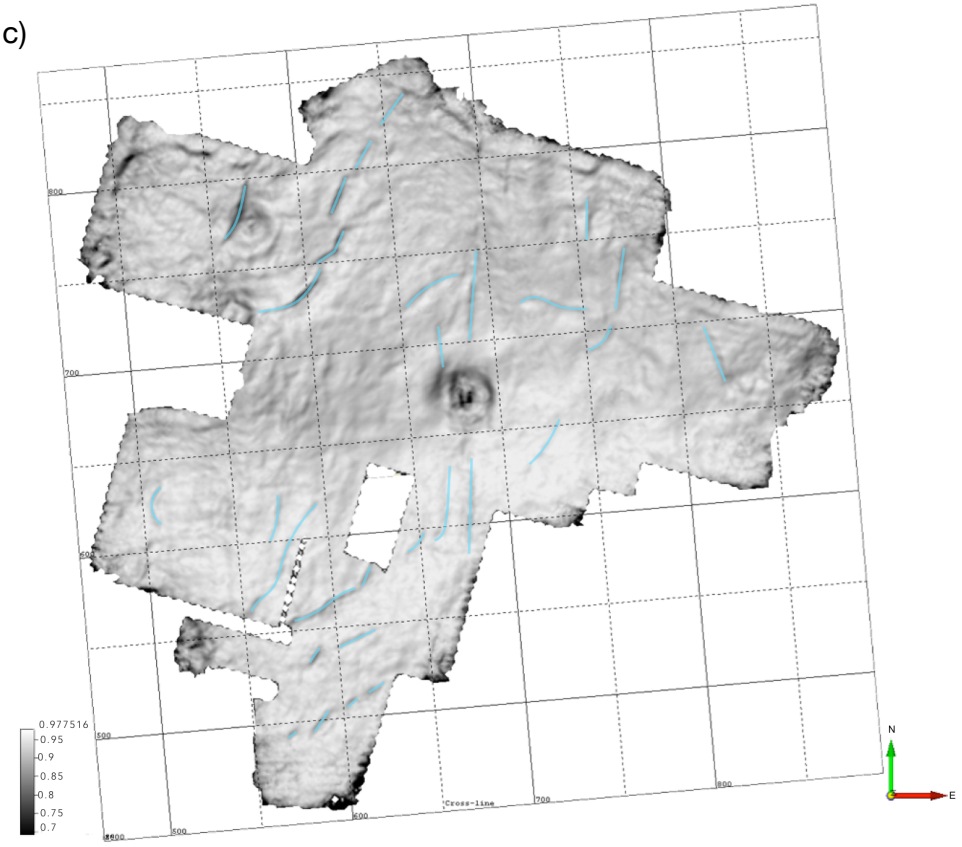
0.977516
0.95
0.9
0.85
0.8
0.75
0.7
Cross-line
N
E

Figure 32 a) Time-structure map of the BEF horizon b) amplitude map for the BEF horizon c) similarity attribute map for the BEF horizon. Faults are indicated by blue lines.

Top of Lower Eagle Ford

The top of the LEF was tracked as a waveform trough (Fig 26), at depths ranging between approximately 5180 and 6558 ft (Fig 33a). This negative reflection event is associated with the contact between more carbonate-rich, organic-poor, tighter porosity UEF mudstone with LEF that has an average velocity of 13294 ft/s. Vertical and lateral resolutions for the LEF are 73 ft and 146 ft, respectively. This change can be seen in the sonic log on the synthetic seismogram- the velocity values in the sonic log begin to decrease significantly as it moves into the LEF and slows until it reaches the top of the Buda. Amplitude values for the LEF event range from -2100 to -11220, with the areas of highest amplitude concentrated between overlying volcanic mounds (Fig 33B). Lowest LEF amplitudes appear to be concentrated along faults and inside rings that surround the volcanic mounds, perhaps due to local development of high velocity material within the mounds. As previously mentioned, the palagonite tuff mounds are much less dense than surrounding carbonates, but without density logs it is not possible to quantify the effect this has on horizon amplitude.

The LEF isochron (Fig 33D) ranges from 68-100 ft so that the structure of the LEF, like that of the BEF, is relatively flat and dipping to the east. Although no fault displacement in the LEF/BEF interval was recognized in vertical seismic lines, subresolution faults were detected and tracked using the similarity attribute map (Fig 33C). The major difference between the top and the base events of the Eagle Ford formation is the area beneath VM1 in which LEF could not be mapped. This is the area where the palagonite tuff of the volcanic mound intrudes down into the LEF section. This characteristic of the top of the LEF provides clues as to the nature and timing of the initial volcanic eruption. As mentioned above, the initially explosive eruptions caused by the

exposure of magma to seawater were violent enough to excavate the country rock surrounding the vent to form a crater and fracture nearby country rock. In the particular instance of VM1, the explosion excavated at least as far as the top of the LEF. Given that the top of the initial structure of VM1 roughly coincides with the top of the Austin, the Santonian explosion excavated rocks that were Coniacian and Turonian in age. The excavations of rocks this far down could also indicate the depth of the phreatic zone in this area at the time of eruption. For these volcanic eruptions to occur, the magma did not necessarily have to reach the seafloor, it only had to reach water. If magma reached the phreatic zone, it would have erupted by steam explosion just as if it reached the seafloor- vaporization of water into a fluidized jet that exploded out. This would excavate a crater more deeply because it would have been initiated deeper. Given this evidence, we can speculate that in the Santonian, the phreatic zone below VM1 was somewhere around 470 feet below the seafloor.

a)

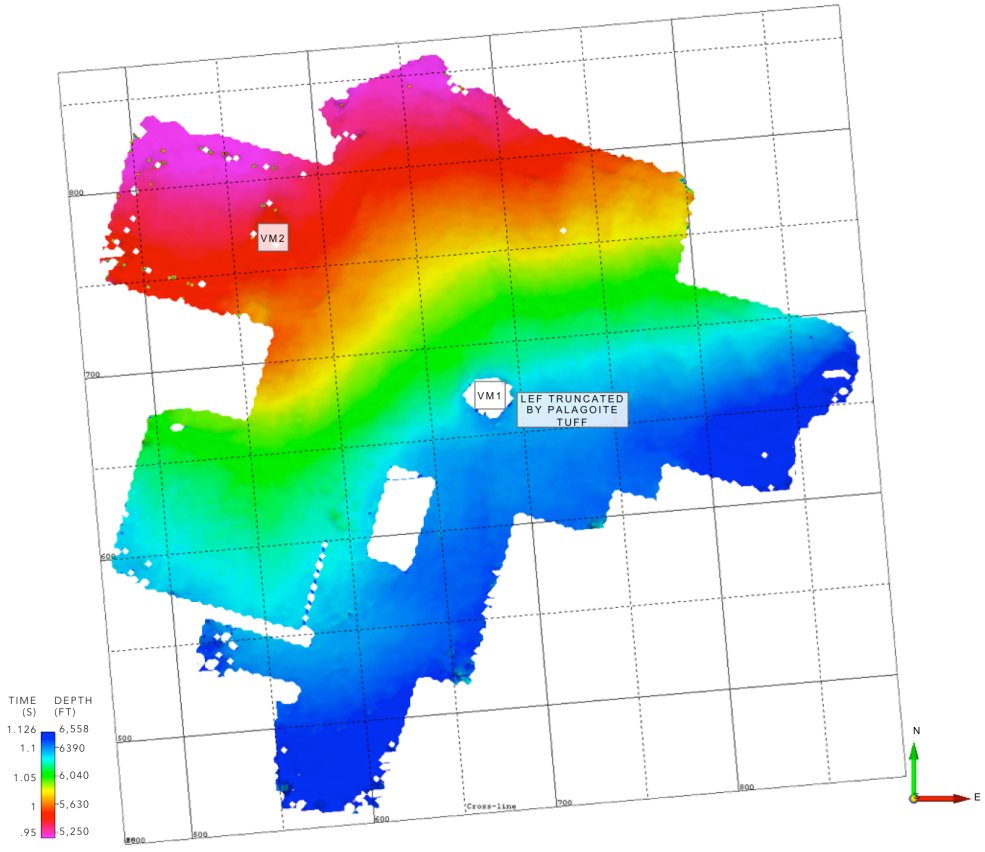

b)

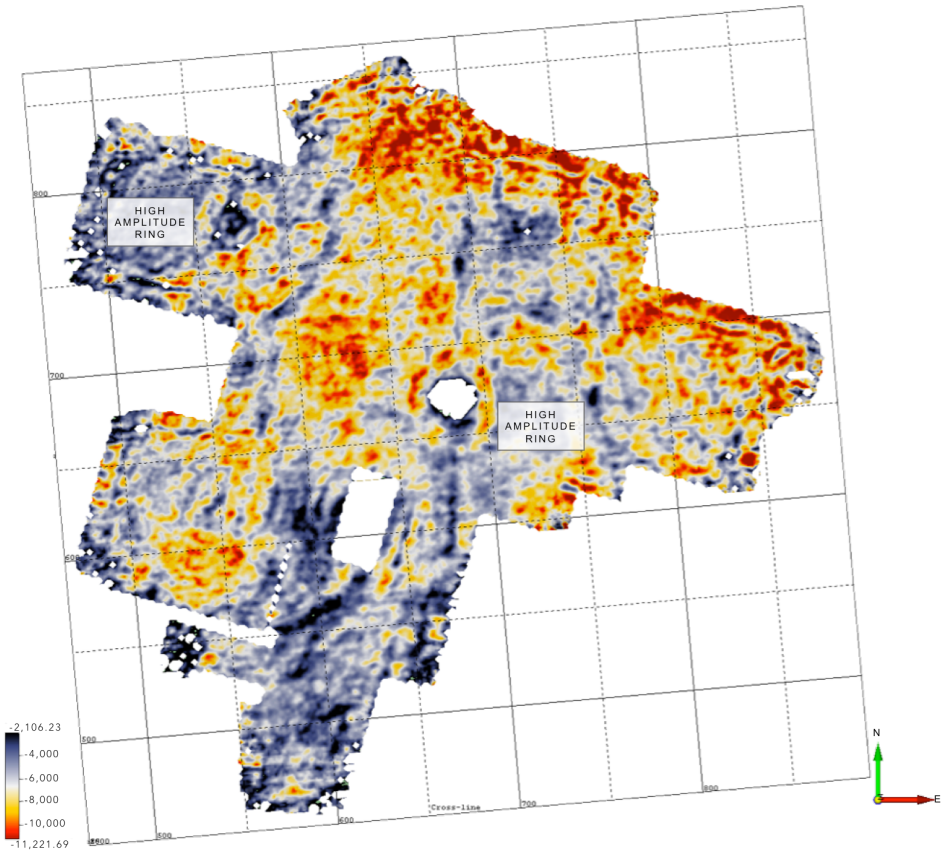
HIGH AMPLITUDE RING
HIGH AMPLITUDE RING
-2,106.23
-4,000
-6,000
-8,000
-10,000
-11,221.69
Cross-line
N
E

c)

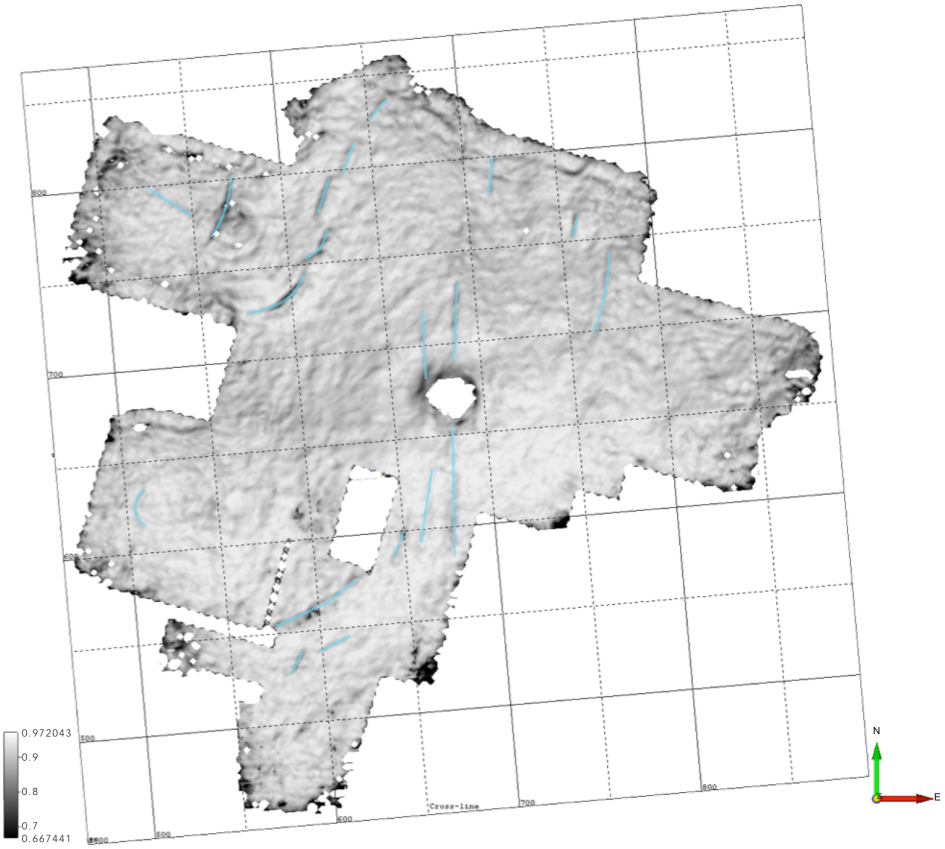
0.972043
0.9
0.8
0.7
0.667441
Cross-line
N
E

d)

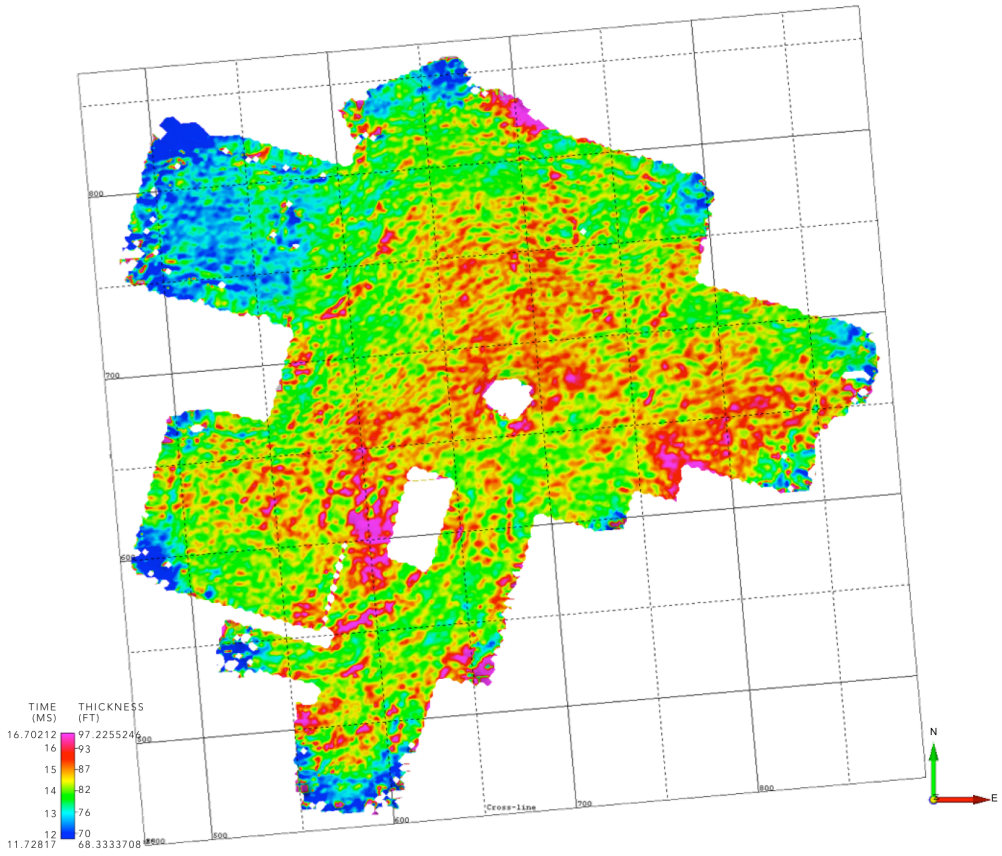

Figure 33 a) Time-structure map of the LEF horizon b) amplitude map for the LEF horizon c) similarity attribute map for the LEF horizon. Faults are indicated by blue lines. d) isochron map from the LEF horizon to the BEF horizon

Top of Upper Eagle Ford

The top of the UEF, like the LEF, was tracked as a waveform trough, at depths between approximately 4985 ft to 6385 ft (Fig 34a). The average velocity of the UEF is 13770 ft/s, and vertical and lateral resolutions for the UEF are 86 ft and 172 ft, respectively. This relatively weak event represents the Austin-UEF carbonate-on-carbonate contact. Even in core and well-log analysis, the Austin Group and the UEF are not wholly distinguishable due to similar lithology. Consequently, the UEF event has relatively low amplitude values of -1000 and -5000 (Fig 34b). The amplitude map shows amplitude variations and orientation with acquisition that is characteristic of acquisition footprint. General lateral amplitude trends are likely associated with geological impedance changes, but local amplitude striping are not. Close inspection of the UEF time structure map shows a dimple pattern also representing acquisition footprint. Acquisition footprint also obscures structural interpretation of the UEF, including fault mapping. Similarity only further reveals the acquisition footprint (Fig 34 C) and gives no indication of much weaker fault patterns. It therefore must be inferred that faults seen in the overlying Austin and the underlying LEF must also cut through the UEF.

Using the UEF horizon, the thicknesses of the UEF formation as well as the thickness of the entire Eagle Ford Group were calculated from isochron maps (Fig 34d and Fig 35). The UEF Formation ranges in thickness from 119 ft to 256 ft and thickens to the southwest, towards the Maverick Basin depocenter in Maverick County. Similarly, the Eagle Ford Group thickens to the southwest and ranges in thickness from 220 ft to 350 ft.

a)

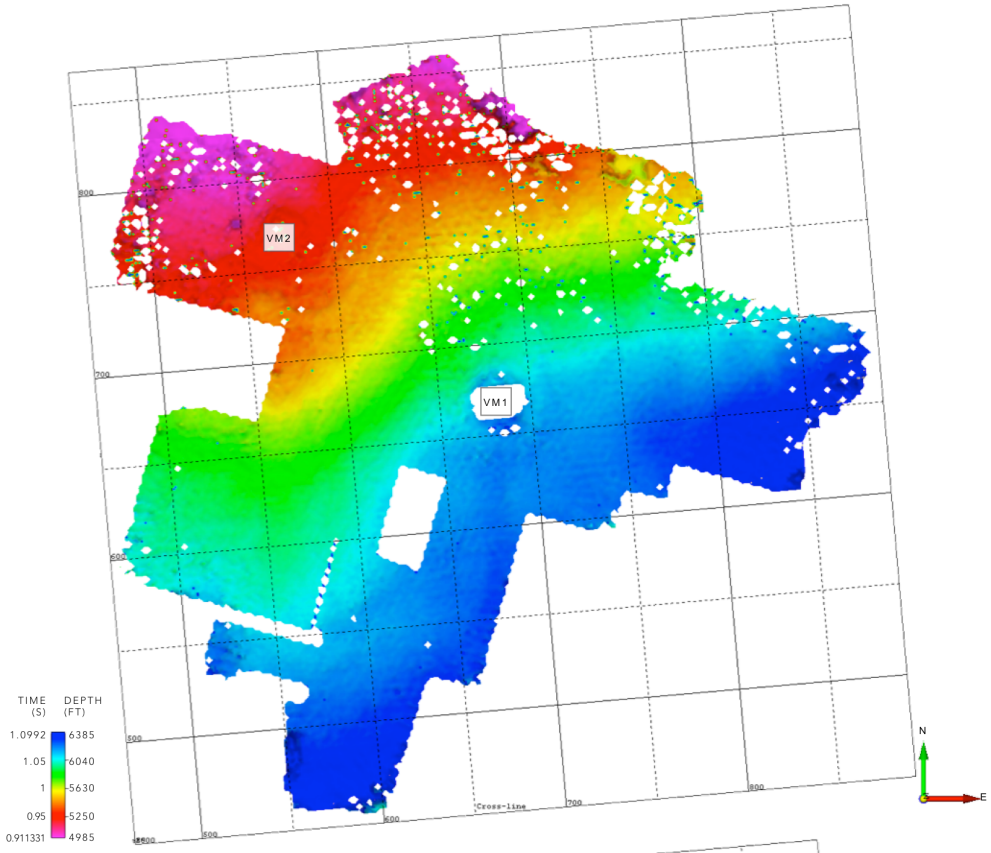
VM2
VM1
TIME (S)
DEPTH (FT)
1.0992
1.05
1
0.95
0.911331
6385
6040
5630
5250
4985
Cross-line
N
E

b)

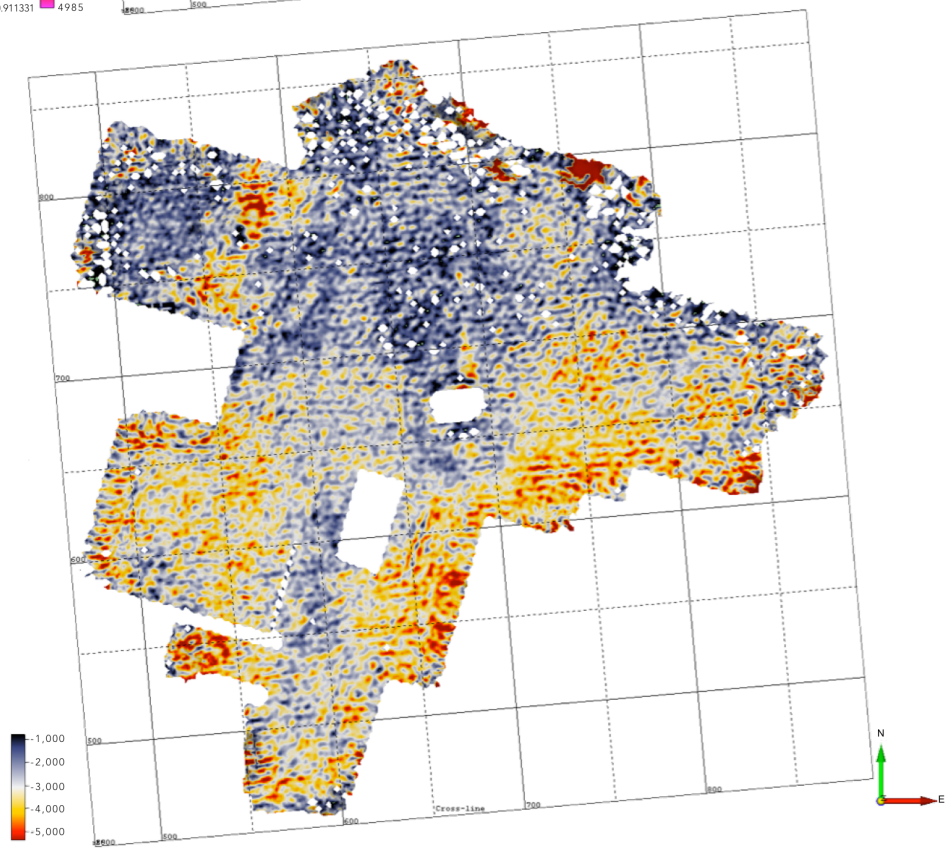
-1,000
-2,000
-3,000
-4,000
-5,000
Cross-line
N
E

c)

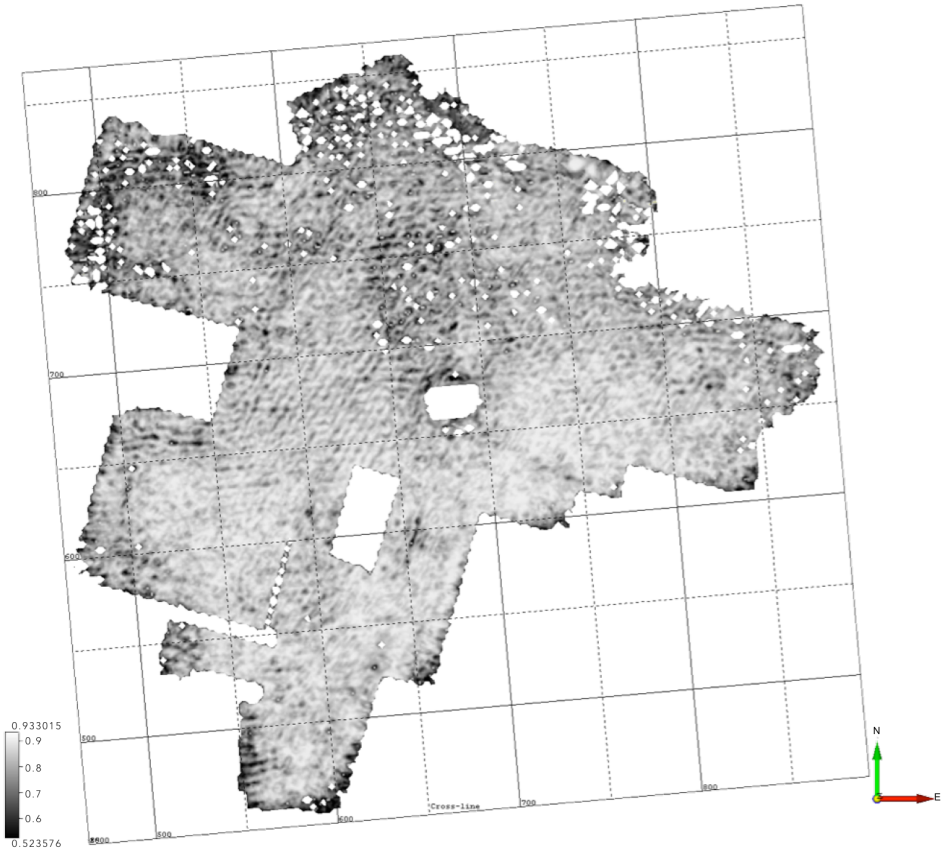
0.933015
0.9
0.8
0.7
0.6
0.523576
Cross-line
N
E

d)

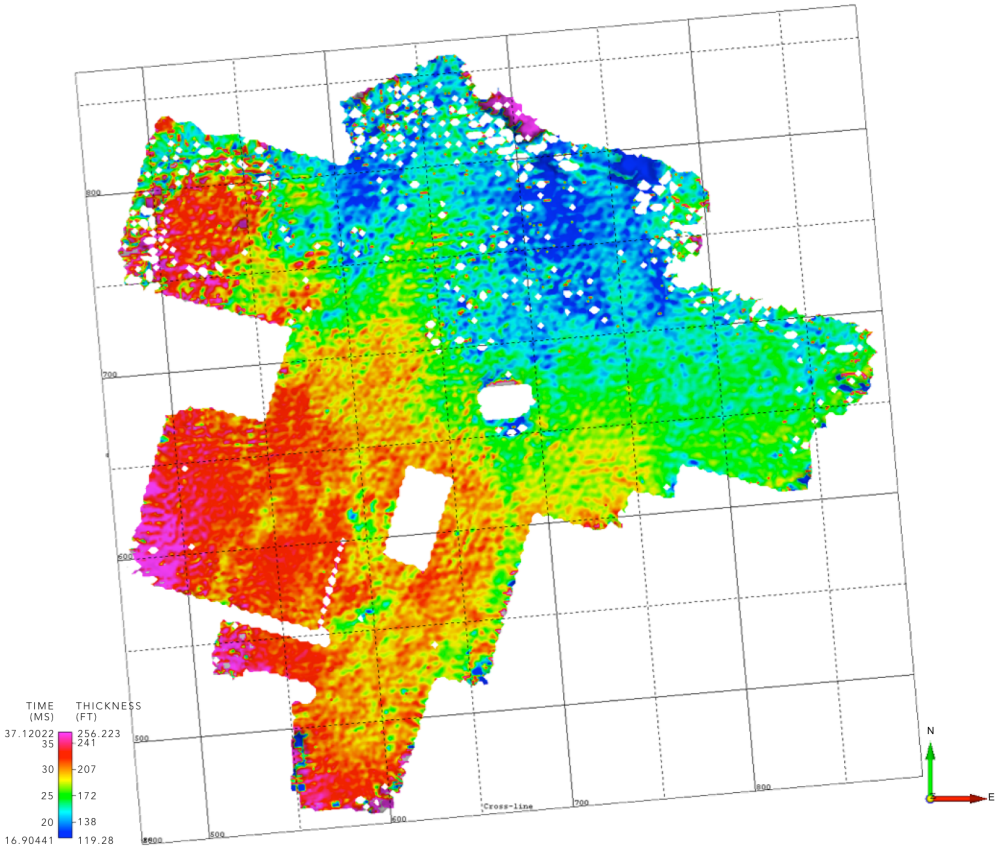
TIME (MS)
THICKNESS (FT)
37.12022
35
30
25
20
16.90441
256.223
241
207
172
138
119.28
Cross-line
N
E

Figure 34 a) Time-structure map of the LEF horizon b) amplitude map for the LEF horizon c) similarity attribute map for the LEF horizon. Faults are indicated by blue lines. d) isochron map from the LEF horizon to the BEF horizon

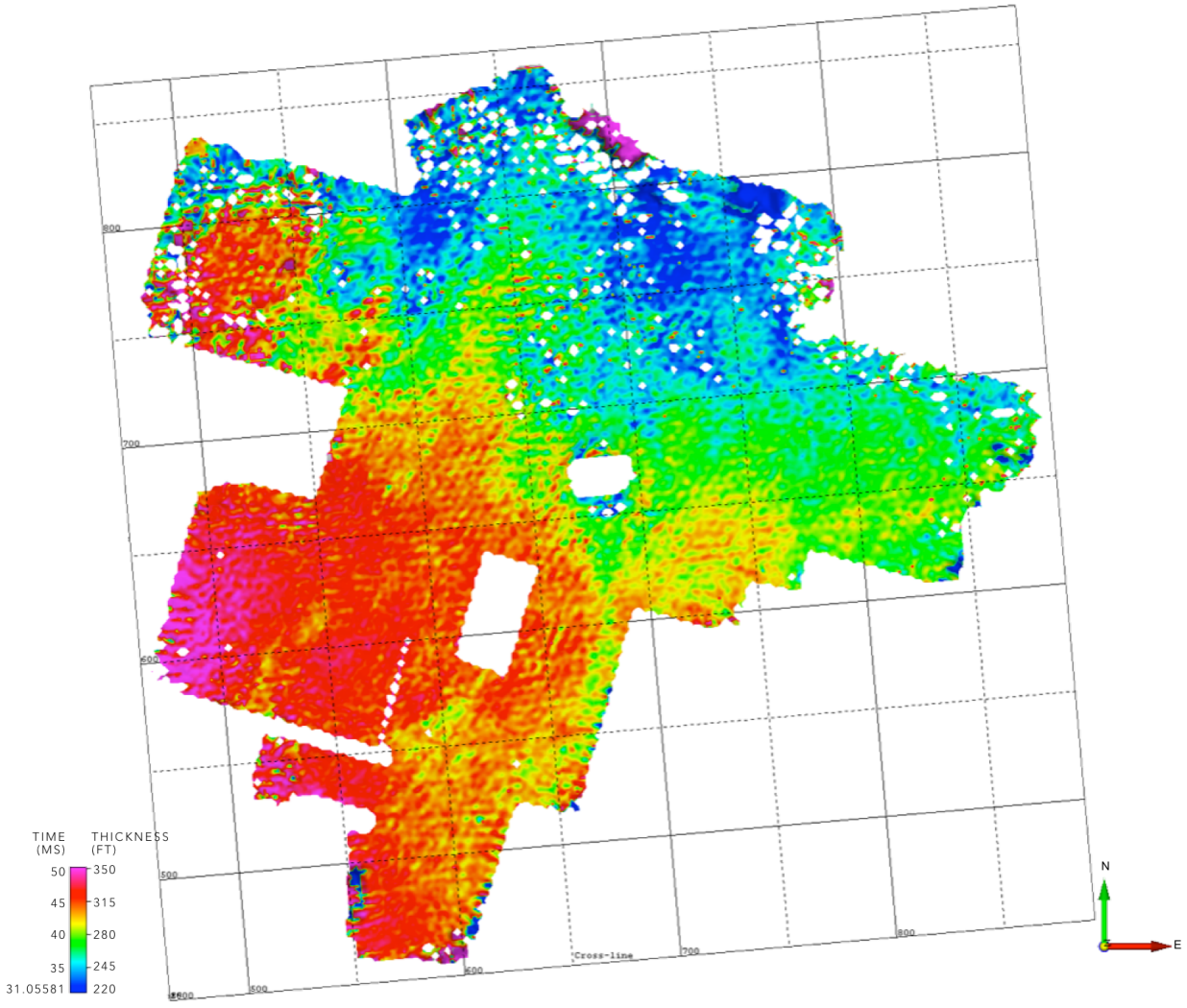

Figure 35 Isochron map from the LEF horizon the the BEF horizon

Top of Austin

The Austin group is intensely fractured, so the horizons within the Austin seismic package tend to be less smooth and easy to track. The top of the Austin was tracked between depths of 4405 ft and 5560 ft (Fig 36a) as a event between two positive reflection coefficients (Fig 26). Two closely spaced, opposite polarity reflection events merge into one large reflection event in a process called thin bed tuning (Liner, 2004). The small positive reflections are a result of the transition from the slightly more porous overlying Anacacho limestone into the chalks and marls of the Austin. Because of the nature of the relationship between the Austin, the volcanic mounds, and the Anacacho Limestone, and the way in which the volcanic mound formation interrupted deposition of both the Anacacho and the Austin, the stratigraphy and seismic data can become complicated. Depending on the bed thickness, the tuned event may become dominantly positive or negative, or appear to have a phase shift. The AUS horizon had to be tracked very carefully, at times using the line tracking function instead of volume tracking, and many auto-picked tracks from the volume tracking cube had to be manually corrected.

The palagonite tuff of VM1 and VM2 intrudes into the top of the Austin, disrupting the continuity of the tracked horizons and resulting in a complicated arrangement of horizons that are difficult to match up. Not only do the volcanic mound byproducts intrude into the Austin, the mixing of the tuff into the formation as eruptions disrupted deposition resulting in lateral lithology variations. In the case of the Top Austin horizon, the older and larger VM1 seems to be the only mound that could have disrupted Austin deposition and possibly result in the mixture of volcanic material into the deep-water carbonates. This would result in lateral acoustic impedance variations in the Austin, which is evident as a low-amplitude halo around mound VM1 in the amplitude map (Fig 36b). Areas to the

southwest have generally lower amplitude values, perhaps the result volcanic material broadcast by prevailing northeast winds.

The Austin time structure map (Fig 36a) and similarity attribute map (Fig 36c) show the dip to the southeast, and gaps under both mounds VM1 and VM2. Major faults with visible offset could be seen in vertical seismic lines and are visible on both maps and highlighted by line overlays. In addition to faults, the similarity attribute indicates fractured country rock surrounding VM1. The entire Austin Group ranges in thickness between 542 ft and 832 ft, thins to the southeast (Fig 36d) and shows clear influence of VM1 on thickness. Average velocity of the entire Austin group is 16125 ft/s and vertical and lateral resolutions for the Austin are 101 ft and 202 ft, respectively.

a)

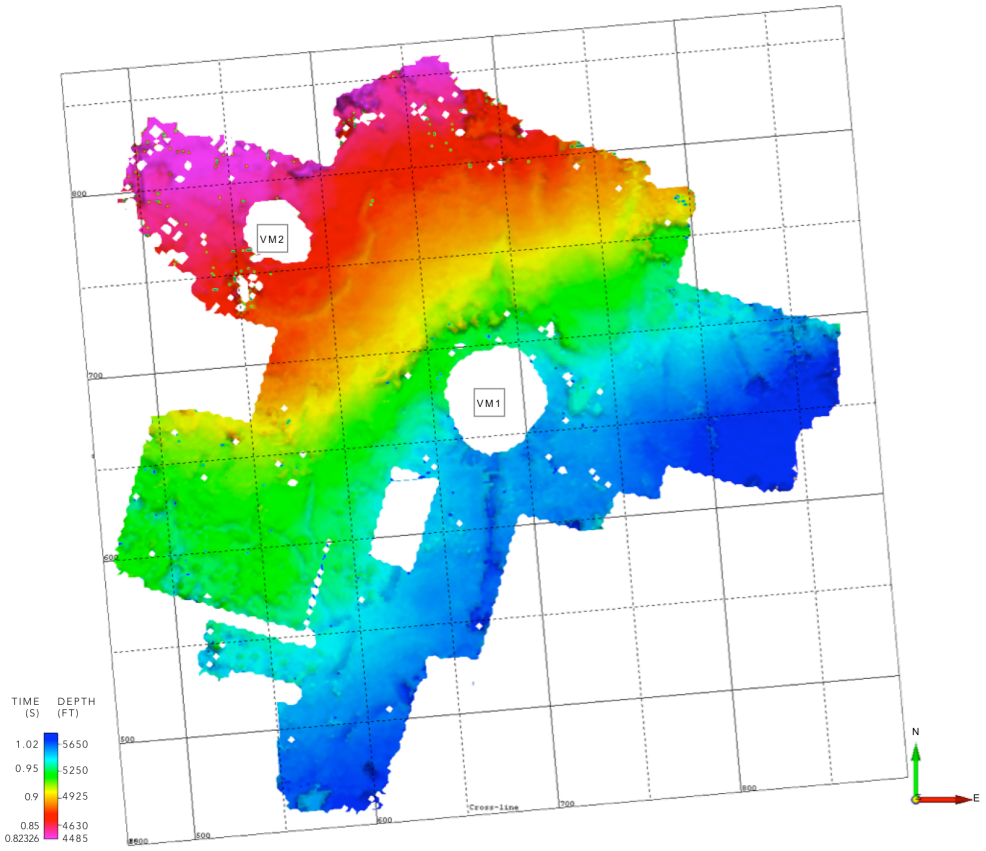

b)

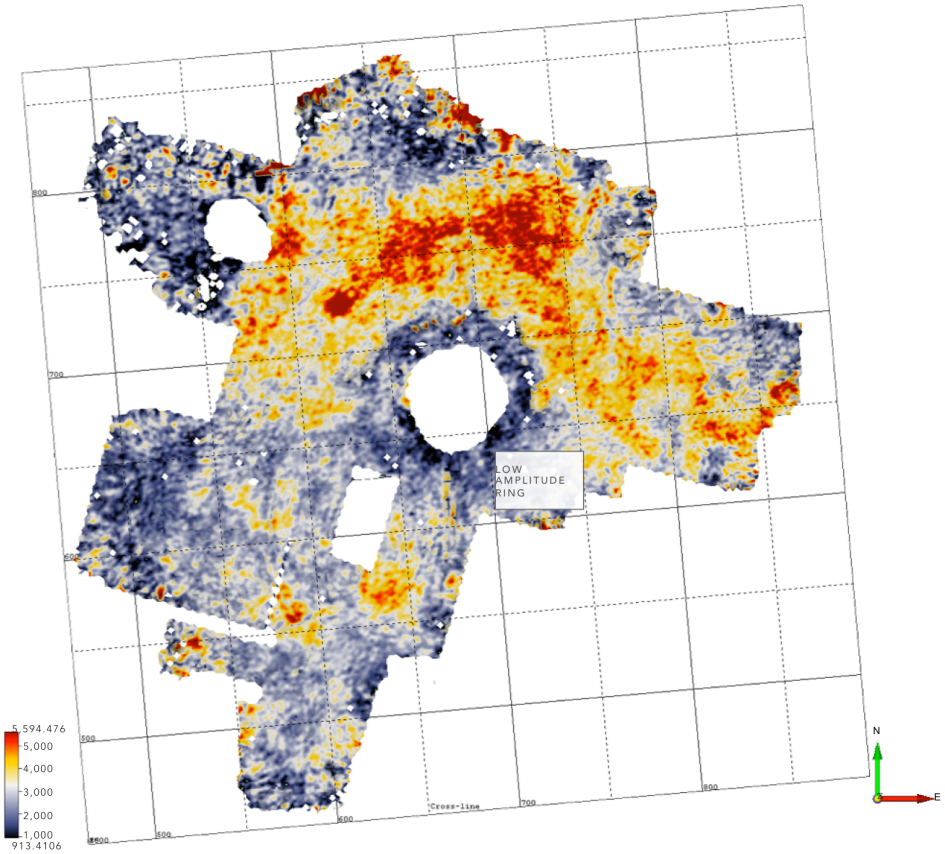
LOW AMPLITUDE RING
5,594.476
5,000
4,000
3,000
2,000
1,000
913.4106
Cross-line
N
E

c)

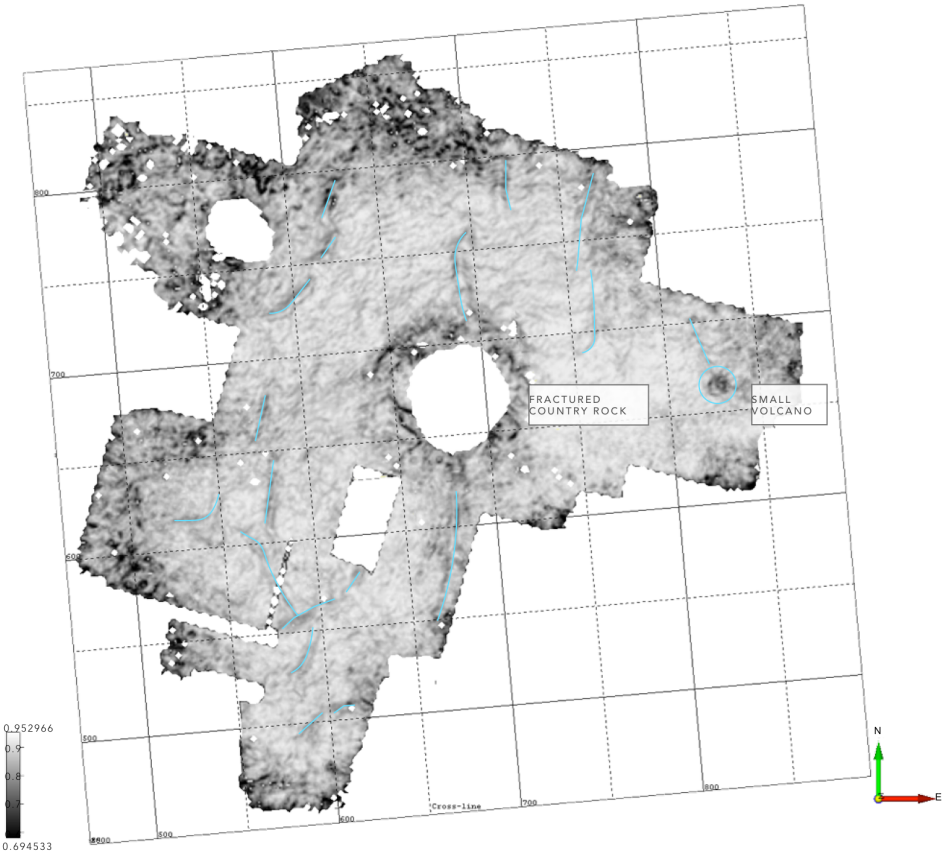
FRACTURED COUNTRY ROCK
SMALL VOLCANO
0.952966
0.9
0.8
0.7
0.694533
Cross-line
N
E

d)

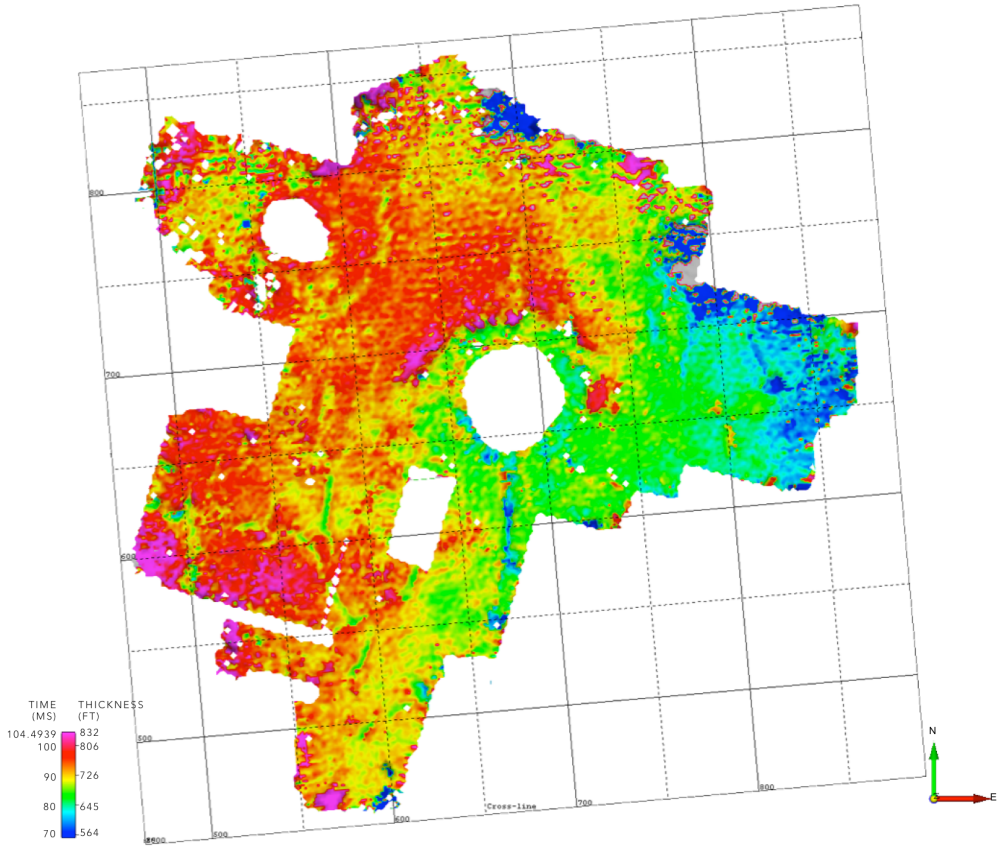

Figure 36 a) Time-structure map of the AUS horizon b) amplitude map for the AUS horizon c) similarity attribute map for the AUS horizon. Faults are indicated by blue lines. d) isochron map from the AUS horizon to the LEF horizon

Top of Anacacho

The top of the Anacacho Limestone (ANA) in the study area occurs at depths between 4100 ft and 5250 ft (Fig 37a). ANA was tracked as a weak waveform peak, representing the transition from the lower velocity porous siliciclastic delta deposits of the overlying San Miguel formation to higher velocity tighter limestones of the Anacacho, with an average velocity of 14383 ft/s (Fig 26) and vertical and lateral resolutions of 90 ft and 180 ft, respectively. ANA horizon amplitude values range from +1970 to +11590 (Fig 37b). Low amplitude rings are observed around VM1 and VM2, indicating the extent of influence of the volcanic mounds. Above VM1, the low-amplitude ring is likely from displacement along a fault that resulted from collapse of the mound from overburden. Such faults do not exist over VM2 due to flatter shape of the top of the mound, so the low amplitude ring must be the result of some other factor, perhaps mixing of volcanic ash into the biohermal reef rock through younger eruptions from VM2 or nearby mounds.

The time-structure map in Fig 37a shows that the Anacacho limestone dips to the southeast and is evenly draped over the volcanic mounds. Fault displacement increases significantly at the top of the Anacacho, which is also evident by both the time-structure and the similarity attribute maps (Fig 37c). In the Anacacho, faults were mapped in vertical seismic sections and the horizon maps enhanced the interpretation. Of all horizons in this study, the greatest number of faults cut the top of the Anacacho. As previously mentioned, the group of faults overlying VM1 is the result of collapse. Other faults in the area are normal faults with varying throw direction, mostly trending approximately north-south with a few trending approximately east-west.

Atop the volcanic mounds, the structure of the top of the Anacacho closely resembles that of the volcanic mound tops themselves. Furthermore, the smaller SVM1

can be seen in the ANA horizon, in addition to its connection to faults in the western area of the survey (Fig 37c).

The Anacacho Limestone generally thickens to the south (Fig 37d), and particularly thickens around VM1, and in areas where there are clusters of mounds-the northwest area including VM2 and VM3, and the southwest area. The nature of reef accumulation in relation to the mounds accounts for these thicker areas. Reefs would have accumulated thickest around individual lone mounds, like VM1, and in lagoons between mounds in large clusters. Areas southwest of the mounds display the thickest Anacacho as a result of the preferential reef development due to the prevailing winds and currents from the northeast.

a)

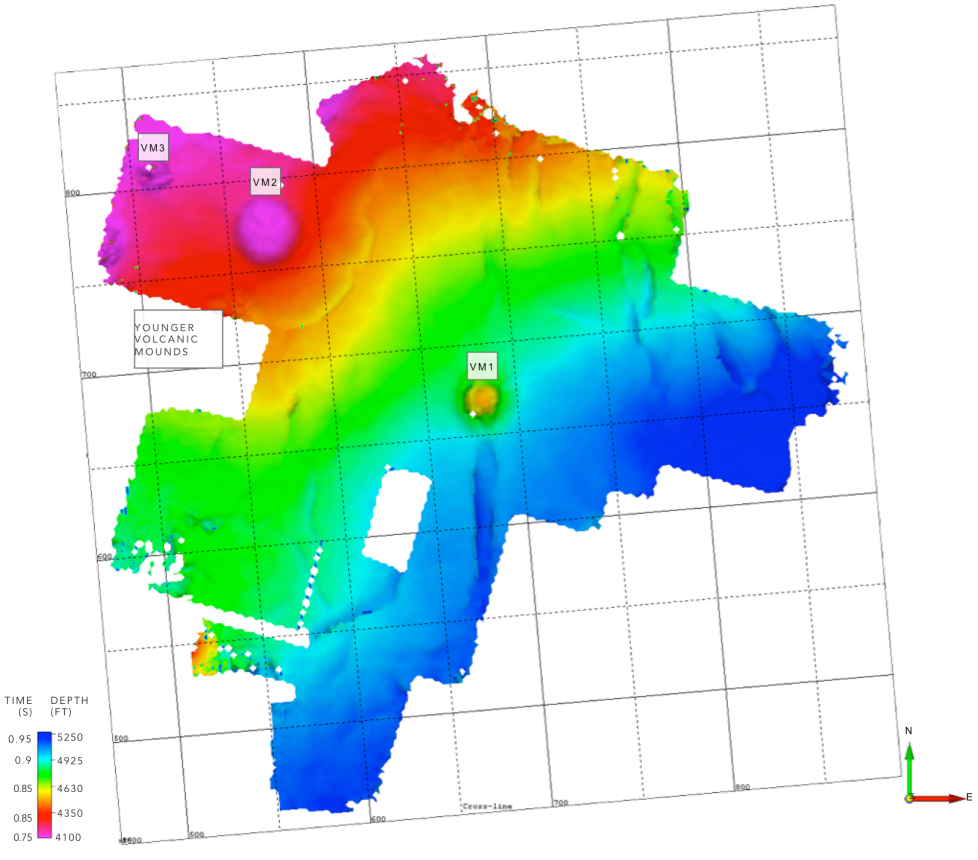

b)

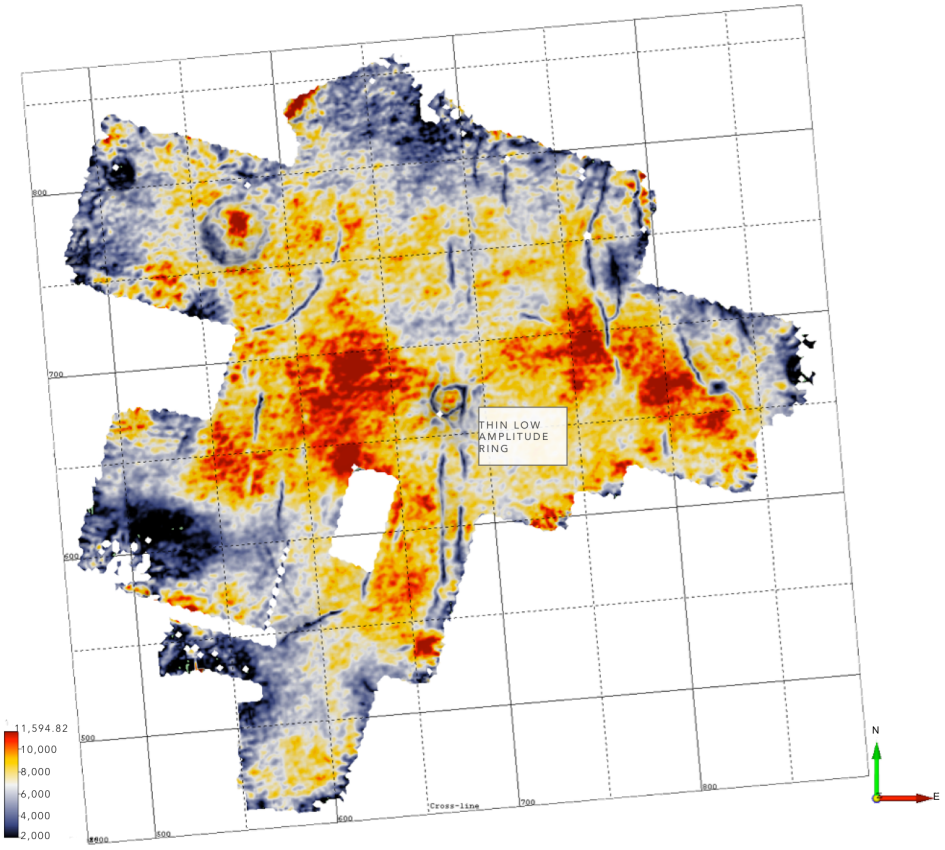
THIN LOW AMPLITUDE RING
11,594.82
10,000
8,000
6,000
4,000
2,000
Cross-line
N
E

c)

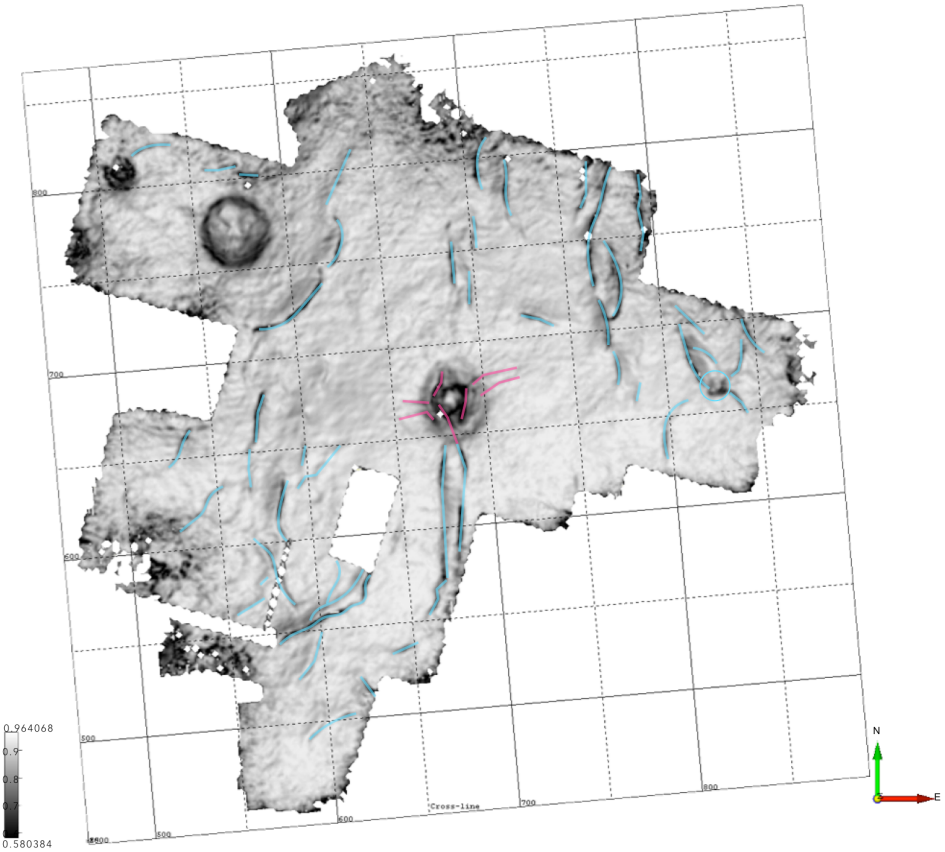
0.964068
0.580384
Cross-line
N
E

d)

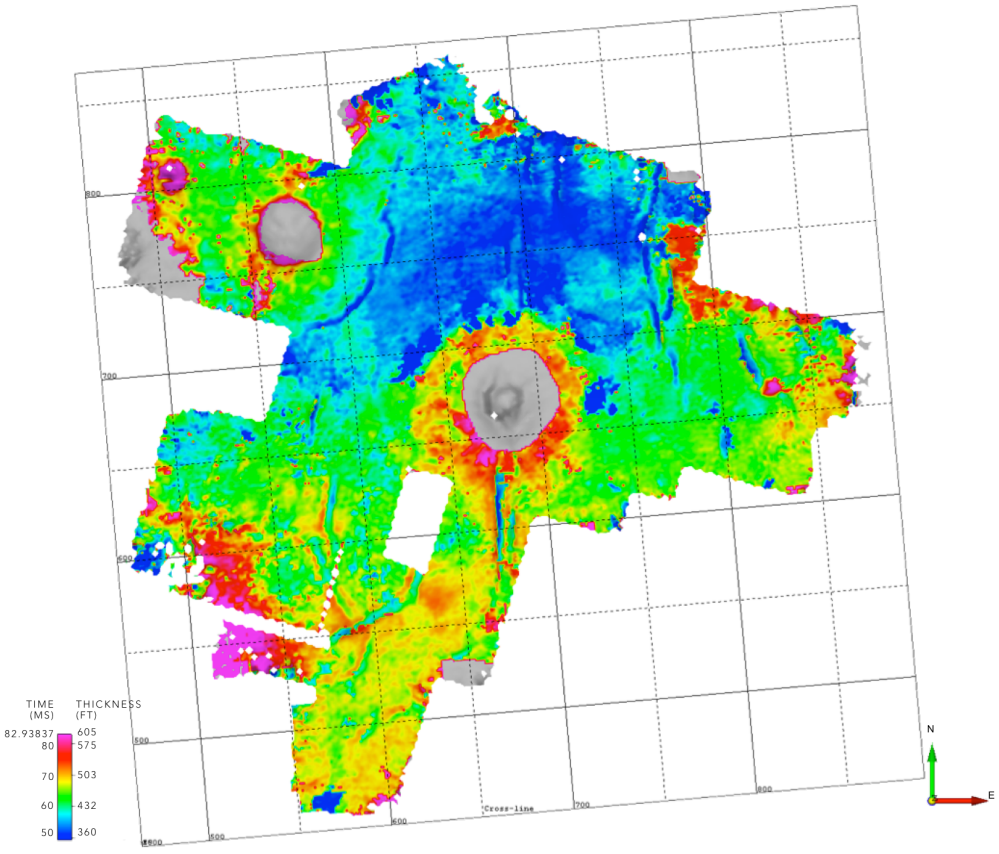

Figure 37 a) Time-structure map of the ANA horizon b) amplitude map for the ANA horizon c) similarity attribute map for the ANA horizon. Faults are indicated by blue lines. d) isochron map from the ANA horizon to the AUS horizon

Top of San Miguel

The top of the San Miguel (SM) was picked on the well log in the exact spot that a fault displaced the San Miguel, yielding a poor match to the synthetic (Fig 26). With a questionable correlation, a better-defined waveform peak event in the overlying Olmos was tracked as a proxy for the San Miguel. This horizon likely represents the transition from sandstone to shale, which is a typical sequence in both the Olmos and the San Miguel. Although this horizon is not technically within the San Miguel, it is representative of the formation because the Olmos Formation above has almost identical depositional packages as the San Miguel. More importantly, there was no break in deposition or structural events that separated the deposition of the formations, so the horizon overlying the top of the San Miguel would have the same structural features as the top itself. Average velocity of the San Miguel is 13294 ft/s and vertical and lateral resolutions are 83 ft and 166 ft, respectively.

Fig 38 a and c show structural features at the top of the San Miguel. The SM horizon dips to the southeast from depths of 3730 ft to 4835 ft (Fig 38a), and thins considerably to the east (Fig 38d) away from the Taylor-aged western depocenter. The formation also thins above volcanic mounds. Because of the regional variability of delta sandstone formation in this area, the variations in amplitude are most likely the result of lateral changes in lithology from different sandstone bodies. The density of normal faults decreases at the top of the San Miguel relative to the Anacacho, but radial faults overlying the volcanic mounds increase, perhaps indicating the critical weight of overburden atop the mounds. The Anacacho formation was draped atop VM2, which appears to have been slightly younger than VM1, but there were no radial faults observed in the Anacacho. However, moving up, radial faults begin to appear. Looking further up into the Olmos, the

number of faults overlying VM2 increases. Although to a lesser extent, this is similar to what occurs over VM1. The number of radial faults overlying the older VM1 increases upward from the Anacacho to the San Miguel, indicating the readjustment from the collapse of the mound structure intensified upward from the mounds. The isochron map in Fig 38d shows interval thickness from 422 ft to 645 ft and highlights the structural features, including the mounds, radial faults and normal faults.

a)

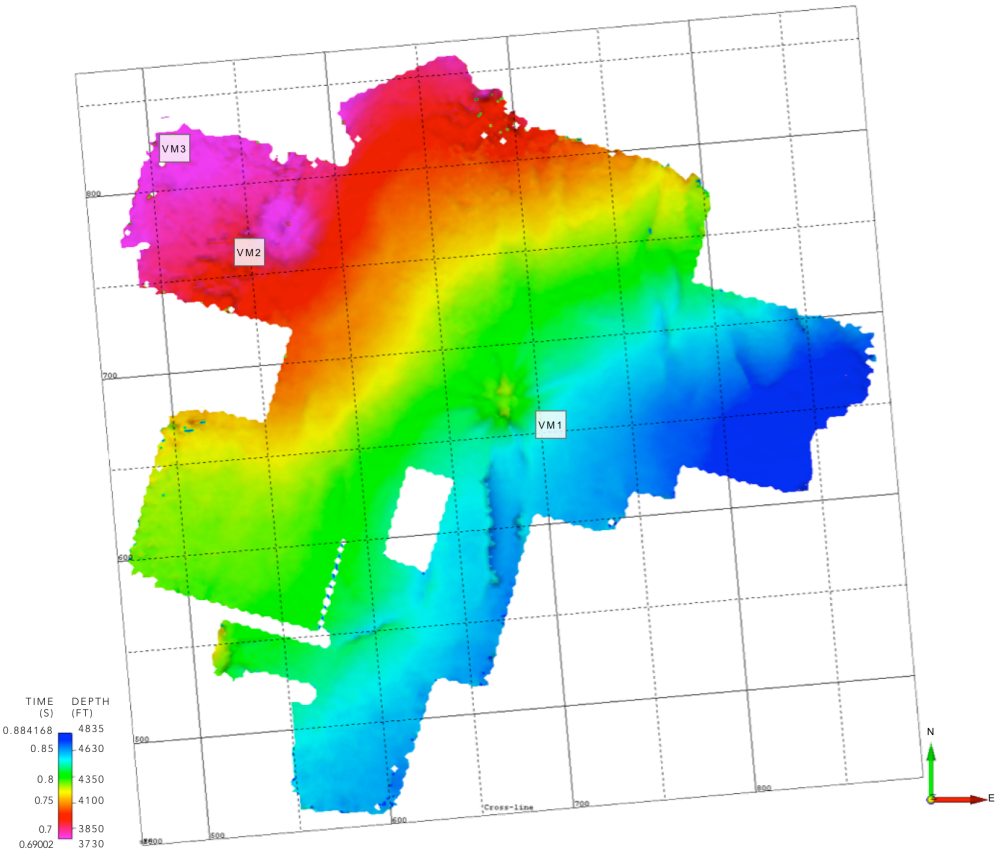

b)

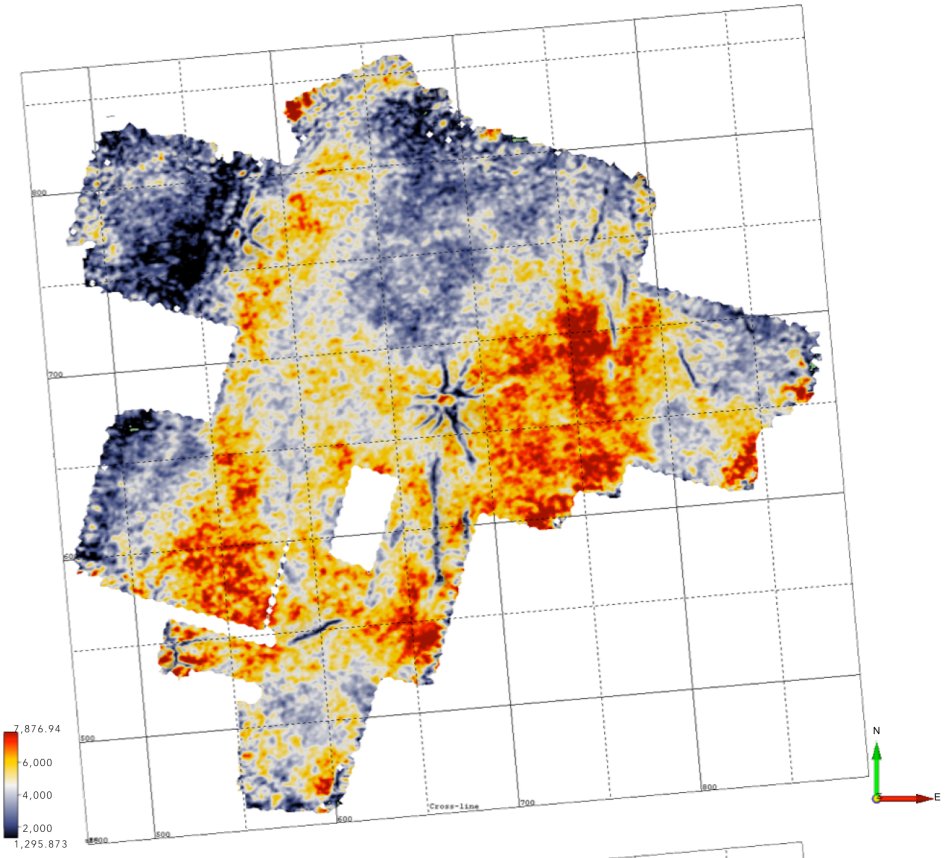
7,876.94
6,000
4,000
2,000
1,295.873
Cross-line
N
E

c)

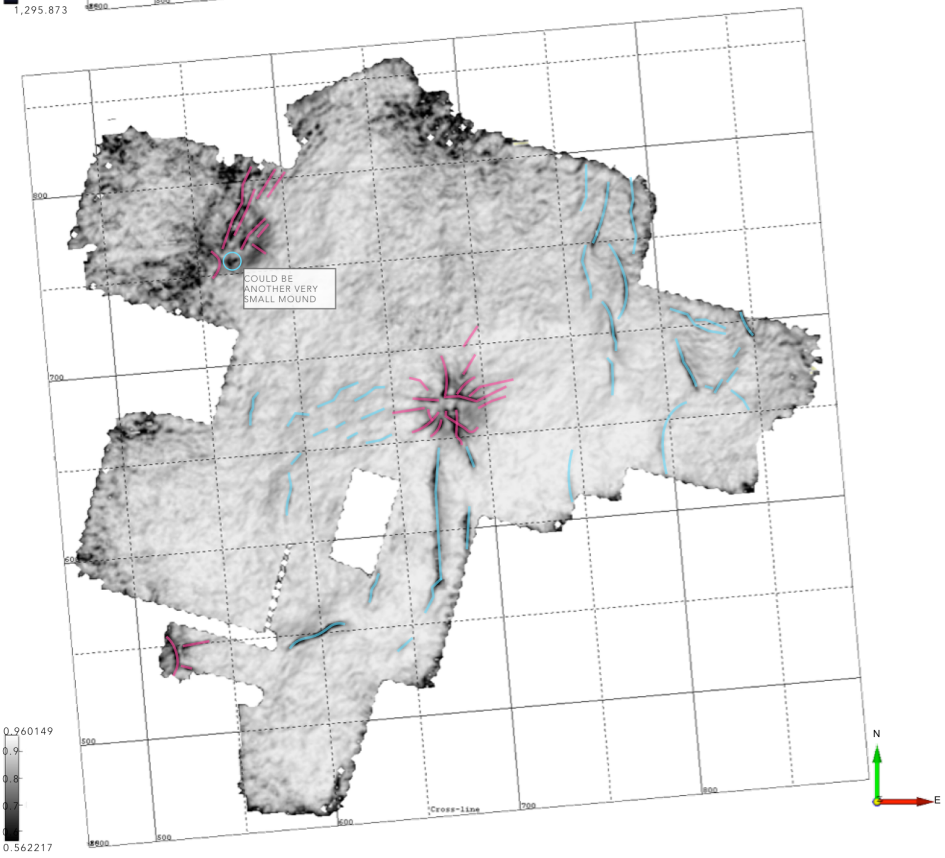
COULD BE ANOTHER VERY SMALL MOUND
0.960149
0.562217
Cross-line
N
E

d)

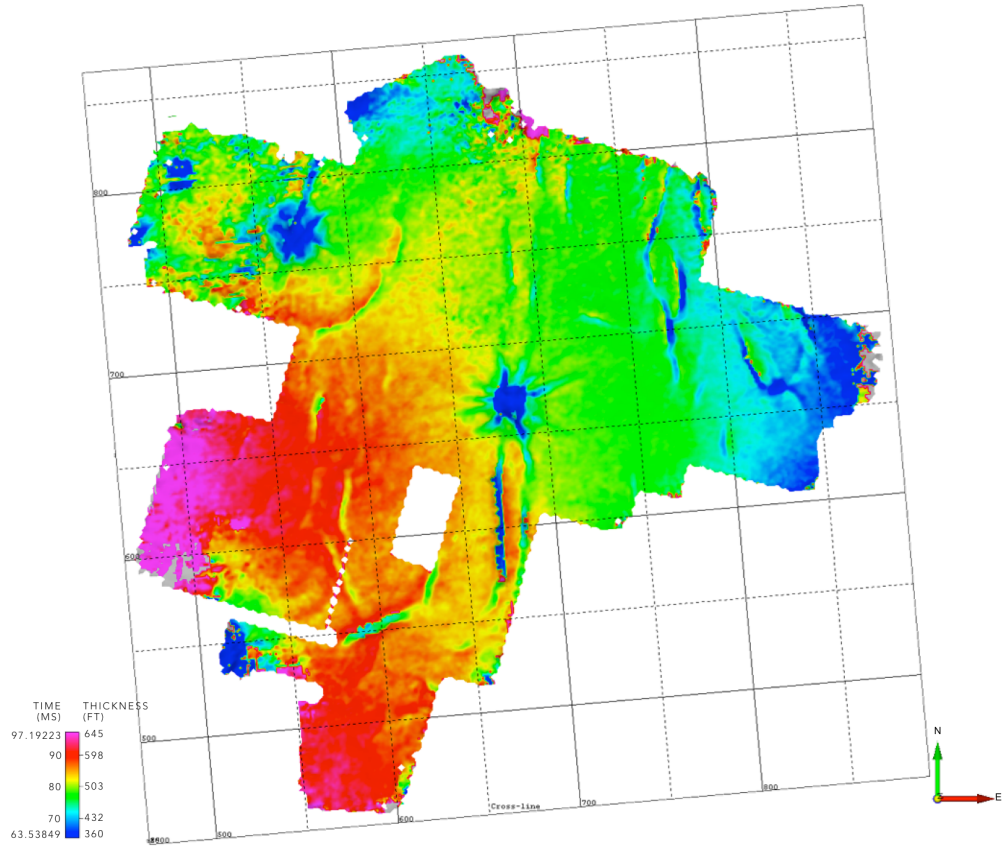

Figure 38 a) Time-structure map of the ANA horizon b) amplitude map for the ANA horizon c) similarity attribute map for the ANA horizon. Faults are indicated by blue lines. d) isochron map from the ANA horizon to the AUS horizon

Using the SM and BEF horizons, an isochron map was generated to show the thickness of the entire studied section (Fig 39). From the top of the San Miguel formation to the base of the Eagle Ford (top of the Buda), the rocks thicken to the southwest from1724 to 2164 ft. This isochron map also highlights the largest features of the entire section that have the greatest effect on structure: faults 1 and 3 and volcanic mounds VM1 and VM2. Thickened bands that extend radially from the mounds are also visible, as well as very large incomplete mound to the east that was not analyzed for this study.

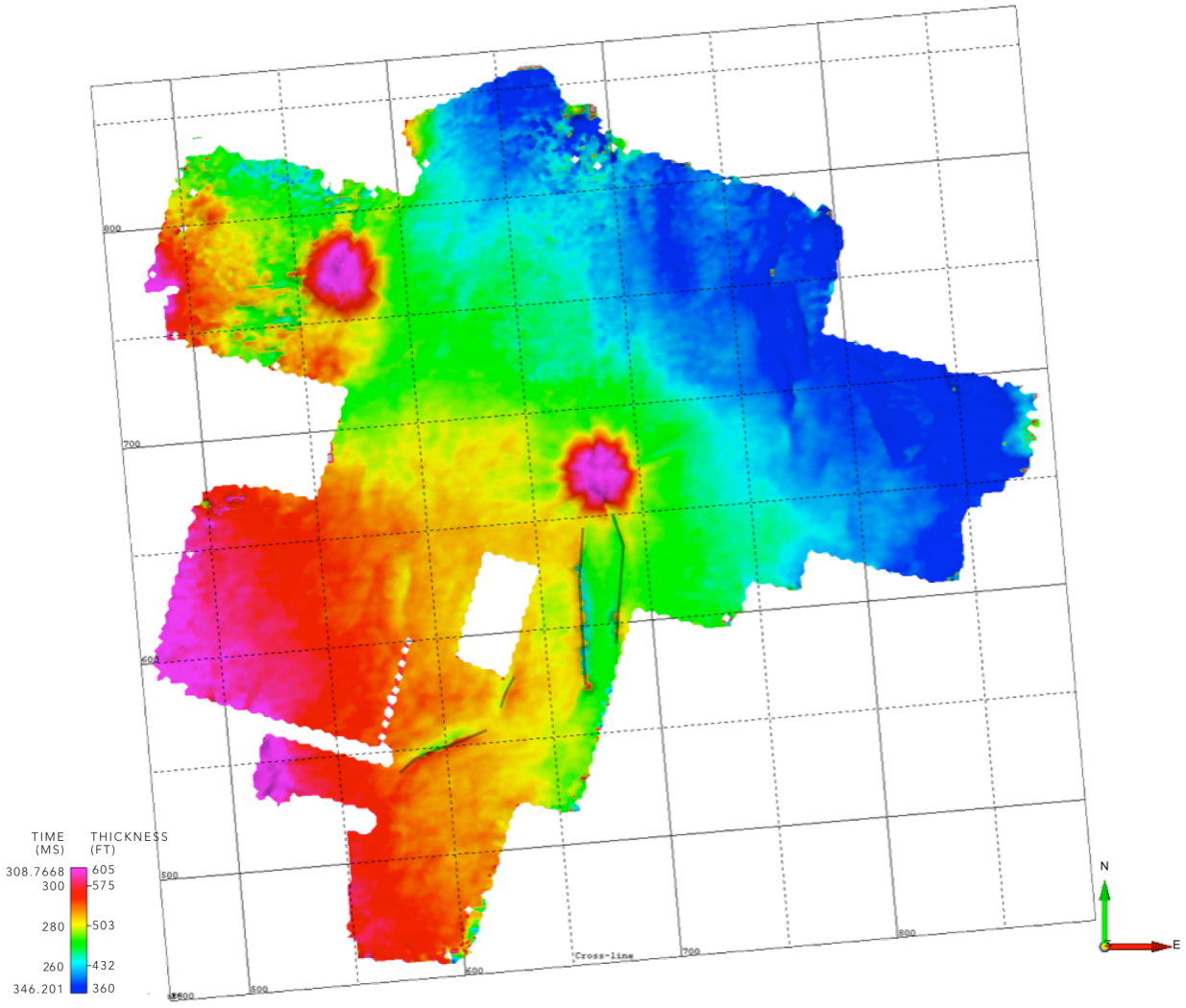

Figure 39 Isochron from SM horizon to BEF horizon showing thickness of entire section

V. Conclusions and Suggestions for Future Work

Without well log data or core from wells that penetrate the mounds, these mounds cannot be definitively proven to be volcanic mounds composed of palagonite tuff. However, using the seismic profile by Ewing and Caran (1991), as well as identifying known associated characteristics, this study is able to state with certainty that these structures seen in 3D seismic data are volcanic mounds. Known characteristics include overlying faults related to overburden, associated grabens, fracturing of country rock around the crater, and lithology changes due to mixing of ash and volcanic tuff with carbonates. The associated faults can be identified using vertical seismic lines, as well as similarity/coherency maps, in which the smaller-scale fracturing of country rock surrounding the mound can also be identified. Amplitude maps assist in identifying larger faults, as well as identifying lithology changes related to the volcanic eruptions. Additionally, velocity pull-down below the volcanic mounds related to the low velocity tuff is known to occur in 3D seismic data. Although not experimented in this work, the extent of velocity pull-down could be used to quantify the size and amount of palagonite tuff in the mound. This would be possible because larger amounts of the low-density tuff within the mounds would slow the seismic P-wave velocity more than smaller amounts.

Future works on these volcanic mounds should focus on identification of fracture systems that served as the conduit for magma to travel upward, as well as the massive dike/sill bodies that were the magma feeders for individual volcanic vents. The magma did not travel through a single fault to the surface but through a system of fractures, which is more difficult to identify in the vertical resolution of the 3D seismic data. The fact that the mounds are found some distance away from the fracture zones further complicates identification. However, these fracture zones could be identified using similarity/coherency

attributes on vertical seismic lines, as well as a calculated curvature attribute (commonly used for fracture identification) in time slices. Identifying these zones could be aided by the interpretation of bright spots that were found in an Early Cretaceous positive horizon in the Pedernales survey. Because of the lithology of the sill/dike bodies, they have very high p-wave velocity. Therefore, the magma feeders would be recognizable in 3D seismic as bright, positive reflectors. Identification as described would further assert the characterization of these mounds as volcanic mounds of the Uvalde Field. Combined with identification methods used in this study, further volcanic mound identification and characterization can be done using 3D seismic without well data.

Mapping these volcanic mounds in the seismic isolated them from surrounding horizons and connected them to geologic features, enabling further interpretation of surrounding formations and the mounds themselves. Prior to mapping the tops and bases of the volcanic mounds, horizon tracking of the surrounding formation tops was difficult and chaotic. This led to a very extensive literature study and geologic setting analysis to understand all the details of the carbonate formations of the Gulfian series, as well as the mounds themselves. An in-depth and comprehensive knowledge of all of these is necessary for accurate mapping and interpretation. Attempts were made to map the formation tops and volcanic mound tops/bases with a general, less extensive understanding of the series in the early stages of this study that produced messy and, more importantly, incorrect results. Once a full understanding of the geology and formation of the volcanic mounds is gained and the tops and bases are mapped, the surrounding formations become much simpler to track. It should also be noted that the top chosen for the volcanic mounds is subject to interpretation of event timing- the top could also be mapped as the bright, negative horizon located above the mapped horizon in

this study.

Timing of events, extent of the mounds, associated faults, and geologic setting could also be interpreted once the forms were identified. Argon-argon dating done in the Uvalde Field in 2002 by Miggins et al. gave an age range for the mounds between 78-71 Ma. This age date restricts volcanic mound formation to the Campanian, during which the Taylor Group was deposited. However, this study found that initial eruption of VM1 likely occurred during the late Santonian, based on the coincidence of the base of the mound with the AUS horizon (top of the Austin Group) and the apparent mixing of volcanic material with the deep water carbonates to the southwest of the mound, interpreted from the amplitude map of the AUS horizon. Based on the interplay of horizons above, as well as the associated faults above and adjacent to the mound, the accumulation of VM1, and therefore volcanic activity, likely ended before onset of San Miguel deposition in the mid-Campanian. And while it is thought that volcanic activity lasted through the Maasrichtian due to the presence of interbedded bentonitic clay thought to be altered pyroclastic material, the extent of structural features associated with mounds do not extend to the Escondido in the seismic. These analyses can be applied to other volcanic mounds to asses the same characteristics that can usually only be determined using well data, core, or geochemical analysis, which only give information about one small area within a larger field. By using 3D seismic data, the entire mound can be interpreted and put in context with other mounds nearby as well as surrounding formations, which can be interpreted and understood more fully. This can all be done without the additional expense and analysis of other data.

As the first student to be given access to the Pedernales 3D seismic survey, this research was also meant to serve as a general overview and starting point for future in-

depth analysis. Through the mapping of the Gulfian formations and structures, several features were observed that should be analyzed in further detail in many other graduate theses.

Firstly, the rest of the major horizons should be mapped in this seismic, going all the way down to the Jurassic. Not only would a complete understanding of the area be gained, but basement structure could be interpreted and possibly applied to overlying structure. An in-depth fault analysis should be completed to best understand the nature of the faults in the area, as they do not match the alignment of fault zones in the Rio Grande Embayment. This would also include relation of the faults to the volcanic mounds themselves, as the major faults appear to be connected to these volcanic mounds. Above the section analyzed in this work, prograding sequences of the Navarro Group should be interpreted and prograding structures identified. This work in particular would be beneficial for tying together MArkUP projects. Analysis of late-Cretaceous prograding structures could be compared to structures in Pennsylvanian formations in Osage County, Oklahoma that were identified as shelf clinoforms and analyzed by West (2015).

VI. References

Bahorich, M. and Farmer, S., 1995, 3-D seismic discontinuity for faults and stratigraphic features: The coherence cube: The Leading Edge, 14, no. 10, 1053-1058.

Blakey, R., 2011, Paleogeography library, Retrieved November 12, 2014, from http://cpgeosystems.com/globaltext2.html

Berg, R.R., and Gangi, A.F., 1999, Primary migration by oil-generating microfracturing in low-permeability source rocks- Application to the Austin Chalk, Texas: American Association of Petroleum Geologists Bulletin, v. 83, no. 5, p.727-756.

Collingwood, D.M., and Rettger, R.E., 1926, The Lytton Springs oil field, Caldweel County Texas: American Association of Petroleum Geologists Bulletin, v. 10, no. 10, p. 953-975.

Condon, S. M., and T. S. Dyman, 2003, 2003 Geologic assessment of undiscovered conventional oil and gas re- sources in the Upper Cretaceous Navarro and Taylor Groups, Western Gulf Province, Texas: Petroleum Systems and Geologic Assessment of Undiscovered Oil and Gas, Navarro and Taylor Groups, Western Gulf Province, Texas: U. S. Geological Survey Western Gulf Province Assessment Team, U. S. Geological Survey Digital Series DDS-69-H, Chapter 2, 42 p.

Conrad, K.T., Snedden, J.W., and Cooke, J.C., 1990, Recognition of fifth-order cycles in a biodestratified shelf sandstone parasequence—Olmos Sandstone, south Texas [abs.]: American Association of Petroleum Geologists Bulletin, v. 74, no. 5, p. 633.

Cooper, J.D., 1971, Maestrichtian (Upper Cretaceous) biostratigraphy, Maverick County, Texas and northern Coahuila, Mexico: Gulf Coast Association of Geological Societies Transactions, v. 21, p. 57-65.

Cooper, J.D., 1973, Cretaceous-Tertiary transition—Rio Grande outcrop section: American Journal of Science, v. 273-A, p. 431-443.

Dawson, W.C., 2000, Shale microfacies: Eagle Ford Group (Cenomanian-Turonian) north-central Texas outcrops and subsurface equivalents: Gulf Coast Association of Geological Societies Transactions, v. 50, p. 607-621

Dawson, W.C., Katz, B., Robison, V.D., 1995, Austin Chalk petroleum system, Upper Cretaceous, southeastern Texas-A case study: Gulf Coast Association of Geological Societies Transactions, v. 45, p. 157-163.

Dennis, J.G., 1987, Depositional environments of A.W.P. Olmos field, McMullen County, Texas: Gulf Coast Association of Geological Societies Transactions, v.37, p. 55-63.

Dravis, J., 1981, Porosity evolution in Upper Cretaceous Austin Chalk Formation, south-central Texas [abs.]: American Association of Petroleum Geologists Bulletin, v. 65, no. 5, p. 922.

Ewing, T.E., The Frio River Line in south Texas- Transition from Cordilleran to Northern Gulf tectonic regimes: Gulf Coast Association of Geological Societies Transactions, v. 37, p. 87-94

Ewing, T. E., and S. C. Caran, 1982, Late Cretaceous volcanism in south and central Texas—Stratigraphic, structural, and seismic models: Gulf Coast Association of Geological Societies Transactions, 32, 137–145.

Galloway, W.E., 2008, Depositional Evolution of the Gulf of Mexico Sedimentary Basin, in Miall, A.D., eds., The Sedimentary Basins of the United States and Canada: New York, Elsevier, 610 p.

Grabowski, G.J., Jr., 1984, Generation and migration of hydrocarbons in the Upper Cretaceous Austin Chalk, south-central Texas, in Palacas, J.G., ed., Petroleum geochemistry and source rock potential of carbonate rocks: American Association of Petroleum Geologists Studies in Geology no. 18, p. 97-115.

Harbor, R.L., 2011, Facies characterization and stratigraphic architecture of organic-rich mudrocks, Upper Cretaceous Eagle Ford Formation, South Texas: M.S. Thesis, The University of Texas at Austin.

Harville, L.L., 1959, Petrology of the Anacacho Limestone of southwest Texas: Gulf Coast Association of Geological Societies Transactions, v. 9, p. 161-165.

Hill, R.T., 1889, A preliminary annotated checklist of the Cretaceous invertebrate fossils of Texas, accompanied by a short description of the lithology and stratigraphy of the system: Austin, Texas Geological Survey Bulletin, 4, 57p.

Hentz, T. F., & Ruppel, S. C., 2011, Regional stratigraphic and rock characteristics of Eagle Ford shale in its play area: Maverick basin to east Texas basin: AAPG Search and Discovery

Jacka, A.D., 1982, Composition and diagenesis of the Upper Cretaceous San Miguel Sandstone, northern Webb County, Texas: Gulf Coast Association of Geological Societies Transactions, v. 32, p. 147-151.

Jennings, D. S., & Antia, J., 2013, Petrographic Characterization of the Eagle Ford Shale, South Texas: Mineralogy, Common Constituents, and Distribution of Nanometer-scale Pore Types, 101–114, doi:10.1306/13391708M1023586

Layden, R.L., 1976, Big Wells field, Dimmit and Zavala Counties, Texas, in Braunstein, J., ed., North American oil and gas fields: American Association of Petroleum Geologists Memoir 24, p. 145-156.

Lewis, J.O., 1977, Stratigraphy and entrapment of hydrocarbons in the San Miguel sands of southwest Texas: Gulf Coast Association of Geological Societies Transactions, v. 27, p. 90-98.

Matthews, T.F., 1986, The petroleum potential of “serpentine plugs” and associated rocks, central and south Texas: Baylor Geological Studies Bulletin, no. 44, fall, 43 p.

McDonald, M.A., 1986, Escondido Sands of the Lemin field in Bexar, Atascosa, and Wilson Counties, Texas, in Stapp, W.L., ed., Contributions to the geology of south Texas, 1986: San Antonio, Tex., South Texas Geological Society, p. 323-329.

Merritt, L.C., 1980, Sandstone diagenesis and porosity development in Olmos, San Miguel, and Upson Formations (Upper Cretaceous), northern Rio Escondido Basin, Coahuila, Mexico: Gulf Coast Association of Geological Societies Transactions, v. 30, p. 459-464.

Miggins, D., Blome, C.D., and Smith, D.V., 2002, Preliminary 40Ar/39Ar age constraints for the Uvalde igneous intrusions west of San Antonio, Texas: Geological Society of America Abstracts with Programs, v. 34, no. 6, p. 512.

Ogiesoba, O.C., Eastwood, R. (2013) Seismic multiattribute analysis for shale gas/oil within the Austin Chalk and Eagle Ford Shale in a submarine volcanic terrain, Maverick Basin, South Texas. Interpretation 1(2):61–83.

Pessagano, E.A., Jr., 1969, Upper Cretaceous stratigraphy of the western Gulf Coast area of Mexico, Texas, and Arkansas: Geological Society of America Memoir 111, 139 p.

Phelps, R. M., Kerans C., Loucks R. G., Gama R. D., Jeremiah, J., and Hull, D., 2014, Oceanographic and eustatic control of carbonate platform evolution and sequence stratigraphy on the Cretaceous (Valanginian-Campanian) passive margin, northern Gulf of Mexico: Sedimentology, v. 61 (2), p. 461-496.

Roy, E.C., Jr., Eidelbach, M., and Trumbly, N., 1981, A Late Cretaceous calcarenite beach complex associated with submarine volcanism, Wilson County, Texas: Gulf Coast Associations of Geological Societies Transactions, v. 31, p. 173-178.

Salvador, A., ed., 1991, Origin and development of the Gulf of Mexico basin, in Salvador, A., ed., The Gulf of Mexico Basin: Boulder, Colo., Geological Society of America, Geology of North America, v. J, p. 389-444.

Simmons, K.A., 1967, A Primer on “serpentine plugs” in south Texas, in Ellis, W.G., ed., Contributions to the geology of south Texas, 1967: San Antonio, Tex., South Texas Geological Society, p. 125-132.

Snedden, J.W., 1991, Origin and sequence stratigraphic significance of large dwelling traces in the Escondido Formation (Cretaceous, Texas, USA): Palaios, v. 6, no. 6, p. 541-552.

Snedden, J.W., and Jumper, R.S., 1990, Shelf and shoreface reservoirs, Tom Walsh-Owen field, Texas, in Barwis, J.H., McPherson, J.Q., and Studlick, R.J., eds., Sandstone petroleum reservoirs: New York, Springer-Verlag, p. 415-436.

Snedden, J.W., and Kersey, D.G., 1982, Depositional environments and gas production trends, Olmos Sandstone, Upper Cretaceous, Webb County, Texas: Gulf Coast Association of Geological Societies Transactions, v. 32, p. 497-518.

Snyder, R. H., and Craft, M., 1977, Evaluation of Austin and Buda Formations from core and fracture analysis: Gulf Coast Association of Geological Societies Transactions, v. 27, p. 376-385.

Spencer, A.B., Alkalic igneous rocks of the Balcones province, Texas: Journal of Petrology, v. 10, part 2, p. 272-306.

Texas Railroad Commission, Eagle Ford Shale information, 2015. Retrieved March 15, 2015, from http://www.rrc.state.tx.us/oil-gas/major-oil-gas-formations/eagle-ford-shale/

Thomas, W. A., 1977, Evolution of Appalachian-Ouachita salients and recesses from reentrants and promontories in the continental margin: American Journal of Science, v. 277, p. 1233-1278.

Treadgold, Galen, Bill McLain, and Steven Sinclair, 2011, Eagle Ford Shale Prospecting with 3D Seismic Data: Proc. of Society of Economic Geologists Annual Meeting, Denver, 2270-2273.

Tyler, N., and Ambrose, W.A., 1986, Depositional systems and oil and gas plays in the Cretaceous Olmos Formation, south Texas: Austin, Tex., University of Texas, Bureau of Economic Geology Report of Investigations no. 152, 42 p.

Tyler, N., Gholston, J.C., Ambrose, W.A., 1986, Genetic Stratigraphy and Oil Recovery in an Upper Cretaceous Wave-Dominated Deltaic Reservoir, Big Wells (San Miguel) Field, south Texas: Austin, Tex., University of Texas, Bureau of Economic Geology Report of Investigations no. 153, 38 p.

Weise, B.R., 1980, Wave-dominated delta systems of the Upper Cretaceous San Miguel Formation, Maverick Basin, south Texas: Austin, Tex., University of Texas, Bureau of Economic Geology Report of Investigations no. 107, 39 p.

West, A., 2015, Pennsylvanian subsurface and stratigraphy based on 3D seismic and wireline data in western Osage County, Oklahoma: M.S. Thesis, The University of Arkansas.

Wilson, W.F., and Wilson, D.H., 1984, Meteor impact site, Anacacho asphalt deposits: San Antonio, Tex., South Texas Geological Society, Field trip guidebook, 97 p.

Winkler, C. D., and Buffler, R. T., 1988, Paleogeographic evolution of early deep-water Gulf of Mexico and margins, Jurassic to Middle Cretaceous (Comanchean): American Association Petroleum Geologists Bulletin, v. 72, p. 318-346.

Wittke, J.H., and Mack, L.E., 1993, OIB-like mantle source for the continental alkaline rocks of the Balcones province, Texas—Trace-element and isotopic evidence: Journal of Geology, v. 101, no. 3, p. 333-344.

VII. Appendix

A

The Pedernales 3D seismic survey was acquired and processed for Stephens Production in 2008 with characteristics:

- Area approximately 79 sq. mi.
- Bin size 110 ft x 110 ft
- 424 inlines (approx. north-south)
- 429 crosslines (approx. east-west)
- Z range: 0-4996 ms
- Grid azimuth 4.99°
- Time sample rate 4 ms
- Frequency range is 8-70 Hz; dominant frequency of 40 Hz

B

PROCESSING WORKFLOW
SEG-Y CONVERSION
RESAMPLE TO 4 MS
LIFT NOISE REDUCTION (LFAF/TFCLEAN)
3-D GEOMETRY INITIALIZATION AND QC
REFRACTION/DATUM STATIC CALCULATIONS (REFRACTION STATIC NOT NEEDED)
SPHERICAL DIVERGENCE SCALING
WAVELET SHAPING, MINIMUM PHASE 8 -80
SURFACE CONSISTENT DECONVOLUTION (SPIKING)
SURFACE CONSISENT BALANCING
3-D VELOCITY ANALYSIS (ONE PER SQ. MILE, NEAR SURFACE DATUM)
SURFACE CONSISTENT AUTOMATIC STATICS 2 PASSES
TFCLEAN CDP ORDER (SECOND PASS)
3-D TSUNAMI PSTM VELOCITY LINES EVERY 660 FEET
3-D PSTM CONTINUOUS VELOCITY ANALYSIS
3-D TSUNAMI PSTM VELOCITY LINES EVERY 660 FEET
3-D CONTINUOUS RESIDUAL VELOCITY ANALYSIS
APERTURE AND PSTM PARAMETER TESTING
3D TSUNAMI KIRCHHOFF CURVED RAY PSTM
STACK AT SEALEVEL DATUM 8000 FT/SEC
TIME VARIANT BANDPASS FILTERING
BALANCING (RMS 2500)